Front. Phys. 13(4), 138113 (2018)
https://doi.org/10.1007/s11467-018-0809-8

Review article

Two-dimensional materials: Emerging toolkit for construction of ultrathin high-efficiency microwave shield and absorber

Mingjun Hu[1,†], Naibo Zhang[2], Guangcun Shan[3], Jiefeng Gao[4], Jinzhang Liu[1], Robert K. Y. Li[5,‡]

[1] *School of Materials Science and Engineering, Beihang University, Beijing 100191, China*
[2] *Beijing Research and Development Center, the 54th Research Institute, Electronics Technology Group Corporation, Beijing 100070, China*
[3] *School of Instrumentation Science and Opto-electronics Engineering, Beihang University, Beijing 100191, China*
[4] *School of Chemistry and Chemical Engineering, Yangzhou University, Yangzhou 225002, China*
[5] *Department of Materials Science and Engineering, City University of Hong Kong, Hong Kong, China*
Corresponding authors. E-mail: † mingjunhu@buaa.edu.cn, ‡ aprkyl@cityu.edu.hk
Received March 22, 2018; accepted May 29, 2018

Two-dimensional (2D) materials generally have unusual physical and chemical properties owing to the confined electro-strong interaction in a plane and can exhibit obvious anisotropy and a significant quantum-confinement effect, thus showing great promise in many fields. Some 2D materials, such as graphene and MXenes, have recently exhibited extraordinary electromagnetic-wave shielding and absorbing performance, which is attributed to their special electrical behavior, large specific surface area, and low mass density. Compared with traditional microwave attenuating materials, 2D materials have several obvious inherent advantages. First, similar to other nanomaterials, 2D materials have a very large specific surface area and can provide numerous interfaces for the enhanced interfacial polarization as well as the reflection and scattering of electromagnetic waves. Second, 2D materials have a particular 2D morphology with ultrasmall thickness, which is not only beneficial for the penetration and dissipation of electromagnetic waves through the 2D nanosheets, giving rise to multiple reflections and the dissipation of electromagnetic energy, but is also conducive to the design and fabrication of various well-defined structures, such as layer-by-layer assemblies, core–shell particles, and porous foam, for broadband attenuation of electromagnetic waves. Third, owing to their good processability, 2D materials can be integrated into various multifunctional composites for multimode attenuation of electromagnetic energy. In addition to behaving as microwave reflectors and absorbers, 2D materials can act as impedance regulators and provide structural support for good impedance matching and setup of the optimal structure. Numerous studies indicate that 2D materials are among the most promising microwave attenuation materials. In view of the rapid development and enormous advancement of 2D materials in shielding and absorbing electromagnetic wave, there is a strong need to summarize the recent research results in this field for presenting a comprehensive view and providing helpful suggestions for future development.

Keywords electromagnetic interference shielding, microwave absorber, graphene, MXenes, polymer nanocomposites

PACS numbers 41.20.Jb, 62.23.Kn, 78.70.Gq, 81.05.ue, 81.07.Pr, 84.40.-x

Contents

*Special Topic: Graphene and other Two-Dimensional Materials (Eds. Daria Andreeva, Wencai Ren, Guangcun Shan & Kostya Novoselov).

1 Introduction

Since the discovery of graphene in 2004, research interest in two-dimensional (2D) materials has drastically increased across various scientific and technical fields owing to their exceptional properties, which can resolve the shortcomings of many traditional materials. Novel physicochemical properties of 2D materials are continuously discovered [1–8], suggesting that 2D materials will play a significant role in future functional-material systems for the establishment of new smart platforms. Compared with their bulk counterparts, the main advantages of exfoliated 2D materials are their remarkable physical properties due to quantum confinement effects resulting from the extreme thinning in one dimension and their distinctive chemical features due to their ultralarge specific surface area and unique atom-thick sheet-like morphology, which provide great flexibility for composition control, structural design, and function integration. Currently, studies on 2D materials focus on several topics, such as optoelectronics, catalysis, energy storage and conversion, and pollutant absorption, owing to their unique semiconductor features, enormous surface areas, specific electrical behavior, and good chemical stability [9–12]. The most studied 2D materials in these fields are graphene, transitional-metal chalcogenides, and MXenes.

Recently, with the explosive increase of electronic devices and the fast development of telecommunication technology towards a high frequency, high density, and high power, electromagnetic pollution is becoming a serious global problem. Undesirable electromagnetic radiation disturbs the transmission of normal electromagnetic signals, causes the leakage of confidential information and targets, leads to the malfunction of normal electronic devices, and probably impairs human health. Thus, the inhibition of the harm done by electromagnetic waves is necessary. It is imperative to develop accessible and all-purpose electromagnetic-wave shields or eliminators. However, conventional electromagnetic-wave shielding and absorbing materials, such as metals, ceramics, and concretes, are usually heavy and unfoldable, making them unfavorable with regard to wearability and portability, which significantly limits their application. Thus, materials with a high electromagnetic interference (EMI) attenuation ability, light weight, good flexibility, high strength, excellent thermal resistance, and corrosion resistance are highly desirable. Owing to their unique 2D morphology, atomic-scale thickness, specific mechanical properties, low mass density, and controllable electromagnetic performance, 2D materials satisfy the increasing requirements and are among the best candidate materials for constructing ultrathin lightweight high-strength high-efficiency microwave shields and absorbers [13, 14]. Thus far, several typical 2D nanomaterials—including graphene, graphene oxides (GOs), MoS_2, MXenes, layered oxides or hydroxides, boron nitrides, and black phosphorus (BP)—have been employed for EMI shielding and microwave absorption, and their electromagnetic performances have been intensively investigated. In this review, we comprehensively introduce the utilization of 2D materials for electromagnetic-pollution prevention over the past decade and consider next steps in development.

According to electromagnetic-wave theory, when a wave encounters a barrier during propagation, owing to the mismatching impedance between the different media, part of the electromagnetic wave is reflected at the interface. The reflection coefficient depends on the impedance discrepancy and can be expressed as $\varGamma = (Z_{\mathrm{in}} - Z_0)/(Z_{\mathrm{in}} + Z_0)$, where Z_0 and Z_{in} are the impedances of the propagation medium and the barrier, respectively. The remainder of the electromagnetic wave penetrates the barrier. The transmission of the electromagnetic wave in the barrier can be expressed by the transmission coefficient $T = \mathrm{e}^{-\gamma t}$, where t is the propagation distance of the electromagnetic wave in the barrier, and γ is the propagation constant. γ is a complex number whose real and imaginary parts are related to the energy loss and energy storage, respectively. Because the barrier has a certain thickness, the electromagnetic wave dissipates in the propagation path and is converted into thermal energy via two principal mechanisms: dielectric loss and magnetic loss. This is defined as microwave absorption. Dielectric loss is mainly ascribed to the hysteresis effect of the dielectric conduction and dielectric polarization, generally involving Joule loss as a result of eddy current and polarization loss derived from interfacial polarization, dipolar polarization, electronic polarization, ionic polarization, etc. Magnetic loss arises from the magnetic hysteresis effect of magnetic materials under an electromagnetic field and mainly comprises magnetic hysteresis loss, eddy current loss, magnetic aftereffect loss, magnetic resonance loss, etc.

To achieve a high EMI attenuation ability, the materials should follow several basic principles, in accordance with electromagnetic theory.

1) The materials must have suitable electromagnetic parameters, i.e., the complex magnetic permeability μ and complex permittivity ε. These can be described by the typical formulas $\mu = \mu' - \mathrm{j}\mu'' = \mu'(1 - \mathrm{j}\tan\delta_m)$ and $\varepsilon = \varepsilon' - \mathrm{j}\varepsilon'' = \varepsilon'(1 - \mathrm{j}\tan\delta_e)$, where δ_m and δ_e represent the magnetic loss angle and electric loss angle of the medium, respectively. The terms μ' and ε' are related to the electromagnetic energy storage, and μ'' and ε'' are associated with the energy loss. The reflection coefficient can be expressed as $\Gamma = (Z_{in} - Z_0)/(Z_{in} + Z_0) = (\sqrt{\frac{\mu_r}{\varepsilon_r}} - 1)/(\sqrt{\frac{\mu_r}{\varepsilon_r}} + 1)$. This coefficient is directly related to the magnetic permeability μ and permittivity ε and represents the magnitude of the reflected electromagnetic wave normalized to the incident electromagnetic wave. The transmission coefficient is described by $T = \mathrm{e}^{-\gamma t}$, where the propagation constant γ is given as $\gamma = \mathrm{j}\omega\sqrt{\mu\varepsilon}$, and is also related to μ and ε. Thus, the electromagnetic parameters of materials directly determine the propagation behavior of the electromagnetic wave at the interface and in the interior of media. By tuning the electromagnetic parameters of materials, the attenuation behavior of the electromagnetic wave can be regulated. For the shielding materials, the transmissivity of the electromagnetic wave is usually required to be as small as possible, indicating that the materials should have strong reflection or absorption ability to electromagnetic waves. Thus, in this case, a large μ and ε are highly desirable for the improvement of the shielding performance. For the absorbing materials, the reflection should be avoided to the greatest extent possible while increasing the absorption, which means that the materials should have good impedance matching to avoid the reflection as well as a strong dissipation ability to incident electromagnetic waves. This requires that the materials have suitable electromagnetic parameters rather than unilateral excellent properties. According to the aforementioned description, several types of materials are preferred for the shielding or absorption of electromagnetic waves. These generally include conductive materials with a high conductivity σ, dielectric materials with a suitable permittivity ε, and ferromagnetic and ferrimagnetic materials with an appropriate permeability μ, which can play different roles in microwave shielding and absorption for the inhibition of electromagnetic pollution.

2) In addition to suitable electromagnetic parameters, electromagnetic-wave shields and absorbers should have optimal structures. In general, the popular structures employed for EMI shielding include conductive slabs, metal mesh structures, and various conductive composites, and the structures used for microwave absorption chiefly include multilayer boards, sandwich structures, frequency-selective surfaces, lattice structures, perpendicular pyramidal structures, and resonant cavity-like structures. The primary purpose of the structural design is to realize the full potential of microwave absorbers for dissipating electromagnetic energy by elongating the propagation path of electromagnetic waves in the medium and preventing the escape of electromagnetic pollution via surface reflection. The specific implementation measures chiefly involve increasing the occurrences of reflection and scattering by increasing the interfacial area and improving the impedance matching by introducing void space or high-impedance materials.

3) To satisfy special requirements, electromagnetic-wave shields and absorbers should also have certain specific physical and chemical properties. For instance, in some cases, the materials must be lightweight, ultrathin, strong, flexible, wearable, thermal resistant, corrosion resistant, optically transparent, etc. The integration of multiple functions can broaden the applications of shielding and wave-absorbing materials.

In each of the aforementioned three aspects, 2D nanomaterials exhibit unrivalled advantages. They constitute a large family of materials and involve a wide range of material types, such as conductors, semiconductors, dielectric isolators, and ferromagnets. Thus, they can be used to construct a variety of multifunctional hybrid systems for the multimode attenuation of electromagnetic waves. Additionally, 2D materials are ultrathin and have a large aspect ratio, which is favorable for building a variety of optimal structures, such as highly oriented layer-by-layer assemblies, core–shell particles, hierarchical constitutions, and porous foams, in a flexible manner, for high-efficiency microwave shielding or absorbing. Moreover, 2D materials are generally highly dispersible via suitable processing and have a low mass density and good mechanical strength; thus, they can act as the fillers of various polymers or other matrices for the fabrication of a variety of lightweight high-strength composite shields and absorbers. Consequently, 2D materials are among the most promising microwave shielding and absorbing materials and will play an increasingly important role in this field.

2 Electromagnetic theory for microwave shielding and absorption

To study the electromagnetic shielding effectiveness (SE) and microwave-absorbing ability (WAA) of the materials accurately and qualitatively, it is necessary to establish a direct connection between the SE/WAA and the electromagnetic parameters of materials. According to the electromagnetic shielding theory of S. A. Schelkunoff [15], we use a monolayer slab as a typical example to describe the effects of various electromagnetic parameters on the SE and WAA of materials.

In Fig. 1(a), an electromagnetic wave enters medium II perpendicularly from medium I. It then penetrates through medium II and reenters medium I. At the incident interface, part of the electromagnetic wave is reflected, and the other part continues to propagate in medium II towards the output interface and is partially reflected again, experiencing a similar process to that at the incident interface. This process is repeated until the energy is dissipated completely, after multiple occurrences of reflection and transmission. According to the electromagnetic theory, we set the magnitude of the incident wave as 1; thus, $T_{11} = 1 + \Gamma_{01}$. The first-, second-, third-, and n-pass transmissivity is given as $T'_{11} = (1+\Gamma_{01})(1+\Gamma_{11})\mathrm{e}^{-\gamma_c t}$, $T'_{12} = (1+\Gamma_{01})(1+\Gamma_{11})\Gamma_{11}\Gamma_{12}\mathrm{e}^{-3\gamma_c t}$, $T'_{13} = (1+\Gamma_{01})(1+\Gamma_{11})\Gamma_{11}^2\Gamma_{12}^2\mathrm{e}^{-5\gamma_c t}$, and $T'_{1n} = (1+\Gamma_{01})(1+\Gamma_{11})\Gamma_{11}^n\Gamma_{12}^n\mathrm{e}^{-(2n-1)\gamma_c t}$, respectively. Thus, the total transmissivity of the monolayer composite slab can be expressed as follows:

$$
\begin{aligned}
T'_{1t} &= (1+\Gamma_{01})(1+\Gamma_{11})\mathrm{e}^{-\gamma_c t} \\
&\quad +(1+\Gamma_{01})(1+\Gamma_{11})\Gamma_{11}\Gamma_{12}\mathrm{e}^{-3\gamma_c t} \\
&\quad +(1+\Gamma_{01})(1+\Gamma_{11})\Gamma_{11}^2\Gamma_{12}^2\mathrm{e}^{-5\gamma_c t}+\cdots \\
&\quad +(1+\Gamma_{01})(1+\Gamma_{11})\Gamma_{11}^n\Gamma_{12}^n\mathrm{e}^{-(2n-1)\gamma_c t}+\cdots \\
&= (1+\Gamma_{01})(1+\Gamma_{11})\mathrm{e}^{-\gamma_c t}[1+\Gamma_{11}\Gamma_{12}\mathrm{e}^{-2\gamma_c t} \\
&\quad +\Gamma_{11}^2\Gamma_{12}^2\mathrm{e}^{-4\gamma_c t}+\cdots+(\Gamma_{11}\Gamma_{12}\mathrm{e}^{-2\gamma_c t})^{n-1}+\cdots] \\
&= (1+\Gamma_{01})(1+\Gamma_{11})\mathrm{e}^{-\gamma_c t}\frac{1}{1-\Gamma_{11}\Gamma_{12}\mathrm{e}^{-2\gamma_c t}},
\end{aligned} \tag{1}
$$

where γ_c is the propagation constant of the absorber, and t is the thickness of the absorber. The SE can be expressed in logarithmic form, as follows:

$$
\begin{aligned}
\mathrm{SE(dB)} &= 20\log\frac{1}{|T'_{1t}|} \\
&= -20\log\ |(1+\Gamma_{01})(1+\Gamma_{11})| + 20\log\ |\mathrm{e}^{\gamma t}| \\
&\quad +20\log\ |1-\Gamma_{11}\Gamma_{12}\mathrm{e}^{-2\gamma t}| \\
&= SE_R + SE_A + SE_M,
\end{aligned} \tag{2}
$$

where the first item is only related to the surface reflection coefficient, representing the reflection part of the electromagnetic power; the second item is only related to the propagation path, representing the absorption of the electromagnetic wave in the propagation process; and the third item is related to both the reflection at the inside interfaces and inside propagation paths, representing the part arising from multiple reflections. The propagation constant γ can be expressed as $\gamma = \alpha + \mathrm{j}\beta = \mathrm{j}\omega\sqrt{\mu\varepsilon}\sqrt{1-\mathrm{j}\frac{\sigma}{\omega\varepsilon}}$. When the medium is highly conductive, $\sigma \gg \omega\varepsilon$, the propagation constant is $\gamma = \mathrm{j}\omega\sqrt{\mu\varepsilon}\sqrt{\frac{\sigma}{\mathrm{j}\omega\varepsilon}} = (1+\mathrm{j})\sqrt{\frac{\omega\mu\sigma}{2}}$, the skin depth is $\delta = \frac{1}{\alpha} = \sqrt{\frac{2}{\omega\mu\sigma}}$, the impedance of the composite slab is $Z = \sqrt{\frac{\mu}{\varepsilon_c}} = \sqrt{\frac{\mu}{\varepsilon+\frac{\sigma}{\mathrm{j}\omega}}} = \sqrt{\frac{\mathrm{j}\omega\mu}{\mathrm{j}\omega\varepsilon+\sigma}} = (1+\mathrm{j})\sqrt{\frac{\omega\mu}{2\sigma}}$, and the reflection coefficient is $\Gamma = \frac{Z-Z_0}{Z+Z_0}$.

Because

$$
\begin{aligned}
SE_R &= -20\log\ |(1+\Gamma_{01})(1+\Gamma_{11})| \\
&= 20\log\left|\frac{(Z+Z_0)^2}{4Z_0 Z}\right|
\end{aligned} \tag{3}
$$

and for metals, $Z_0 \gg Z$,

$$
SE_R = 20\log\frac{|Z_0|}{4|Z|} = 10\log\frac{|Z_0|^2}{16|Z|^2} = 10\log\frac{\sigma}{16\omega\mu_r\varepsilon_0}. \tag{4}
$$

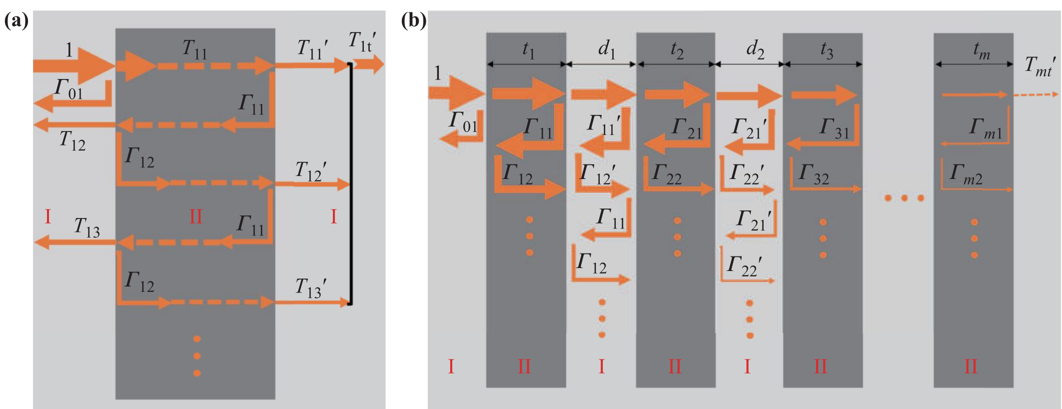

Fig. 1 **(a)** The propagation of electromagnetic wave in monolayer slab; **(b)** electromagnetic wave travels through multilayer structure, in which, I stands for the matrix, II stands for the wave absorber, T means transmission coefficient, Γ means reflection coefficient, t is the thickness of absorber, and d is the space distance between the absorbers.

Similarly, we obtain

$$SE_A = 8.69t\sqrt{\frac{\omega\mu_r\sigma}{2}} = A, \tag{5}$$

$$\begin{aligned} SE_M &\approx 20\log\ |1-\mathrm{e}^{-2\gamma t}| \\ &\approx 20\log\ |1-10^{-0.1A}\mathrm{e}^{-\mathrm{j}0.23A}|, \end{aligned} \tag{6}$$

where $\sigma = \omega\varepsilon_0\varepsilon'' = 2\pi f\varepsilon_0\varepsilon''$, with $\varepsilon_r = \varepsilon' - \mathrm{j}\varepsilon''$. The aforementioned expressions clearly indicate that for a monolayer conductive slab, the conductivity σ, the permeability μ, and the permittivity ε all play the important roles in attenuating electromagnetic waves, and with higher conductivity, the reflection and absorption are both enhanced.

In Fig. 1(b), the multilayer sandwiched structured composites with the same matrix are described, and the corresponding formula can be expressed as follows:

$$\begin{aligned} SE_m &= 20\log\frac{1}{|T'_{mt}|} \\ &= -20\log|(1+\Gamma_{01})(1+\Gamma_{11})(1+\Gamma'_{11})(1+\Gamma_{21}) \\ &\quad (1+\Gamma'_{21})(1+\Gamma_{31})(1+\Gamma'_{31})\cdots(1+\Gamma_{m1})| \\ &\quad +20\log|\mathrm{e}^{\gamma_c(t_1+t_2+t_3+\cdots+t_m)+\gamma_d(d_1+d_2+\cdots+d_{m-1})}| \\ &\quad +20\log|(1-\Gamma_{11}\Gamma_{12}\mathrm{e}^{-2\gamma_c t_1})(1-\Gamma'_{11}\Gamma'_{12}\mathrm{e}^{-2\gamma_d d_1}) \\ &\quad (1-\Gamma_{21}\Gamma_{22}\mathrm{e}^{-2\gamma_c t_2})(1-\Gamma'_{21}\Gamma'_{22}\mathrm{e}^{-2\gamma_d d_2}) \\ &\quad (1-\Gamma_{31}\Gamma_{32}\mathrm{e}^{-2\gamma_c t_3})(1-\Gamma'_{31}\Gamma'_{32}\mathrm{e}^{-2\gamma_d d_3})\cdots \\ &\quad (1-\Gamma_{m1}\Gamma_{m2}\mathrm{e}^{-2\gamma_c t_m})|, \end{aligned} \tag{7}$$

where γ_c is the propagation constant of the absorber, γ_d is the propagation constant of the matrix, t is the thickness of the absorber, and d is the separation distance between two adjacent absorbers. Notably, according to the formula, the deduction of the reflection coefficient should consider the overall effect of the multilayer structure, and the impedance of the composite medium is not the characteristic impedance of the first layer but rather the whole impedance, including all the succeeding layers in the microwave propagation path. Additional details about the reflection coefficient are presented in a previous work [15]. The expression of SE_m indicates that the electromagnetic SE in the multilayer structure is mainly determined by the number of interfaces, the wave propagation path, and the real part of the propagation constant. Generally, a larger amount of heterogeneous particles filling the matrix yields a larger number of interfaces reflecting the electromagnetic wave and a longer propagation path, resulting in a larger dissipation probability of electromagnetic energy in the matrix. This is very important for the study of the electromagnetic energy loss in a composite medium.

To further evaluate the electromagnetic wave absorbing performance of composite materials, more professional parameters have been introduced by researchers, such as the reflection loss (RL) and the attenuation constant α (the real part of the propagation constant). These can be expressed as follows:

$$RL = 20\log|\Gamma| = 20\log\left|\frac{Z_{in}-Z_0}{Z_{in}+Z_0}\right| = 20\log\left|\frac{\frac{Z_{in}}{Z_0}-1}{\frac{Z_{in}}{Z_0}+1}\right|, \tag{8}$$

where Z_{in} is the overall impedance of the composite material that the electromagnetic wave enters, and Z_0 is the impedance of free space or the medium through which the wave travels before entering the composite material. In the case of a monolayer slab with a perfect electric conductor as the substrate for completely reflecting the electromagnetic wave, according to the transmission-line theory, the RL can be expressed as follows [16]:

$$RL = 20\log\left|\frac{\sqrt{\frac{\mu_r}{\varepsilon_r}}\tanh\left(\mathrm{j}\frac{2\pi fd}{c}\sqrt{\mu_r\varepsilon_r}\right)-1}{\sqrt{\frac{\mu_r}{\varepsilon_r}}\tanh\left(\mathrm{j}\frac{2\pi fd}{c}\sqrt{\mu_r\varepsilon_r}\right)+1}\right|. \tag{9}$$

The attenuation constant is given as

$$\begin{aligned} \alpha &= \mathrm{Re}(\gamma) = \mathrm{Re}(\mathrm{j}\omega\sqrt{\mu\varepsilon}) = \mathrm{Re}\left(\frac{\mathrm{j}\omega\sqrt{\mu_r\varepsilon_r}}{c}\right) \\ &= \frac{\omega}{\sqrt{2}c}\sqrt{\mu''\varepsilon''-\mu'\varepsilon'+\sqrt{(\mu'^2+\mu''^2)(\varepsilon'^2+\varepsilon''^2)}}, \end{aligned} \tag{10}$$

where c is the speed of light, and μ', ε' and μ'', ε'' are the real and imaginary parts of the relative complex permeability and permittivity, respectively. For reducing the RL to the greatest extent possible, the absolute value of the RL should be maximized. Generally, $\frac{Z_{in}}{Z_0} < 1$ owing to the larger impedance of free space than common media; thus, $\sqrt{\frac{\mu_r}{\varepsilon_r}}\tanh\left(\mathrm{j}\frac{2\pi fd}{c}\sqrt{\mu_r\varepsilon_r}\right) < 1$. Therefore, to achieve good impedance matching, $\sqrt{\frac{\mu_r}{\varepsilon_r}}\tanh\left(\mathrm{j}\frac{2\pi fd}{c}\sqrt{\mu_r\varepsilon_r}\right)$ must be maximized to keep $\left|\frac{\sqrt{\frac{\mu_r}{\varepsilon_r}}\tanh\left(\mathrm{j}\frac{2\pi fd}{c}\sqrt{\mu_r\varepsilon_r}\right)-1}{\sqrt{\frac{\mu_r}{\varepsilon_r}}\tanh\left(\mathrm{j}\frac{2\pi fd}{c}\sqrt{\mu_r\varepsilon_r}\right)+1}\right|$ as small as possible. For a nonmagnetic sample, $\mu_r = 1 + 0\mathrm{j} = 1$; thus, $\sqrt{\frac{1}{\varepsilon_r}}\tanh\left(\mathrm{j}\frac{2\pi fd}{c}\sqrt{\varepsilon_r}\right)$ should be as large as possible. In the general case, $\left|\mathrm{j}\frac{2\pi fd}{c}\sqrt{\varepsilon_r}\right| < 1$, and the Taylor expansion yields the following expression.

$$\begin{aligned} &\sqrt{\frac{1}{\varepsilon_r}}\tanh\left(\mathrm{j}\frac{2\pi fd}{c}\sqrt{\varepsilon_r}\right) \\ &= \mathrm{j}\frac{2\pi fd}{c}+\mathrm{j}\left(\frac{2\pi fd}{c}\right)^3\frac{\varepsilon_r}{3}+\mathrm{j}\left(\frac{2\pi fd}{c}\right)^5\frac{2\varepsilon_r^2}{15}+\cdots \end{aligned} \tag{11}$$

When $\left|\mathrm{j}\frac{2\pi fd}{c}\sqrt{\varepsilon_r}\right| \ll 1$, we can neglect the higher-order terms, and

$$\sqrt{\frac{1}{\varepsilon_r}}\tanh\left(\mathrm{j}\frac{2\pi fd}{c}\sqrt{\varepsilon_r}\right)\approx\mathrm{j}\frac{2\pi fd}{c}+\mathrm{j}\left(\frac{2\pi fd}{c}\right)^3\frac{\varepsilon_r}{3}, \quad (12)$$

$$\begin{aligned}&\left|\sqrt{\frac{1}{\varepsilon_r}}\tanh\left(\mathrm{j}\frac{2\pi fd}{c}\sqrt{\varepsilon_r}\right)-1\right|\\&=\left|\mathrm{j}\frac{2\pi fd}{c}+\mathrm{j}\left(\frac{2\pi fd}{c}\right)^3\frac{\varepsilon_r}{3}-1\right|\\&=\left|\left(\frac{m^3}{3}\varepsilon''-1\right)+\mathrm{j}\left(\frac{m^3}{3}\varepsilon'+m\right)\right|, \end{aligned}\quad (13)$$

where $m=\frac{2\pi fd}{c}>0$. To minimize the RL, $\left|\frac{m^3}{3}\varepsilon''-1\right|$ and $\left|\frac{m^3}{3}\varepsilon'+m\right|$ should be as small as possible. Thus, ε' should be as small as possible, and ε'' should be as close to $\frac{3}{m^3}$ as possible under the condition that $\left|\mathrm{j}\frac{2\pi fd}{c}\sqrt{\varepsilon_r}\right|\ll 1$. Additionally, because $\sigma=\omega\varepsilon_0\varepsilon''=2\pi f\varepsilon_0\varepsilon''$, the following relationship can be obtained:

$$\sigma=\frac{3\lambda^3 f\varepsilon_0}{4\pi^2 d^3}. \quad (14)$$

For magnetic materials, $\mu_r\neq 1$, and the equation for achieving perfect impedance matching is as follows:

$$\sqrt{\frac{\mu_r}{\varepsilon_r}}\tanh\left(\mathrm{j}\frac{2\pi fd}{c}\sqrt{\mu_r\varepsilon_r}\right)=\sqrt{\frac{\mu_r}{\varepsilon_r}}\tanh\left(\mathrm{j}\frac{2\pi d}{\lambda}\sqrt{\mu_r\varepsilon_r}\right)=1. \quad (15)$$

When the frequency of the electromagnetic wave ranges from 1 to 20 GHz, the wavelength is > 15 mm in free space, which is generally greater than the thickness of thin-film materials. Additionally, μ_r and ε_r are relatively small at a high frequency and under a weak magnetic field. Thus, usually, $\left|\mathrm{j}\frac{2\pi d}{\lambda}\sqrt{\mu_r\varepsilon_r}\right|<1$.

When $\left|\mathrm{j}\frac{2\pi d}{\lambda}\sqrt{\mu_r\varepsilon_r}\right|\ll 1$, $\tanh\left(\mathrm{j}\frac{2\pi fd}{c}\sqrt{\mu_r\varepsilon_r}\right)\approx \mathrm{j}\frac{2\pi fd}{c}\sqrt{\mu_r\varepsilon_r}$; thus,

$$\sqrt{\frac{\mu_r}{\varepsilon_r}}\tanh\left(\mathrm{j}\frac{2\pi d}{\lambda}\sqrt{\mu_r\varepsilon_r}\right)\approx\mathrm{j}\frac{2\pi fd}{c}(\mu_r'-j\mu_r'')=1. \quad (16)$$

This reduces to

$$\mu_r'=0,\quad \mu_r''=\frac{c}{2\pi fd}=\frac{\lambda}{2\pi d}. \quad (17)$$

When $\left|\mathrm{j}\frac{2\pi d}{\lambda}\sqrt{\mu_r\varepsilon_r}\right|\ll 1$ is not satisfied and $\left|\mathrm{j}\frac{2\pi d}{\lambda}\sqrt{\mu_r\varepsilon_r}\right|<1$, we can apply the Taylor expansion, yielding the following formula:

$$\begin{aligned}&\sqrt{\frac{\mu_r}{\varepsilon_r}}\tanh\left(\mathrm{j}\frac{2\pi fd}{c}\sqrt{\mu_r\varepsilon_r}\right)\\&=\mathrm{j}\frac{2\pi fd\mu_r}{c}+\mathrm{j}\left(\frac{2\pi fd}{c}\right)^3\frac{\mu_r^2\varepsilon_r}{3}+\mathrm{j}\left(\frac{2\pi fd}{c}\right)^5\frac{2\mu_r^3\varepsilon_r^2}{15}+\cdots.\end{aligned}\quad (18)$$

Because $\left|j\frac{2\pi d}{\lambda}\sqrt{\mu_r\varepsilon_r}\right|<1$, we neglect the higher-order items, and the following formula is used to optimize the impedance matching:

$$\begin{aligned}&\sqrt{\frac{\mu_r}{\varepsilon_r}}\tanh\left(\mathrm{j}\frac{2\pi fd}{c}\sqrt{\mu_r\varepsilon_r}\right)\\&=\mathrm{j}\frac{2fd\mu_r}{c}+\mathrm{j}\left(\frac{2\pi fd}{c}\right)^3\frac{\mu_r^2\varepsilon_r}{3}=1.\end{aligned}\quad (19)$$

Thus,

$$\varepsilon_r=-\frac{c^2}{(2\pi fd)^2\mu_r}-\mathrm{j}\frac{3c^3}{(2\pi fd)^3\mu_r^2}. \quad (20)$$

For the condition of $\left|\mathrm{j}\frac{2\pi d}{\lambda}\sqrt{\mu_r\varepsilon_r}\right|\geq 1$, a detailed description of the relationship between the electromagnetic parameters is presented in a previous work [17].

Furthermore, for composites filled with magnetic nanoparticles, under a weak magnetic field and a high frequency, the magnetic loss from magnetic domain-wall displacement and magnetic hysteresis is small because there are few domain walls in nanoscale materials and there is little irreversible magnetization under a weak external magnetic field; thus, the natural resonance loss and eddy current loss play the dominant roles in the total magnetic loss [18].

Generally, for eddy current loss, the following relationship holds:

$$\frac{\mu_r''}{\mu_r'}\propto\frac{\mu_r' fD^2}{\rho}, \quad (21)$$

where D is the diameter of the nanoparticles, and ρ is the electrical resistivity of magnetic nanoparticles. We observe that $\tan\delta_m=\mu_r''/\mu_r'$, which is related to μ_r', f, D, and ρ. In addition, for specific magnetic nanoparticles, the value of $\mu_r''\mu_r'^{-2}f^{-1}$ is only associated with D and ρ and thus can principally remain constant at a high frequency.

In the meantime, for natural resonance loss, the following equations hold [16]:

$$f_r=\frac{\gamma}{2\pi}H_a, \quad (22)$$

where $\frac{\gamma}{2\pi}=2.8$ MHz/Oe is the gyromagnetic ratio, and H_a is the anisotropy field, which can be expressed as

$$H_a=\frac{2|K|}{\mu_0 M_s}. \quad (23)$$

Here, K is the anisotropy constant, and M_s is the saturation magnetization. A larger H_a yields higher natural resonance frequency and thus larger high-frequency loss, and the growth of M_s generally results in the redshift of f_r and an increase in low-frequency loss. In addition, according to Snoek's law [19],

$$\int_0^\infty \mu''(f) f \mathrm{d}f = k_A \frac{\pi}{2}(\bar{\gamma} 4\pi M_s)^2, \tag{24}$$

where k_A is a dimensionless factor associated with the distribution of the orientation of the magnetization in the sample, and $\bar{\gamma} = \frac{\gamma}{2\pi}$ is the gyromagnetic ratio. The equation indicates that the right-hand side is constant for a specific material with a definite shape; thus, there is a trade-off between the resonance frequency and the frequency bandwidth. With the redshift of the resonance frequency f_r, the absorption frequency bandwidth increases. Therefore, generally, the addition of magnetic materials with a high M_s can broaden the microwave absorbing bandwidth while enhancing the absorbing intensity by introducing magnetic loss.

In addition to the electromagnetic parameters of materials, the film thickness has a large influence on the microwave absorption performance. According to the 1/4-wavelength equations [14],

$$d = \frac{(2n+1)\lambda_r}{4} = \frac{(2n+1)c}{4 f_m \sqrt{\mu_r \varepsilon_r}}, \quad n = 0, 1, 2, \ldots, \tag{25}$$

where d is the optimal film thickness, λ_r is the electromagnetic wavelength in the composite film, c represents the light velocity in free space, f_m is the peak absorption frequency, μ_r is the relative magnetic permeability of the composite film, and ε_r is the relative permittivity. Thus, for the same f_m, a larger μ_r and ε_r result in a smaller d, meaning that the film thickness can be thinned greatly.

On account of aforementioned electromagnetic theory, several basic principles should be followed in order to obtain high-efficiency microwave shields and absorbers. First, the composites should contain as many interfaces as possible for multiple reflections and interfacial polarization loss; second, the composites should have a suitable conductivity for both good impedance matching and electromagnetic energy dissipation; third, the propagation path of electromagnetic waves should be as long as possible to maximize the energy consumption in the propagation process; fourth, the magnetic absorber should have a high M_s and low resistivity, to generate a large magnetic loss for microwave attenuation; fifth, optimal film-thickness design is an effective approach for enhancing the microwave absorption. Thus, the fabrication of multicomponent microwave shields and absorbers with a reasonable structure and composition is an absolute necessity for the further enhancement of the EMI SE and WAA, and 2D materials provide a perfect toolkit for the construction of a variety of microwave shields and absorbers to enable high-efficiency prevention of electromagnetic pollution.

3 Characterization of EMI SE and microwave-absorbing ability (WAA)

In modern instrumentation, S-parameters at two ports measured by a scalar or vector network analyzer based on a coaxial or waveguide setup are typically used for the analysis of the reflected, absorbed, and transmitted power in a given frequency range. Here, $|S_{11}|^2$ and $|S_{21}|^2$ correspond to the electromagnetic power reflected at port 1 P_{ref} and the power transmitted from port 1 to port 2 P_{out}, normalized to the incident power P_{in}, respectively, and satisfy the following relationships [20]:

$$|S_{11}|^2 = \frac{P_{ref}}{P_{in}}, \tag{26}$$

$$|S_{21}|^2 = \frac{P_{out}}{P_{in}}, \tag{27}$$

$$P_{in} = P_{ref} + P_{out} + P_{abs}. \tag{28}$$

For a monolayer composite slab, in a two-port network, a single-chain matrix T_c can be expressed as follows:

$$T_c = \begin{bmatrix} A_0 & B_0 \\ C_0 & D_0 \end{bmatrix} = \begin{bmatrix} \cosh \gamma_c t & Z_c \sinh \gamma_c t \\ Y_c \sinh \gamma_c t & \cosh \gamma_c t \end{bmatrix}, \tag{29}$$

where $Z_c = \sqrt{\frac{\mu}{\varepsilon}}$ is the wave impedance of the composite slab, $Y_c = 1/Z_c$ is the wave admittance, and $\gamma_c = j\omega\sqrt{\mu_r \varepsilon_r}/c_0$ is the propagation constant in the medium. According to the reciprocity formulation and the transformation relationship between the S-matrix components and the single-chain matrix T_c components, in combination with the definition $\Gamma_c = (Z_c - Z_0)/(Z_c + Z_0)$ and $T_l = \mathrm{e}^{-\gamma t}$, we obtain

$$S_{11} = S_{22} = \frac{A_0 + B_0/Z_0 - C_0 Z_0 - D_0}{A_0 + B_0/Z_0 + C_0 Z_0 + D_0} = \frac{\Gamma_c(1 - T_l^2)}{1 - \Gamma_c^2 T_l^2}, \tag{30}$$

$$S_{21} = S_{12} = \frac{2(A_0 D_0 - B_0 C_0)}{A_0 + B_0/Z_0 + C_0 Z_0 + D_0} = \frac{T_l(1 - \Gamma_c^2)}{1 - \Gamma_c^2 T_l^2}. \tag{31}$$

As the definition indicates,

$$SE = \frac{P_{in}}{P_{out}} = \frac{1}{|S_{21}|^2} = \left|\frac{1 - \Gamma_c^2 T_l^2}{T_l(1 - \Gamma_c^2)}\right|^2, \tag{32}$$

$$R = \frac{P_{ref}}{P_{in}} = |S_{11}|^2 = \left|\frac{\Gamma_c(1 - T_l^2)}{1 - \Gamma_c^2 T_l^2}\right|^2, \tag{33}$$

$$A = \frac{P_{abs}}{P_{in}} = 1 - |S_{11}|^2 - |S_{21}|^2 = \frac{(1 - \Gamma_c^2)(1 - T_l^2)(1 + \Gamma_c^2 T_l^2)}{(1 - \Gamma_c^2 T_l^2)^2}, \tag{34}$$

and the electromagnetic SE can be written logarithmically in decibels as follows:

$$SE = 10\log\frac{P_{in}}{P_{out}} = 10\log\frac{1}{|S_{21}|^2}. \tag{35}$$

Regarding the relationship between S_{11}, S_{21} and $\varGamma_c$, T_l, the following equations can be obtained [21]:

$$\frac{S_{11}^2 - S_{21}^2 + 1}{2S_{11}} = \frac{1+\varGamma_c^2}{2\varGamma_c}. \tag{36}$$

Suppose that

$$\frac{S_{11}^2 - S_{21}^2 + 1}{2S_{11}} = K. \tag{37}$$

Thus,

$$\varGamma_c = K \pm \sqrt{K^2-1} \quad (|\varGamma_c| \leq 1) \tag{38}$$

$$T_l = \frac{S_{21}}{1 - S_{11}\varGamma_c} = \mathrm{e}^{-\gamma_c t} = \mathrm{e}^{-\frac{\mathrm{j}\omega\sqrt{\mu_r\varepsilon_r}}{c_0}t}, \tag{39}$$

and

$$\varGamma_c = \frac{Z_c - Z_0}{Z_c + Z_0} = \frac{Z_c/(Z_0-1)}{Z_c/(Z_0+1)} = \frac{\sqrt{\frac{\mu_r}{\varepsilon_r}}-1}{\sqrt{\frac{\mu_r}{\varepsilon_r}}+1}. \tag{40}$$

Accordingly,

$$\frac{\mu_r}{\varepsilon_r} = \left(\frac{1+\varGamma_c}{1-\varGamma_c}\right)^2 = b_1, \tag{41}$$

$$\mu_r\varepsilon_r = -\left(\frac{c_0\ln T_l}{\omega t}\right)^2 = b_2, \tag{42}$$

and we obtain the following expressions:

$$\mu_r^2 = b_1 b_2, \tag{43}$$

$$\varepsilon_r^2 = \frac{b_2}{b_1}. \tag{44}$$

After obtaining the values of μ_r and ε_r, using Eq. (9) we can obtain the RL–frequency curves and evaluate the frequency dependence of RL and the wave-absorbing performance of materials.

Using the coaxial-line testing method, we can obtain the S parameters and determine the electromagnetic-wave SE of materials; determine the reflection coefficient $\varGamma$ and transmission coefficient T; obtain the electromagnetic parameters of composite materials, such as the complex permeability μ_r and complex permittivity ε_r; and calculate the RL and attenuation constant α for evaluating the microwave absorbing ability (WAA) of materials. Obviously, the coaxial-line method is an indirect measurement method for testing the electromagnetic performance of materials and can yield electromagnetic parameter information for materials in a wide frequency range. It has been widely adopted for the evaluation of electromagnetic shielding and absorbing properties. In addition to the coaxial-line method, other methods—the such as NRL-arch method and waveguide method, etc.—have also been employed to evaluate the EMI SE and WAA of materials [22, 23].

4 Graphene and graphene-based composites as microwave shield and absorber

4.1 Graphene and graphene-filled polymer composites for microwave attenuation

Graphene was first exfoliated mechanically from graphite by Novoselov *et al.* in 2004 [24] and was found to show an extremely high mechanical strength and electron mobility. The study indicated that graphene is a single-atom-thick carbon layer with a honeycomb-like structure and has a superhigh aspect ratio. As a microwave shield and absorber, graphene was usually deposited on the surface of various substrates or dispersed in different matrices for the fabrication of freestanding films or composites. These composites contain numerous interfaces for reflecting and scattering electromagnetic waves. Additionally, owing to the large specific surface area, graphene-based composites usually possess a very low percolation threshold (∼0.1 vol.%) [25], and even with a very small amount of graphene loading, a continuous conductive network can be formed in the matrix, increasing the dielectric loss of electromagnetic energy. Additionally, when graphene is oxidized into GOs, numerous functional groups containing oxygen are introduced, giving rise to strong dipolar polarization and interfacial polarization for the further enhancement of the microwave attenuation ability.

Generally, graphene-based materials used for shielding and absorbing electromagnetic waves can be divided into three categories: graphene, GOs, and their composites. The EMI SE of monolayer chemical vapor deposition (CVD)-grown graphene was studied by Hong *et al.*, and it was found that there was an average EMI SE value of 2.27 dB for a single-carbon atom layer, amounting to shielding of 40% of the incident electromagnetic waves, where the absorption played a dominant role. This absorbance gradually decreased with an increasing number of layers owing to the enhancement of the conduction. Further modeling indicated that perfect monolayer graphene can shield approximately 97.8% of EMI; thus, an ultrathin high-efficiency monolayer or few-layer transparent graphene film with high EMI SE can be achieved [26]. Shen *et al.* reported the production of ultrathin graphited graphene films by annealing evaporation-induced deposited GO films at 2000 °C.

These films not only possess good EMI SE of approximately 20 dB even for an 8.4-μm-thick film, but also have excellent mechanical flexibility and structural integrity during bending [27]. Furthermore, the electromagnetic properties of chemically reduced GOs were investigated. It was found that compared with pure graphene and carbon nanotubes (CNTs), GOs have better impedance matching with free space, more prompt energy-level transitions from contiguous states to the Fermi level, and more defect polarization relaxation and electron dipole relaxation of functional groups owing to the existence of residual defects and functional groups on the surface, resulting in easier penetration and absorption of electromagnetic waves during propagation and a stronger WAA [28]. Reduced large-area GO (rLGO) with a super-large surface area was also prepared, through a cost-effective chemical reduction method. The results indicated that the as-prepared rLGO films had electrical conductivity of 243 ± 12 S·cm^{-1} and thermal conductivity of 1390 ± 65 W·m^{-1}·K^{-1}, which are significantly better than those of common small-area GOs. Additionally, the films exhibited remarkable EMI SE of ∼20 dB even with a thickness of 15 μm, which is superior to that of small-area graphene [29].

However, for pure graphene-based materials, i.e., graphene or GOs, as the thickness increases, the conduction increases rapidly, resulting in large surface reflection, which is not beneficial for the absorption of electromagnetic energy. Thus, when graphene-based materials are used as a microwave absorber, to reduce the surface reflection, the conduction should be limited in order to achieve good impedance matching with free space. Thus, dielectric or magnetic materials with relatively low conductivity are usually added to graphene for reducing the surface reflection and allowing the multimode dissipation of electromagnetic energy. Compared with pure-graphene materials, graphene-based composites have lower cost, better processability, and a superior macroscale mechanical property and are thus used more frequently in electromagnetic-wave shielding and absorbing fields.

Graphene- and GO-filled polymer composites are the most widely studied composite materials for microwave attenuation. Liang *et al.* described the utilization of solution-processable functionalized graphene epoxy composites in shielding EMI. They found that the percolation threshold of functionalized graphene epoxy composites was approximately 0.52 vol.% owing to the good dispersion of modified graphene in the epoxy matrix, and the EMI SE of the composites could reach 21 dB when the graphene content was 15 wt.%, indicating the great potential of the graphene-based epoxy composites as lightweight and high-efficiency EMI shielding materials [31]. Bai *et al.* investigated the microwave absorption properties of graphene-based poly(ethylene oxide) (PEO) composites. They considered that uniformly dispersed chemically reduced graphene sheets in the polymer matrix can form abundant electrical pathways to dissipate electromagnetic energy into heat energy, while dielectric relaxation and interface scattering also frequently occurred owing to the numerous graphene/PEO interfaces. The multiple roles of graphene in the PEO matrix yield a strong microwave absorption ability [32]. Batrakov *et al.* investigated the microwave attenuation performance of graphene/PMMA multilayer films, paying great attention to the study of the absorption of electromagnetic radiation. They determined the ideal number of graphene/PMMA layers for optimizing the absorption. Typically, when the number of graphene/PMMA double layers is six, the portion of microwave absorptionis the maximum, approaching ∼55%. At less than six layers, with an increasing number of graphene layers, the absorption percentage increased rapidly, and once the number of layers surpassed six, the absorption portion gradually declined with a continuously increasing thickness. This indicates that graphene has excellent microwave absorption performance with a suitable structural design. In this case, an effective graphene layer with a total thickness of only approximately 2 nm generated ∼50% wave absorption while maintaining high light transmission, indicating the great potential of graphene films as transparent microwave shielding and absorbing materials [33]. The electromagnetic shielding performance of a graphene/polyethylene terephthalate (PET) multilayer structure was reported by Lu *et al.* This structure was prepared via the membrane transfer method. Monolayer graphene was first deposited on copper foil using CVD. Then, the copper foil was etched by $FeCl_3$, and the graphene layer was transferred onto a PET film. Subsequently, the graphene/PET films were stacked layer-by-layer to obtain a multilayer structure. A diagram of the multilayer structure and its electromagnetic shielding performance is presented in Fig. 2. With the increase of the number of graphene layers, the EMI SE was continuously enhanced, and with the increase of the thickness of the PET layer, the portion of microwave absorption in the total EMI SE in the K-band increased. When the total thickness of the graphene layers reached 4 nm, the graphene/PET multilayer film had an average SE of 19.14 dB in the frequency range of 18–26.5 GHz, with a maximum microwave absorption ratio of ∼95.82% at 25.7 GHz, while maintaining light transmission of 80.5%. In this graphene/PET multilayer structure, the microwave absorption played a dominant role in the total EMI SE, and the absorption ratio exceeded 96% [30]. In this study, the microwave absorption portion in the total EMI SE increased monotonically with the number of layers once the separation between the

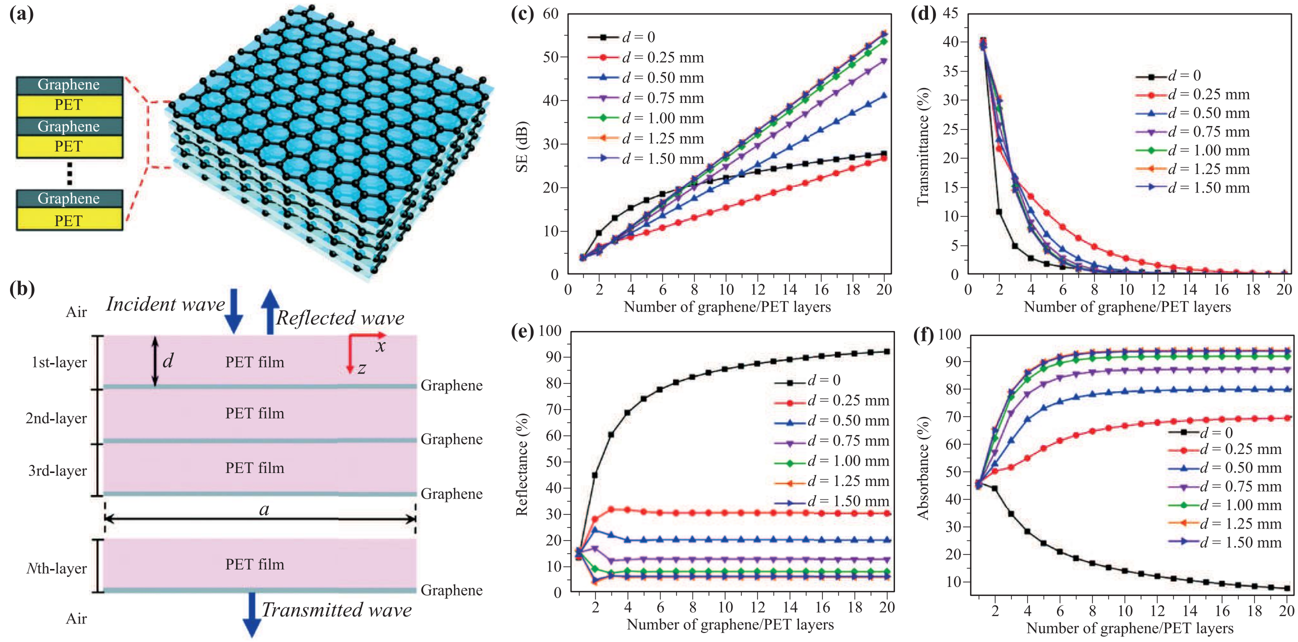

Fig. 2 **(a)** Diagram of the multi-layer graphene/PET structure; **(b)** description of the wave dispersion in the multi-layer graphene/PET structure; the calculated microwave **(c)** SE, **(d)** transmittance, **(e)** reflectance, and **(f)** absorbance for the mono- to the twenty-layer graphene/PET structures with various PET thicknesses: d = 0, 0.25, 0.50, 0.75, 1.00, 1.25, and 1.50 mm; the frequency of the incident microwaves is 25 GHz [30]. Reproduced from Ref. [30]. Copyright © 2016, with permission from the Royal Society of Chemistry.

graphene layers exceeded 0.25 mm. This differs from Batrakov's study, where the absorption percentage first increased and then decreased, possibly owing to different separation distances between the graphene layers. In the graphene/PET multilayer film of Batrakov's study, the PET thickness was far larger than the thickness of the PMMA layer. However, the discrepancy does not affect the general conclusion that the insertion of lowly conductive substances between the graphene layers increases the microwave absorption percentage in the total EMI SE. The microwave absorbing performance of a thermally reduced GO (RGO)/nitrile butadiene rubber (NBR) polymer composite was also investigated, revealing that even at a very low concentration of RGO, the composites exhibited high values of the dielectric loss tangent. The calculated RL for the composite with 10 wt.% RGO filling reached −57 dB at 9.6 GHz, and the bandwidth with RL less than −10 dB ranged from 7.5 to 12 GHz at a thickness of 3 mm, indicating that RGO-NBR composites have a very strong microwave absorbing ability [34]. Graphene nanosheets with grafted aminoethyl methacrylate were prepared via free-radical polymerization, and the modified graphene nanosheets showed good dispersion and high compatibility with a waterborne polyurethane (PU) matrix grafted by sulfonated functional groups as a result of electrostatic attraction. The results indicate that the modified graphene-filled composites had better conductivity, which is attributed to the superior graphene dispersion. When the graphene loading amount was 5 vol.%, the electrical conductivity of the composites reached ∼43.64 S/m, and the EMI SE in the frequency range of 8.2–12.4 GHz reached 38 dB [35].

4.2 Graphene-based multifunctional composites for microwave attenuation

Increasingly, studies indicate that graphene is a fascinating material for the attenuation of electromagnetic waves. Therefore, a current pivotal research topic is the thorough exploration of the potential of graphene-based materials for inhibiting electromagnetic waves. It is well-known that the electromagnetic shielding and microwave absorption performance of a material usually depends on two main factors—the composition and structure—which directly determine the dissipation mode and propagation path of electromagnetic waves, thus influencing the EMI SE and microwave absorption properties of the material. Accordingly, in the following chapters, we focus on the composition and structure of graphene-based materials for optimizing the electromagnetic performance.

4.2.1 Component-oriented graphene-based composites

Graphene is a good conductor and has a large dielectric constant, large specific surface area, good mechanical strength, and low mass density; thus, it offers exceptional advantages for shielding and absorbing electromagnetic waves. However, it is inadequate as a microwave absorber because of its high conductivity, which gives rise to great interfacial reflection due to the impedance mismatch with free space. This reflection is undesirable in many situations, such as anechoic chambers, stealth coating, and signal receivers, because it results in interference, leakage of information, signal loss, etc. In addition to the reflection, the effective absorption bandwidth is an important index. For microwave absorbing materials, a large effective absorption bandwidth is commonly preferable. Consequently, to optimize the microwave absorbing performance of graphene-based materials, e.g., decreasing the RL and broadening the absorption bandwidth, a variety of dielectric or magnetic materials are usually introduced into the graphene-based composite system. Typically, these materials include conductive polymers, dielectric organic matter, dielectric inorganic particles, and magnetic materials. They are either directly mixed with graphene to produce multifunctional composites or anchored on graphene nanosheets to generate a stable coupling system for multimode microwave attenuation.

4.2.1.1 Graphene-based dielectric composites

As mentioned previously, the dielectric constant of materials can be expressed as $\varepsilon_r = \varepsilon' - \mathrm{j}\varepsilon''$. The real part ε' represents the polarization capability of materials under an alternating electromagnetic field, which is only related to the energy storage, and is a function of the frequency, generally decreasing with the increase of the frequency. The imaginary part ε'' represents the dielectric loss, which is derived from the combined effect of conduction loss and polarization relaxation [36]. For dielectric materials, the dissipation of an electromagnetic wave is principally determined by ε''. According to the Debye theory, ε'' can be described as $\varepsilon'' = \varepsilon''_p + \varepsilon''_c = \frac{(\varepsilon_s-\varepsilon_\infty)\omega\tau}{1+\omega^2\tau^2} + \frac{\sigma(T)}{\varepsilon_0\omega}$, where ε''_p and ε''_c are associated with the polarization relaxation and conduction loss, respectively; ε_s and ε_∞ represent the static permittivity and the dielectric constant at a limiting frequency, respectively; ω is the angular frequency; τ is the temperature-dependent relaxation time; and $\sigma(T)$ is the temperature-dependent electrical conductivity. Obviously, according to this relationship, ε'' is related to the conductivity, relaxation time, $(\varepsilon_s - \varepsilon_\infty)$, angular frequency, and temperature. Thus, the conductivity, relaxation time, and $(\varepsilon_s - \varepsilon_\infty)$ are directly related to the material, and it can be concluded that dielectric materials with a higher conductivity, larger static dielectric constant, and moderate relaxation time are favorable for the attenuation of electromagnetic waves.

In addition, we consider the Havriliak–Negami (HN) equation [37]:

$$\varepsilon_r = \varepsilon_\infty + \frac{\Delta\varepsilon}{[1+(\mathrm{i}\omega\tau_{HN})^{\alpha_{HN}}]^{\gamma_{HN}}} - \mathrm{i}\frac{\sigma_0}{\omega^s\varepsilon_0}, \tag{45}$$

where $\Delta\varepsilon = \varepsilon_s - \varepsilon_\infty$ is the dielectric relaxation strength, τ_{HN} is the relaxation time, α_{HN} and γ_{HN} $(0 < \alpha_{HN}, \gamma_{HN} \le 1)$ are the shape parameters of the relaxation spectra, and $-\mathrm{i}\frac{\sigma_0}{\omega^s\varepsilon_0}$ is related to the electrical conductivity. When $\alpha_{HN} = \gamma_{HN} = s = 1$, the HN equation well matches the Debye theory, with $\varepsilon' = \varepsilon_\infty + \frac{\varepsilon_s-\varepsilon_\infty}{1+\omega^2\tau^2}$ and $\varepsilon'' = \frac{(\varepsilon_s-\varepsilon_\infty)\omega\tau}{1+\omega^2\tau^2} + \frac{\sigma(T)}{\varepsilon_0\omega}$.

The polarization part of the HN equation corresponds to the Debye polarization relaxation process, which can be expressed by the Debye equation, as follows:

$$\begin{aligned}\varepsilon_r = \varepsilon' - j\varepsilon'' &= \varepsilon_\infty + \frac{\varepsilon_s - \varepsilon_\infty}{1+\mathrm{j}\omega\tau} \\ &= \varepsilon_\infty + \frac{\varepsilon_s - \varepsilon_\infty}{1+\omega^2\tau^2} - \mathrm{j}\frac{(\varepsilon_s - \varepsilon_\infty)\omega\tau}{1+\omega^2\tau^2}.\end{aligned} \tag{46}$$

Thus,

$$\varepsilon' = \varepsilon_\infty + \frac{\varepsilon_s - \varepsilon_\infty}{1+\omega^2\tau^2}, \tag{47}$$

$$\varepsilon'' = \frac{(\varepsilon_s - \varepsilon_\infty)\omega\tau}{1+\omega^2\tau^2}. \tag{48}$$

The relationship between ε' and ε'' can also be written as follows:

$$\left(\varepsilon' - \frac{\varepsilon_s + \varepsilon_\infty}{2}\right)^2 + (\varepsilon'')^2 = \left(\frac{\varepsilon_s - \varepsilon_\infty}{2}\right)^2. \tag{49}$$

Clearly, the plot of ε' versus ε'' is a single semicircle—typically called the Cole–Cole semicircle—and each semicircle corresponds to one Debye relaxation process. For each semicircle, there exists a maximum value of the loss tangent $\frac{\varepsilon''}{\varepsilon'}$, corresponding to the maximum dielectric polarization loss. Additional Debye relaxation processes result in a larger dielectric polarization loss. Normally, Debye polarization relaxation occurs at the interface between different phases owing to the difference in their dielectric properties. Obviously, increasing the number of phase interfaces induces more interfacial polarization, resulting in a larger dielectric polarization loss. This is the theoretical basis for designing a multicomponent dielectric microwave absorber.

Currently, the widely used dielectric materials for microwave attenuation contain dielectric ceramics, dielectric polymers, conductive polymers, carbon, semiconductors, and even metals. Wu *et al.* prepared a three-dimensional (3D) nanocomposite of GO and zinc oxide (ZnO) nanoparticles via a hydrothermal process. The influence of ultraviolet (UV) irradiation on the dielectric properties of the composite was studied. Before UV irradiation, the Cole–Cole semicircle could hardly be found in the plot of ε' versus ε'', whereas after UV irradiation, semicircles could be clearly observed, and the attenuation constant was enhanced greatly in the whole frequency band; thus, the RL of the composite was improved with a minimum value of approximately −25 dB. The effective absorption bandwidth reached 6.4 GHz when the filler loading was 10 wt.% and the absorber thickness was 2.5 mm. It was considered that the UV irradiation removed the oxygen-containing functional groups of the RGOs and enhanced the interfacial polarization relaxation process, thus improving the microwave absorbing properties of the composite [38]. Additionally, TiO_2-loaded RGO (TRGO) nanocomposites were prepared via a facile one-step hydrothermal treatment. The contact area between TiO_2 and RGO could be well controlled by changing the amount of TiO_2 precursors. Increasing the TiO_2 content strengthened the interfacial polarization owing to the increase of polarization points, as indicated by the plot of ε' versus ε'', where more Cole–Cole semicircles could be observed with the increase of the TiO_2 content in the composites. However, stronger interfacial polarization did not always result in better microwave absorbing performance, probably because of the mismatched impedance or poor dielectric loss ability. A good balance between the dissipation ability and impedance matching was important. The study also indicated that interfacial polarization is only one factor giving rise to microwave attenuation; conduction loss might play a more important role in attenuating microwaves. With an optimized composition, the minimum RL of the TRGO nanocomposites at 2.1 mm was −27.2 dB, and an effective frequency bandwidth of 5.2 GHz was achieved [39]. ZnO/nanoporous carbon (NPC)/RGO nanocomposites derived from a hybrid of zinc metalorganic frameworks (MOFs)/RGO were prepared via a simple hydrothermal method. The permittivity of the ZnO/NPC/RGO nanocomposites was regulated by adjusting the addition amount of GOs, and it was found that a good balance between the energy dissipation and the impedance matching could be achieved via the addition of 4 mL of GO. After the composition was optimized, the composites with 40 wt.% ZnO/NPC/RGO in the wax matrix exhibited a minimum RL of −50.5 dB at 14 GHz for a film thickness of 2.4 mm. For a film thickness of 2.6 mm, the effective microwave absorption bandwidth reached 7.4 GHz, indicating that the ZnO/NPC/RGO composites derived from zinc MOFs can behave as a perfect absorber with a broad frequency bandwidth and strong absorption [40]. Graphene/polyaniline (PANI) hybrids were prepared via *in situ* intercalation polymerization in a one-step process by Chen *et al.*, and their electromagnetic properties were studied. The results showed that in the formation of the intercalated structure, vigorous movement of the aniline cations towards the electron-enriched zone of expanded graphite and the exothermic effect in the *in situ* polymerization of aniline played important roles. The composites exhibited extraordinary electromagnetic absorption performance, which was attributed to the combined effect of expanded graphite and PANI. When the film thickness was 3.5 mm, the RL reached −36.9 dB at 10.3 GHz, and the absorption bandwidth reached 5.3 GHz, which are far better than those for pure graphite and pure PANI [41]. Liu *et al.* fabricated novel ternary composites consisting of RGO, a conducting polymer, and Co_3O_4 nanoparticles and investigated their microwave absorption properties. The as-employed conducting polymers included PANI, polypyrrole, and poly(3, 4-ethylenedioxythiophene), and the as-synthesized Co_3O_4 nanoparticles had a diameter of 5–10 nm. They considered that the excellent microwave absorbing properties of the ternary composites stemmed from the dipole polarization, electronic spin, and charge polarization of Co_3O_4 nanoparticles, as well as the synergistic effects of several components. In this system, the maximum RLs differed for different conducting polymers, with PANI, polypyrrole, and poly (3, 4-ethylenedioxythiophene) yielding values of −44.5, −43.5, and −46.5 dB, respectively. Additionally, the absorption bandwidths (RL <−10 dB) were 4.3, 6.4, and 2.1 GHz for film thicknesses of 3.3, 3.2, and 3.1 mm, respectively, indicating that the composite system is highly efficient in attenuating electromagnetic waves [42]. Song *et al.* reported the application of all-carbon composites composed of carbon nanofiber–graphene–carbon nanofiber heterojunctions as flexible lightweight EMI materials. Owing to the replacement of the insulting polymer frames and interfaces with CNF-GN-CNF heterojunctions, the electrical properties of the all-carbon networks were significantly improved, resulting in an enhanced EMI SE. The study showed that the as-fabricated thin all-carbon networks with a low mass density ($\rho < 0.1$ g/cm^3) and small thickness less than 0.3 mm have a comparable EMI shielding performance to carbon-based polymer composites with a significantly larger thickness (> 1 mm) [43]. Gupta *et al.* described the EMI shielding properties of multi-walled CNT–graphene–PANI multiphase nanocomposites, finding that graphene multilayers derived from ball milling *in situ* functioned as a bridge between the CNTs and PANI. When the content of multi-walled CNTs was 10%, the maximum value of the EMI SE was 98 dB, and the absorption was dominant owing to the increase of the charge polarization and the decrease of the carrier mobility [44]. Furthermore, they synthesized dielectric MnO_2-decorated graphene nanoribbons for electromagnetic-wave shielding. The presence of MnO_2 on the graphene enhanced the interfacial polarization, multiple scattering, natural resonance, and effective anisotropy energy, resulting in high-efficiency EMI SEand microwave absorption performance. For a 3-mm-thick sample, the SE value reached 57 dB, mostly owing to the absorption loss caused by the superior permittivity of the composites [45]. Zhang *et al.* prepared RGO/CuS/polyvinylidene fluoride (PVDF) composites via wet chemistry and a hot-press process, where CuS complex microspheres with a relatively uniform size were embedded in the RGO layers to form unique core–shell nanostructures and then hot-pressed into the PVDF matrix. Composites with a filler loading of 15 wt.% showed a dielectric constant of 36 at 2 GHz, which is 10 times higher than that of pure PVDF, and composites with a filler loading of 5 wt.% exhibited a minimum RL of −32.7 dB at 10.7 GHz when the thickness was 2.5 mm. The improved RL is explained by the Debye dipolar relaxation of the composites [46]. Zhang *et al.* reported the fabrication of multifunctional PVDF/RGO composites via a simple thermal reduction method and investigated their dielectric and electromagnetic-wave absorption properties. Owing to the specific interaction between the oxygen-containing functional groups in the GO and the fluorine groups in the PVDF, GO was well-dispersed in the PVDF and thermally reduced into RGO, enhancing the dielectric and microwave absorption properties. The results indicate that for the composites with 3 wt.% GO loading, the minimum RL reached −25.6 dB at 10.8 GHz, the frequency bandwidth (RL <−10 dB) was 4.32 GHz, and the dielectric constant reached 3,801 at a frequency of 1 kHz [47]. Han *et al.* reported the synthesis of graphene-wrapped ZnO hollow spheres via a two-step process including a hydrothermal reaction and surface modification. The hybrids in a wax matrix exhibited enhanced dielectric properties and microwave absorbing performance in the X-band region. The complex permittivity was significantly improved because of the enhanced polarization derived from the graphene/ZnO interfaces, residual functional groups of RGO, and defects of ZnO nanoparticles. The minimum RL was −45.05 dB at 9.7 GHz, and the effective absorption bandwidth reached 2.5 GHz for composites with 50 wt.% ZnO spheres/GO hybrids (mass ratio = 88:12) loading in the wax matrix at a thickness of 2.2 mm [48].

4.2.1.2 Graphene-based magnetic composites

As described previously, according to electromagnetic theory, the reflection coefficient of an electromagnetic wave at a two-phase interface can be expressed as

$$\Gamma = \frac{Z - Z_0}{Z + Z_0} = \frac{\sqrt{\frac{\mu_r}{\varepsilon_r}} - 1}{\sqrt{\frac{\mu_r}{\varepsilon_r}} + 1}. \tag{50}$$

In general, $\mu_r < \varepsilon_r$ for nonmagnetic materials; thus, to reduce the interfacial reflection, we must increase μ_r. Clearly, the addition of magnetic materials can resolve this problem. In addition, the introduction of magnetic materials can increase the magnetic loss, further attenuating the electromagnetic energy. The mechanism whereby magnetic materials attenuate electromagnetic waves is described in the previous chapter and generally involves magnetic hysteresis loss, eddy current loss, magnetic aftereffect loss, domain-wall resonance loss, natural resonance loss, etc. For nanoscale magnetic particle-based composites, owing to the lack of domain walls at the nanoscale size and the low-degree magnetization under a weak electromagnetic field, the domain-wall resonance loss and magnetic hysteresis loss can be neglected; thus, the eddy current loss and natural resonance loss play dominant roles in the magnetic loss.

For spherical ferromagnetic nanoparticles, including ferrites and metals, because the skin depth is far larger than the size of the nanoparticles even at 10 GHz, the power of the eddy current loss and the magnetic loss tangent can be written as follows [50, 51]:

$$P_e = \frac{\pi^2 R^2 f^2 B_m^2}{5\rho}, \tag{51}$$

$$\tan\delta_m = \frac{\mu''}{\mu'} = \frac{4\pi\mu' R^2 f}{5\rho}, \tag{52}$$

where P_e is the power of the eddy current loss, B_m is the amplitude of the magnetic flux density, δ_m is the magnetic loss angle, ρ is the resistivity of spherical nanoparticles, and R is the radius of spherical nanoparticles. We observe that the eddy current loss is related to the resistivity, the real part of the magnetic permeability, and the nanoparticle size. Generally, metal magnetic particles have a larger eddy current loss than ferrites owing to their low resistivity. According to the equation $f_r = \frac{\gamma}{2\pi} H_a$, a stronger magnetocrystalline anisotropic field H_a results in natural resonance at a higher frequency. In ferrites, H_a can be well tuned by adjusting the composition, and through the addition of various ferrites with different compositions, multiple resonance peaks can appear in μ''–f curves, resulting in the broadening of the absorption bandwidth and the enhancement of the microwave absorption.

The typical magnetic materials employed for microwave attenuation in graphene-based composites include ferrites and magnetic metals. Zhang *et al.* synthesized $MnFe_2O_4$ nanoparticles using a simple hydrothermal process and then mixed them with RGO to prepare RGO/$MnFe_2O_4$ nanocomposites via ultrasonication. The microwave absorption properties of $MnFe_2O_4$/wax, RGO/$MnFe_2O_4$/wax, and the RGO/$MnFe_2O_4$/PVDF composites were compared, revealing that the RGO/$MnFe_2O_4$/PVDF composites had the best microwave absorption properties, with a minimum RL of −29.0 dB at 9.2 GHz and a frequency bandwidth of 4.88

GHz (RL <−10 dB) at a filler content of 5 wt.%. The microwave absorption was attributed to the dielectric loss, the magnetic loss, and the synergetic effect of multiple components, indicating that the addition of magnetic particles can greatly improve the microwave absorbing performance of composite materials [52]. Zhu *et al.* prepared RGO-spherical carbonyl iron (SCI) cross-linked composites via a simple wet chemical method, where RGO behaved as an electron-transfer medium between SCI particles. The transport of electrons resulted in strong electron polarization and space-charge polarization, increasing the permittivity and dielectric loss. In the whole frequency range of 7.79–11.98 GHz, the RL of the RGO-SCI composites was less than −10 dB, and a minimum RL of −52.46 dB was achieved [53]. Qing *et al.* reported that graphene nanosheets and flake-like carbonyl iron particle-filled epoxy-silicone composites had excellent microwave absorption performance at a small thickness and wide bandwidth owing to the large magnetic loss and dielectric loss; thus, they can serve as a good microwave absorber. An RL less than −10 dB (> 90% absorption) was obtained in the frequency range of 10.5–18 GHz at a thickness of 1.0 mm [54]. Chen *et al.* described the growth of hexagonal close-packed nickel nanocrystals with an average diameter of 3 nm and face-centered cubic nickel nanoflowers composed of 15 nm of nanoparticles on graphene nanosheets. The composites showed better microwave absorbing performance than pure nickel nanoparticles, indicating that the addition of graphene can enhance the microwave absorption of magnetic materials [55]. Li *et al.* reported the one-pot synthesis of $CoFe_2O_4$/GO hybrids and *in situ* conversion into FeCo/graphene hybrids in an H_2/NH_3 atmosphere. The magnetic nanoparticles were uniformly distributed on the graphene nanosheets without obvious aggregation. After chemical reduction, the FeCo/graphene hybrids showed significantly improved permeability and permittivity owing to the high conductivity and magnetocrystalline anisotropy of the metallic FeCo, resulting in improved microwave absorption performance. The FeCo/graphene hybrids showed a minimum RL of −40.2 dB at 8.9 GHz when the film thickness was 2.5 mm and an absorption bandwidth of 14.6 GHz (RL <−10 dB) when the absorber thickness was 1.5–5 mm. The results suggest that the FeCo/graphene hybrid is an ideal lightweight and high-efficiency microwave absorber [56]. Wang *et al.* described a simple procedure for fabricating a flexible freestanding magnetic film consisting of GO and CNT–Fe_3O_4 via a one-pot co-precipitation *in situ* growth route. Fe_3O_4 nanoparticles with relatively uniform size were used to decorate the surface of GO nanosheets and intercalated between the GO nanosheets with interspersed CNTs. The incorporation of the Fe_3O_4 nanoparticles greatly enhanced the microwave absorption peak value and absorption bandwidth. The minimum RL reached −37.3 dB when the film thickness was 5 mm. Additionally, they considered that in the presence of microwaves, the carbon-based composites generated microplasma to interact with the electromagnetic waves for the further dissipation of electromagnetic energy [57]. Mesoporous Fe_3O_4@ZnO sphere-decorated graphene composites for microwave absorption were reported by Sun *et al.* The as-prepared Fe_3O_4@ZnO spheres with porous and core–shell structures were anchored on both sides of the graphene nanosheets without significant aggregation. The microwave absorption performance of epoxy composites with 30 wt.% graphene-Fe_3O_4@ZnO loading was investigated; a minimum RL of approximately −40 dB was achieved, and the absorption bandwidth (RL <−10 dB) reached 11.4 GHz. The synergy of Fe_3O_4 and ZnO—especially the multi-interfacial effect—was considered as the main cause of the enhanced EM absorption properties [58]. Lv *et al.* demonstrated the preparation of a rod-like MnO_2@Fe-loaded graphene composite. The rod-like MnO_2 with a diameter of 30 nm was synthesized via a simple liquid-phase process. Next, $Fe(CO)_5$ was decomposed, and the generated iron was deposited on the surface of MnO_2. Then, the MnO_2@Fe was anchored on graphene using a liquid deposition technique. The resulting ternary nanocomposites exhibited excellent microwave absorption properties. An optimal RL up to −17.5 dB was obtained at a film thickness of 1.5 mm, and the effective frequency bandwidth was significantly broader than those of pure MnO_2 and MnO_2@Fe, owing to the better synergetic effect of the impedance matching and attenuation capability [59]. Figure 3 shows the synthesis of a quaternary nanocomposite consisting of graphene, Fe_3O_4@Fe core–shell, and ZnO nanoparticles with a considerably wide absorption bandwidth. In a frequency range of > 7.3 GHz, the RL is less than −20 dB, indicating that > 99% of the electromagnetic energy is attenuated even if the content of quaternary composites in the matrix is only 20 wt.%. Such excellent microwave absorption performance suggests that the quaternary nanocomposites are fantastic microwave absorbing materials [49]. A graphene@Fe_3O_4@SiO_2@NiO nanosheet quaternary composite was also synthesized. A hierarchical structure with NiO nanosheets grown perpendicularly on the surface of graphene@Fe_3O_4@SiO_2 was obtained via a sol–gel process and a hydrothermal reaction. Experiments indicated that the graphene@Fe_3O_4@SiO_2@NiO nanosheets had significantly greater microwave absorption than graphene@Fe_3O_4, which is attributed to their higher porosity and larger surface area arising from the hierarchical structure [60]. Singh *et al.* prepared phenolic resin-based composite sheets that were filled with RGO, γ-Fe_2O_3, and carbon fiber and exhibited a conductivity

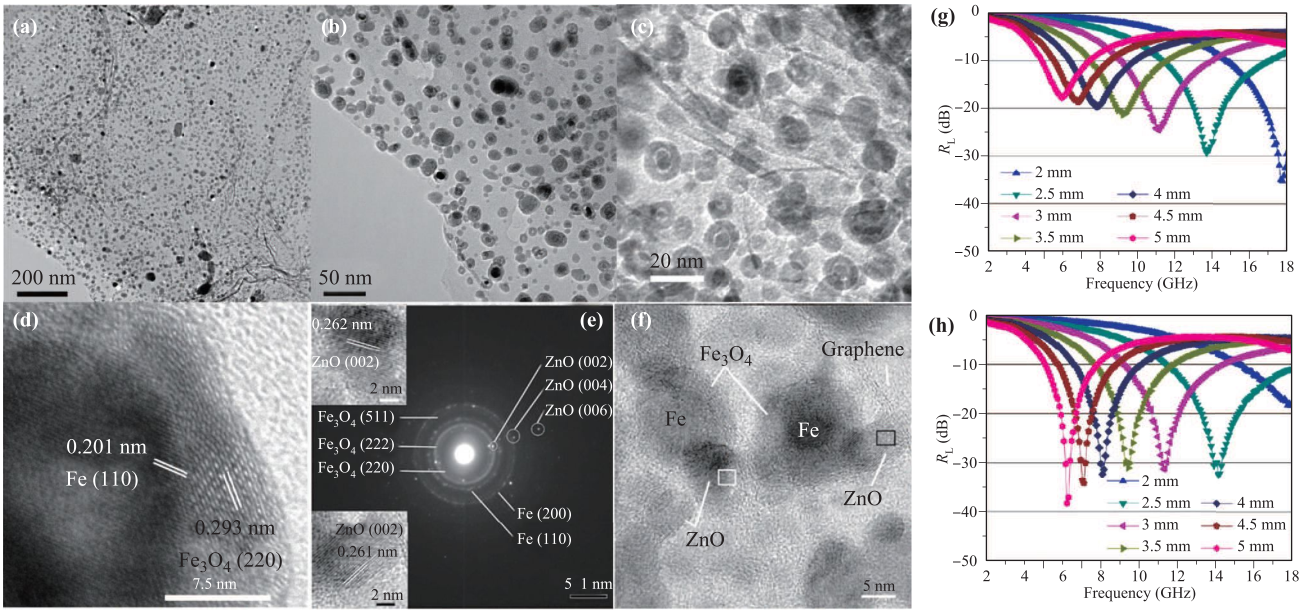

Fig. 3 **(a)** Low-resolution TEM image, **(b, c)** magnified TEM images, and **(d)** HRTEM image of the G/Fe_3O_4@Fe ternary nanocomposites; **(e)** SAED pattern, **(f)** HRTEM image for the triple junctions of the G/Fe_3O_4@Fe/ZnO quaternary nanocomposites; reflection losses of the **(g)** G/Fe_3O_4@Fe ternary nanocomposites and **(h)** G/Fe_3O_4@Fe/ZnO quaternary nanocomposites with thickness 2–5 mm [49]. Reproduced from Ref. [49]. Copyright © 2012, with permission from American Chemical Society.

of 0.48–171.21 S/cm. The insertion of γ-Fe_2O_3 between RGO layers enhanced the interfacial polarization and the effective anisotropy energy, increasing the interface scattering and polarization relaxation, which resulted in high SE (~45.26 dB) and microwave absorbing performance ($SE_A \approx 35.42$ dB). Microwave absorption is dominant in the EMI SE rather than the reflection attributed to the strong magnetic loss of γ-Fe_2O_3 and dielectric loss of RGO. This study indicates that the structure with a conducting shell encapsulating the magnetic core is conducive to microwave absorption [61]. Bowl-like Fe_3O_4 hollow spheres anchored RGO composites were prepared via a facile solvothermal method. In contrast to pristine r-GO, pure Fe_3O_4 nanoparticles, and solid nano-Fe_3O_4/r-GO composites, hollow Fe_3O_4 sphere-anchored r-GO composites have a wider and stronger absorption behavior in the frequency range of 2–18 GHz. When 30 wt.% of hollow Fe_3O_4 spheres/r-GO composites was loaded into the wax matrix, the 2-mm-thick sample had maximum absorption of 24 dB at 12.9 GHz, as well as an effective bandwidth of 4.9 GHz. The enhanced microwave absorption properties are mainly ascribed to the improved dielectric loss and magnetic loss arising from the synergy of the hollow Fe_3O_4 spheres and r-GO [62]. Singh *et al.* built a 3D nanostructure consisting of chemically modified graphene, Fe_3O_4, and PANI, and spectroscopic analysis indicated that the graphene/Fe_3O_4 hybrid structure facilitated the polarization of the composites owing to the solid-state charge transfer between the graphene and PANI. A relatively large imaginary part of the permittivity and permeability ($\varepsilon'' = 30, \mu'' = 0.2$) was obtained, leading to stronger microwave absorption (~26 dB), which is closely correlated to the concentration of graphene/Fe_3O_4 in the PANI matrix [63]. Chen *et al.* reported a similar composite consisting of metallic nanoparticles, graphene, and PANI for EMI shielding. Ni@graphene-filled PANI composites and Ag@graphene-filled PANI composites were prepared, and their electrical conductivity and EMI SE were investigated and compared. The Ag@graphene-filled composites exhibited better EMI shielding effects. PANI composites containing 5.0 wt.% Ag@graphene showed an electrical conductivity of 20.32 S/cm and EMI SE of 29.33 dB. The presence of metal nanoparticles on the graphene surface increased the electrical conductivity and EMI SE, which is mainly attributed to the increased permittivity of the composites [64]. Additionally, many other magnetic materials, such as iron [65, 66], nickel [67], the CoNi alloy [68], Fe_3O_4 [69–72], hematite [73], maghemite [74], $CoFe_2O_4$ [75–77], $NiFe_2O_4$ [78, 79], $Co_{0.5}Ni_{0.5}Fe_2O_4$ [80], Co_3O_4 [81], $BaFe_{12}O_{19}$ [82], Fe_3O_4-Fe [83], and ferrofluids [84] have been used to prepare graphene-based magnetic composites and showed excellent microwave attenuation performance.

4.2.2 Structure-oriented graphene-based composites

As is well-known, electromagnetic waves have remarkable time–space features and are accordingly affected by time and space. Supposing that the influence of the composition of materials on the dissipation of electromagnetic waves has an obvious time feature, e.g., relaxations, the structure of the materials should be designed with regard to the space attribute of electromagnetic waves, e.g., resonances. Obviously, the structure has the same importance as the composition in modulating electromagnetic waves. As mentioned previously, the composition has proven to play an important role in attenuating electromagnetic waves; naturally, the structure also has a significant influence on the propagation of electromagnetic waves. Thus, the structural design of the materials is a crucial aspect for building a high-efficiency microwave shield and absorber. Owing to their ultrathin thickness and specific 2D features, graphene-based materials have significant structural advantages and are easily fabricated into various well-defined assemblies for the improvement of the microwave attenuation performance. Currently, the frequently used structures in 2D material-based composites include multilayer structures, core–shell structures, hierarchical structures, 3D porous foam structures, and combinations of these.

4.2.2.1 Multilayer structure

A multilayer structure of 2D materials has several advantages for microwave attenuation. First, 2D materials have ultrathin thickness far smaller than the skin depth, and electromagnetic waves easily penetrate through the 2D nanosheets and into the interior of the multilayer structure, yielding multiple reflections. Second, the multilayer parallel capacitor-type structure can store electromagnetic energy, increasing the polarization and conduction loss during charging and discharging. Third, multilayer 2D materials can be prepared via facile methods on a large scale and have good mechanical properties allowing practical application. Song *et al.* reported that an aligned graphene-based wax composite prepared via the split–press–merge approach had better microwave shielding and absorption effectiveness than randomly dispersed graphene and graphite composites owing to their higher electrical conductivity [85]. They also investigated the microwave attenuating properties of graphene papers (Fig. 4). Single-layer graphene paper was prepared via vacuum filtration and then transferred and adhered onto a wax substrate using glue. Then, several graphene pa-

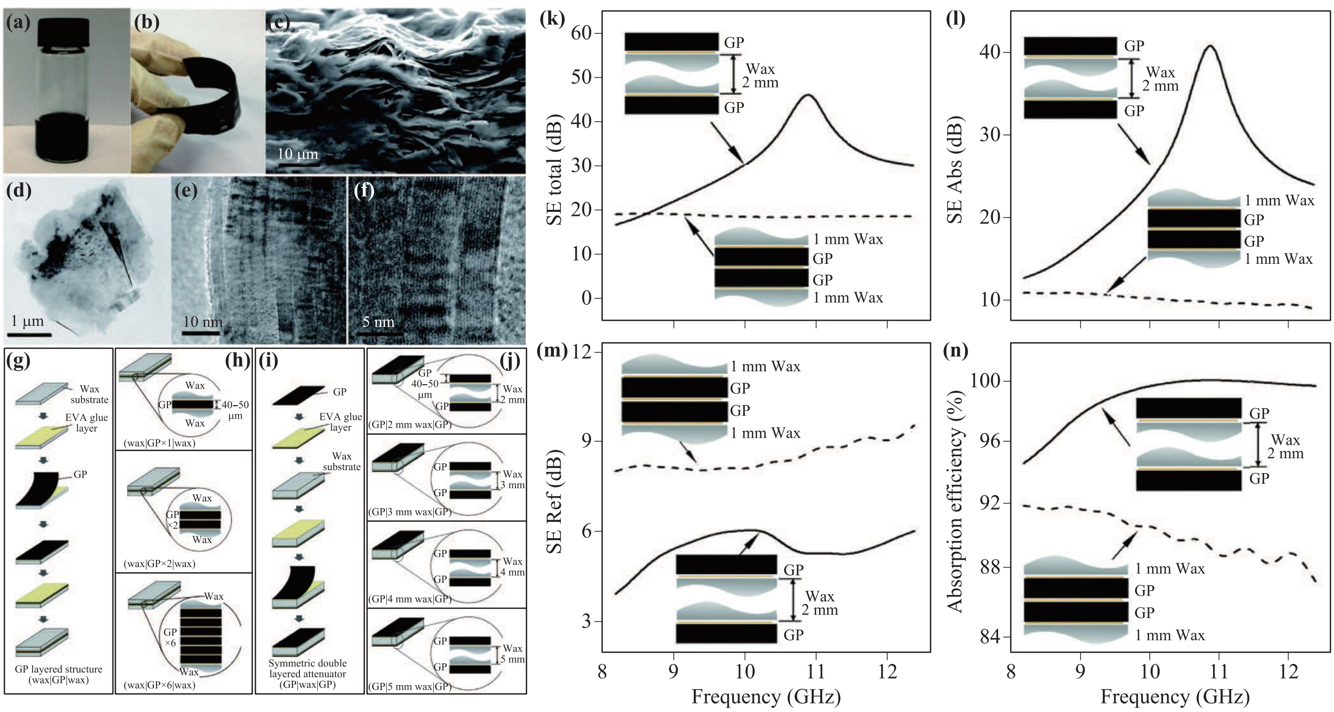

Fig. 4 **(a)** Aqueous suspension of graphene nanosheets; **(b)** flexible graphene paper (GP); **(c)** typical SEM image of GP; **(d)** TEM image of the multilayer graphene (MLG) sheet; **(e, f)** microtome images for cross-sectional views of the GP; **(g, h)** preparation scheme of GP layered structures and the structures of wax/multilayer GP/wax composites; **(i, j)** preparation scheme of symmetric double-layered attenuator and the structures of GP/wax/GP multilayer composites [76]. Reproduced from Ref. [76]. Copyright © 2014, with permission from the Royal Society of Chemistry.

pers were adhered together using glue to form a multilayer structure. The as-prepared graphene papers exhibited high EMI SE, with SE values of ∼19.0 and ∼46.3 dB at the thicknesses of ∼0.1 and ∼0.3 mm, respectively, and the shielding performance of double-layer graphene paper with a 2-mm middle wax layer inserted reached ∼47.7 dB at a total graphene thickness of ∼0.1 mm, which is far better than that of the wax/multilayer GPs/wax structured composites. The authors attributed the high shielding performance to the Fabry–Pérot resonance of the double-layer graphene papers [86]. Multilayer graphene/polymer composite films with good mechanical flexibility were also fabricated. Experimental results showed that the electrical properties of the multilayer films were significant factors influencing the EMI SE. Both experimental and calculated results indicated that the reflection had a dominant effect on the EMI SE. By increasing the thickness of the shielding layer, the absorption performance was improved. The optimized SE reached 27 dB for a 350-μm-thick composite film μ87]. Yousefi *et al.* reported the preparation of a highly self-aligned RGO/polymer nanocomposites via an aqueous casting method. The as-prepared graphene-based epoxy nanocomposites had a significantly low percolation threshold (∼0.12 vol.%) owing to the uniform dispersion and ultrahigh aspect ratios (> 30 000) of the graphene nanosheets. When the filler content was larger than a critical value, the graphene nanosheets aligned into a layered structure in the epoxy matrix, with obvious electrical and mechanical anisotropy. An extremely large dielectric constant (> 14 000) at a frequency of 1 kHz was obtained as a result of the charge accumulation between conductive layers when the graphene content was approximately 3 wt.%. An EMI SE test showed that the composites had remarkable EMI SE of 38 dB, where the wave absorption played a dominant role [88]. Singh *et al.* fabricated layered sandwiched composites composed of vertically aligned CNT, iron oxides, and RGOs, in which Fe_3O_4 nanoparticles were infiltrated into a vertically arrayed CNT forest and then sandwiched by RGO. The sandwiched composites exhibited SE exceeding 37 dB in the Ku-band (12.4–18 GHz) at a thickness of 2 mm [89]. Lv *et al.* described the fabrication of a sandwich-structured flexible film with two conductive carbon electrodes coated on a dielectric layer composed of a SnS/SnO_2 heterojunction and amorphous carbon. The sandwiched film showed excellent microwave absorbing performance in the low-frequency range of 1.5–2 GHz under an applied voltage of 16 V, which was hardly achieved with a conventional absorber. The study indicated that an external voltage can well modulate the dielectric parameters of the sandwiched film to satisfy the ideal range for optimal microwave absorption, providing a new method for achieving strong low-frequency absorption [90].

4.2.2.2 Structure consisting of core–shell particles

In addition to the multilayer structure, the core–shell structure has been widely applied for electromagnetic-wave attenuation. In this kind of structure, graphene or GOs was usually coated on the surface of dielectric or magnetic particles for obtaining multifunctional composite particles, and then these core–shell particles were adhered or compressed together for building heterogeneous bulk composites, where the graphene layer coating formed a continuous conductive network for conduction loss and the dielectric or magnetic core behaved as heterogeneous cavity giving rise to multiple scattering at the interface between the graphene shell and dielectric core for the high-efficiency dissipation of electromagnetic waves.

Feng *et al.* reported the synthesis of hierarchical $ZnFe_2O_4$@SiO_2@RGO core–shell microspheres via a “coating–coating” route (Fig. 5). Compared with binary composites of $ZnFe_2O_4$@SiO_2, the hierarchical $ZnFe_2O_4$@SiO_2@RGO ternary composites exhibited better electromagnetic wave absorption properties. Moreover, the absorption performance of as-prepared composites could be tuned by changing the RGO content and the thickness of the SiO_2 layer. The minimum RL of a 2.8-mm-thick reached −43.9 dB at 13.9 GHz, and its effective bandwidth (RL <−10 dB) reached 6 GHz. These results indicate that the hierarchical core–shell particles composites are excellent microwave absorbers [91]. Similarly, Fe_3O_4@SiO_2@RGO core–shell nanocomposites were prepared by Pan *et al.* and exhibited excellent microwave absorption properties even at a low filler content [92]. Furthermore, Li *et al.* synthesized FeCo@SiO_2@RGO composites via a liquid-phase reduction reaction and a subsequent hydrothermal reaction. Core–shell FeCo@SiO_2 composites with a diameter of approximately 150–200 nm were first formed via a solution-based reduction reaction in an argon atmosphere and then coated with RGO in a hydrothermal process. Compared with FeCo@SiO_2 and FeCo@RGO composites, the as-prepared FeCo@SiO_2@RGO composites exhibited better electromagnetic wave absorption properties. The minimum RL reached −52.9 dB at 9.12 GHz and a thickness of 3.0 mm, and the absorption bandwidth (RL <−10 dB) reached 5.36 GHz (8.8–14.16 GHz) at a film thickness of 2.5 mm, indicating outstanding microwave absorption performance [93]. Liu *et al.* fabricated yolk–shell ZnO-Ni-C hybrid structures wrapped with RGO by annealing an amorphous yolk–shell zinc–nickel microsphere precursor. The core@void@shell structures exhibited excellent electromagnetic wave absorption properties owing to the good impedance matching derived from the adjustable void space. The RGO-wrapped ZnO-Ni-C yolk–

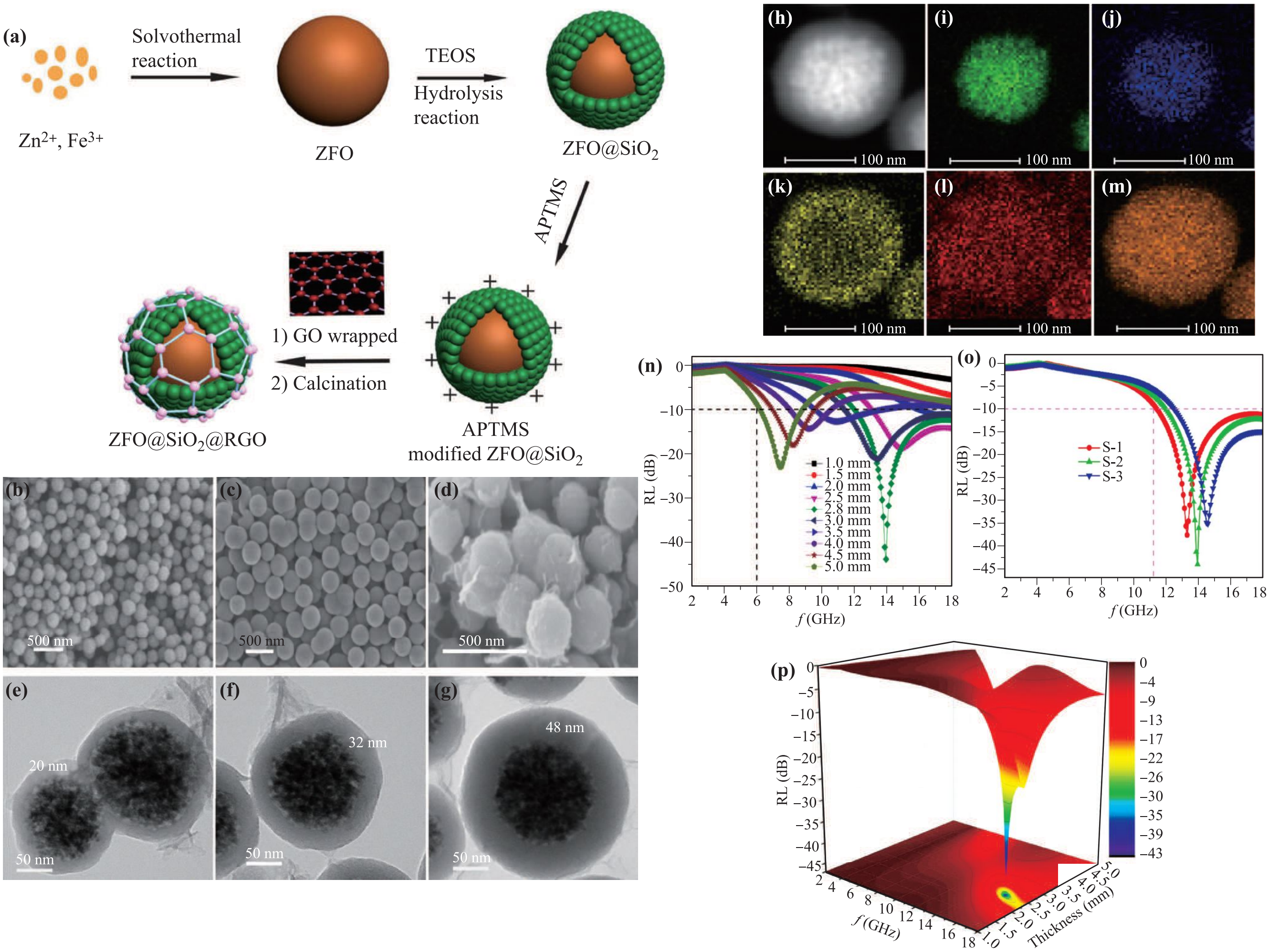

Fig. 5 **(a)** Schematic illustration of the preparation of $ZnFe_2O_4$(ZFO)@SiO_2@RGO; SEM images of **(b)** ZFO, **(c)** ZFO@SiO_2, and **(d)** ZFO@SiO_2@RGO composite; TEM images of ZFO@SiO_2@RGO composites with different thicknesses of silica layer: **(e)** S-1, **(f)** S-2, and **(g)** S-3; STEM of S-2 **(h)** and its corresponding mapping of Fe **(i)**, Zn **(j)**, Si **(k)**, C **(l)**, and O **(m)**; **(n)** reflection loss of S-2 with thickness of 1–5 mm; **(o)** reflection loss of the samples with a thickness of 2.8 mm in the range of 2-18 GHz; **(p)** three-dimensional presentations of the reflection loss of S-2 on EMW [91]. Reproduced from Ref. [91]. Copyright © 2017, with permission from American Chemical Society.

shell microspheres could also increase the content of defects and led to more effective interfacial polarization under microwave radiation. The minimum RL of the ZnO-Ni-C/RGO composites reached −59.3 dB at 15.2 GHz and a film thickness of 2.05 mm, and the effective attenuation bandwidth was 5.6 GHz (12.4–18 GHz) [94]. Yan *et al.* prepared RGO/polymer composites composed of cell-like units with polystyrene (PS) particles as cells and GOs as cell membranes via high-pressure solid-phase compression molding. This special architecture not only provided numerous interfaces for the reflection and dissipation of electromagnetic waves but also significantly decreased the usage amount of RGO by confining the RGO at the interfaces. Moreover, with fabrication under a high pressure of 350 MPa, the mechanical strength of the composite was significantly improved and was superior to that of a composite fabricated under the conventional pressure of 5 MPa. A remarkable EMI SE of 45.1 dB was achieved for composites with only 3.47 vol% RGO loading, which was the highest value among the reported RGO-based polymer composite [95]. Jian *et al.* reported the facile synthesis of nanoscale Fe_3O_4/graphene capsule composites using catalytic CVD and a hydrothermal process and then studied their electromagnetic properties via experiments and simulation based on the transmission-line theory. The results showed that the composites had a minimum RL of −32 dB at 8.76 GHz and that the absorption bandwidth (RL <−10 dB) ranged from 5.4 to 17 GHz. The good microwave absorption performance was derived from the reasonable impedance, numerous interfaces, and polarization of free carriers, which are effective for the preparation of high-performance microwave attenuating materials [96]. Song *et al.* demonstrated all-carbon CNTs-multilayer graphene edge plane (MLGEP) core–shell hybrid foams for ultrahigh-performance EMI shielding. The lightweight, flexible, and conductive core–shell hybrid foam was fabricated using CVD. MLGEPs were seamlessly grown on the CNTs, and the hybrid foam exhibited excellent EMI SE that exceeded 38.4 and 47.5 dB in the X-band at a thickness of 1.6 mm with a density of only 0.0058 and 0.0089 $g \cdot cm^{-3}$, respectively, which are significantly higher than the best values of the reported carbon-based composites. The grafted MLGEPs on CNTs can obviously enhance the penetration losses of microwaves during the propagation process, greatly improving the EMI shielding performance. In addition, the CNT-MLGEP hybrids can act as nano-reinforcements for fabricating high-strength polymer-based composites [97].

4.2.2.3 Hierarchical structure

The hierarchical structure is also effective for achieving high-efficiency electromagnetic-wave attenuation. This structure has numerous interfaces and voids with different sizes, which can greatly increase the multiple reflections and scattering, as well as improve the impedance matching, owing to perfectly matched impedance between the void space and free space. The voids with different sizes might also broaden the absorption bandwidth because of the dimensional resonance of electromagnetic waves.

Wang *et al.* described the fabrication of novel hierarchical graphene@Fe_3O_4 nanocluster@carbon@MnO_2 nanosheet array composites and investigated their microwave absorption performance (Fig. 6). In the synthesis of the composites, Fe_3O_4 nanoclusters were deposited on the surface of graphene via a simple *in situ* hydrothermal method, a carbon coating layer was introduced on the surface of graphene@Fe_3O_4 nanoclusters by the carbonization of glucose in a hydrothermal and heat-treatment process, and the hierarchical graphene@Fe_3O_4 nanocluster@carbon@MnO_2 structure was formed by the reaction between potassium permanganate ($KMnO_4$) and surface carbon. The study indicated that the composites had significantly enhanced microwave absorption properties compared with graphene@Fe_3O_4 nanoclusters, owing to their unique hierarchical structure and large surface area. The maximum RL of the hierarchical composites was −38.8 dB at 15 GHz, and the absorption bandwidth with the RL below −10 dB reached 5.4 GHz in the range of 12.3 to 17.7 GHz at a film thickness of 1.8 mm. Thus, it was considered that such hierarchical structures can act as microwave absorbers over a wide spectrum [98]. Bian *et al.* demonstrated the construction of 3D flexible hierarchical magnetic composites consisting of carbon fiber textiles, graphene, and nickel nanoparticles for strong electromagnetic shielding, and the results showed that the presence of 3D RGO interfaces and bifunctional nickel nanoparticles substantially influenced the magnetic and dielectric properties of the resulting hierarchical composite textiles. The composite textiles had strong SE greater than 61 dB, showing greater advantages than conventional polymer-based and foamy shielding composites. As a polymer-free lightweight structure, flexible CF-RGO-Ni composites comprising all electromagnetic active components offered multi-scale and multiple mechanisms for electromagnetic energy consumption. This novel type of shielding structure in combination with convenient preparation technology highlighted a strategy for achieving high EMI SE and lightweight EMI shielding composites [99]. Wang *et al.* synthesized hierarchical core–shell $NiFe_2O_4$@MnO_2 composite microsphere-decorated graphene nanosheets via a simple hydrothermal method for enhanced microwave absorption, where the $NiFe_2O_4$ nanoparticles were coated with hierarchically MnO_2 shells and distributed on the surface of graphene. The results indicated that the $NiFe_2O_4$@MnO_2@graphene composites had an optimal RL of −47.4 dB at 7.4 GHz when the film thickness was 3 mm, and their maximum absorption bandwidth (RL <−10 dB) was 4.3 GHz (5.1–9.4 GHz). The enhanced microwave absorption performance was attributed to the hierarchical structure of MnO_2, the void space between the MnO_2 and graphene, and the better impedance matching of ternary composites, proving that the hierarchical $NiFe_2O_4$@MnO_2@graphene composite was a promising microwave absorber [100]. Zhang *et al.* synthesized hierarchical structures of graphene@$CoFe_2O_4$@SiO_2@TiO_2 nanosheets by combining the versatile sol–gel process with a hydrothermal reaction and studied their microwave absorption properties. In the hierarchical structures, TiO_2 nanosheets were grown on top of a graphene@$CoFe_2O_4$@SiO_2 support with a random orientation. The microwave absorbing properties of the composites were investigated, revealing that the minimum RL reached −62.8 dB at 6.24 GHz for a film thickness of 4.9 mm and that an RL below −10 dB could be obtained over the whole frequency range with the sample thickness varying from 2.0 to 6.0 mm. The excellent microwave absorption properties of the graphene@$CoFe_2O_4$@SiO_2@TiO_2 nanosheets was attributed to the high interfacial polarization and the existence of void space between $CoFe_2O_4$ and TiO_2 nanosheets for multiple reflections and scattering, which consumed electromagnetic energy [101].

Perpendicular array structures with the microwave absorbing materials perpendicularly growing on graphene can also be classified as hierarchical structures. The classic case that employs such a structure for microwave at-

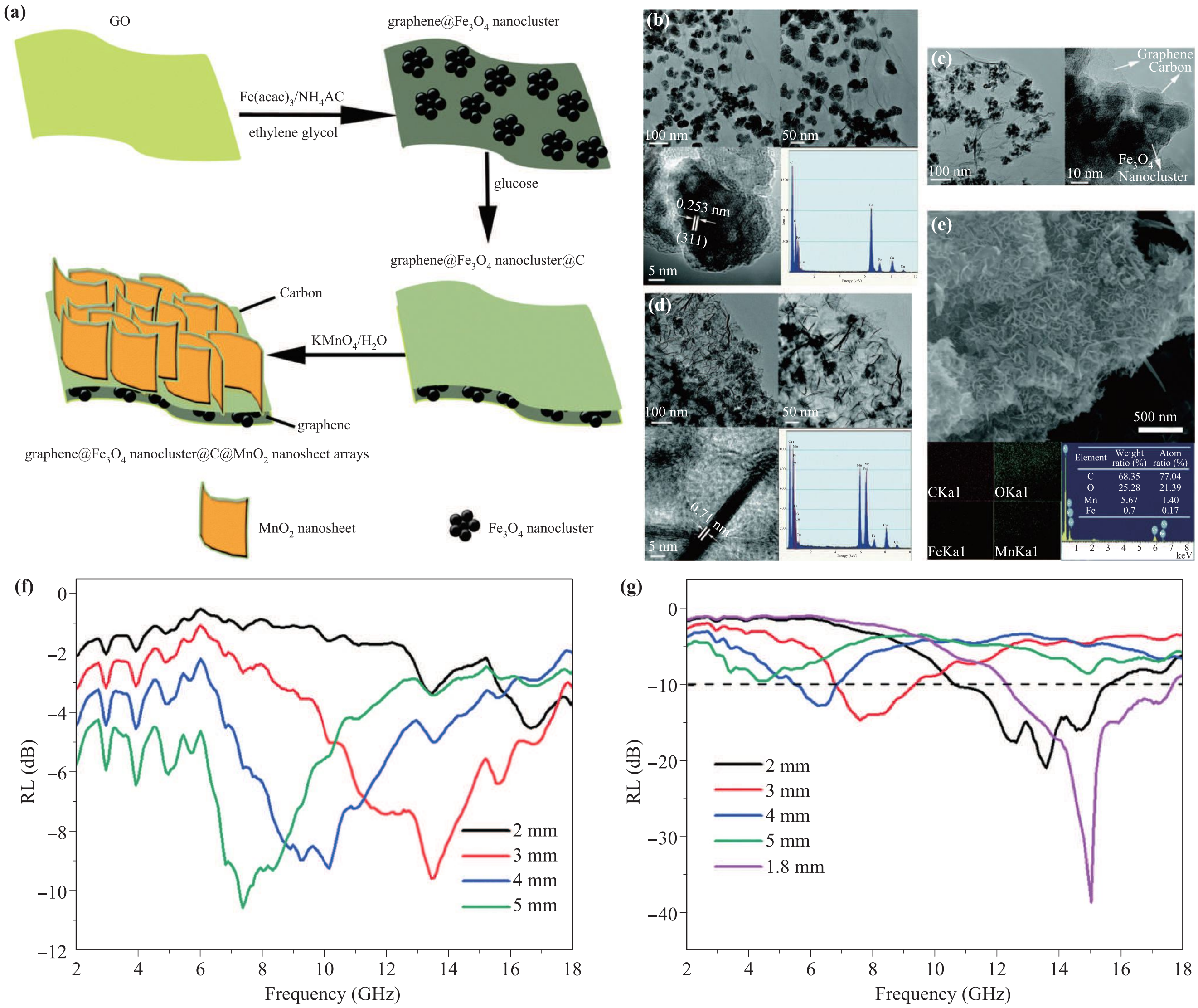

Fig. 6 **(a)** Schematic illustration of the three-step preparation of hierarchical composites of graphene@Fe_3O_4 NC@carbon@MnO_2 nanosheet arrays; **(b)** TEM images of graphene@Fe_3O_4 NC; **(c)** TEM images of graphene@Fe_3O_4 NC@carbon; **(d)** TEM images of graphene graphene@Fe_3O_4 NC@carbon@MnO_2 composite; **(e)** SEM images and the corresponding EDX element maps of C, O, Fe and Mn for graphene@Fe_3O_4 NC@carbon@MnO_2 composite nanosheet arrays; **(f, g)** calculated reflection losses for graphene@Fe_3O_4 NC and graphene@Fe_3O_4 NC@carbon@MnO_2 nanosheet arrays paraffin wax composites with different thicknesses in the frequency range of 2–18 GHz [98]. Reproduced from Ref. [98]. Copyright © 2015, with permission from the Royal Society of Chemistry.

tenuation is that of pyramidal nickel foam arrays perpendicular to the substrate, which were utilized for the absorption of electromagnetic and sound waves in an anechoic chamber. On the micro–nanoscale, the perpendicular micro–nanopillar arrays can be applied for microwave attenuation owing to the numerous interfaces and free voids or space between and inside the pillars, which can not only improve the impedance matching but also increase the interfacial reflection and scattering.

Yu *et al.* synthesized PANI nanorod arrays perpendicularly grown on the surface of graphene via an *in situ* polymerization process, and the composites showed significantly enhanced electromagnetic wave absorption properties. The minimum RL of −45.1 dB was reached at a thickness of only 2.5 mm, and the absorption bandwidth with a RL of <−20 dB reached 10.6 GHz. The results indicate that the enhanced microwave absorption properties were derived from the enhanced dielectric relaxation, the special structural characteristics, and the charge transfer between the graphene and PANI nanorods, suggesting that the deposition of other dielectric nanostructures on the surface of graphene nanosheets is an efficient way to fabricate excellent microwave absorbing materials [102]. Ren *et al.* synthesized a 3D $SiO_2@Fe_3O_4$ core–shell nanorod array/graphene architecture via a multi-step process. 3D β-FeOOH nanorod arrays were grown on graphene via a hydrothermal method, and then SiO_2 was coated on β-FeOOH nanorods to form core–shell structures. After heat treatment, the $SiO_2@Fe_3O_4$ nanorods array/graphene architecture was obtained. The 3D architecture presented excellent microwave absorption properties and attenuated $> 99\%$ of the microwave energy even with only 20 wt.% loading of composites in the paraffin matrix [103].

4.2.2.4 3D porous foam structure

The 3D porous foam structure is highly desirable for preparing lightweight high-efficiency microwave absorbers owing to its excellent impedance matching and extremely high attenuation constant. In this structure, the pores are usually filled with air that has perfect impedance matching with free space, reducing the surface reflection of electromagnetic waves, and the walls are mainly composed of microwave absorbing materials with suitable dielectric and magnetic performance and are used for the dissipation of electromagnetic energy during the propagation of electromagnetic waves. The combined effects of the pores and walls yield efficient absorption of electromagnetic waves.

Eswaraiah *et al.* reported the fabrication of novel foam-like composites comprising functionalized graphene and PVDF and investigated their electrical conductivity and EMI shielding properties. The electrical conductivity of the composites increased with the concentration of graphene, and the conductivity changed drastically at the graphene concentration of 0.5 wt.%. The conductivity increased sharply from 10^{-16} S·m^{-1} for insulating PVDF to 10^{-4} S·m^{-1} for the 0.5 wt.% graphene-reinforced PVDF composite, which was attributed to the formation of a continuous conductive network in the polymer as a result of the high aspect ratio and high conductivity of the graphene nanofillers. The 5 wt.% graphene-loaded foam composites exhibited EMI SE of ~20 dB in the X-band region (8–12 GHz) and 18 dB in the broadband region (1–8 GHz). This study indicates that graphene/PVDF foamy composites can be applied as lightweight EMI shielding materials for broadband EMI shielding [105]. Zhang *et al.* demonstrated the preparation of functional polymethylmethacrylate (PMMA)/graphene nanocomposite microcellular foams through the blending of PMMA and graphene sheets, followed by foaming with subcritical CO_2. The PMMA/graphene nanocomposite foams showed high electrical conductivity and improved EMI SE with a microwave absorption-dominant EMI shielding mechanism. The graphene-PMMA foam with graphene loading of 1.8 vol.% exhibited a conductivity of 3.11 S/m and EMI SE of 13–19 dB in the frequency range of 8 to 12 GHz. In addition, owing to the numerous microcellular cells, the graphene-PMMA foam exhibited far better ductility and tensile toughness than its bulk counterpart. This research indicated that the lightweight and tough graphene-PMMA composite microcellular foams with good electrical conductivity and EMI shielding properties were promising EMI shielding materials [106]. Yan *et al.* described the synthesis of lightweight conductive polymer composites using high-pressure compression molding and a salt-leaching method. As-prepared functionalized graphene sheet/PS composites showed a low density and high EMI SE with an average value of 29 dB, indicating that the porous composites had potential as a lightweight shielding material against electromagnetic radiation. This method for preparing porous composites can be scaled [107]. Zhang *et al.* synthesized a 3D RGO/α-Fe_2O_3 composite hydrogel via a two-step process in a solution phase. The as-prepared composites exhibited an interconnected 3D porous network-like structure with microsize pores, and α-Fe_2O_3 nanoparticles 50–100 nm in size were uniformly dispersed on the surface of graphene nanosheets. Compared with a pristine RGO hydrogel, the RGO/α-Fe_2O_3 composite hydrogel exhibited excellent microwave absorbing performance with a maximum absorption of -33.5 dB at 7.12 GHz and a bandwidth of 6.4 GHz (10.8–17.2 GHz) (RL <-10 dB). The enhanced microwave absorption properties were attributed to the improved impedance matching [108]. Song *et al.* demonstrated a simple and universal method for the scalable fabrication of porous carbon-based 3D hybrid structures. Here, graphene was infiltrated into a modified carbon texture (CT) to obtain graphene aerogel-CT hybrids with an ultra-light feature (0.07 g·cm^{-3} in density) after freeze-drying. The composites exhibited efficient EMI SEup to 27 and 37 dB at thicknesses of 2 and 3 mm, respectively, in the X-band region. The excellent shielding performance coupled with the ultralow density endowed the 3D all-carbon hybrids with enormous advantages for a wide range of EMI shielding applications [109]. Wu *et al.* prepared an RGO-modified spongelike polypyrrole (S-PPy) aerogel. The dispersed GO was locked homogeneously in the chains formed by the gelation of PPy, and then the GO was reduced into RGO via a hydrothermal process. The microwave absorption performance of S-PPy/RGO aerogel-filled paraffin composites was investigated. The results indicated that even with very low filler loading (10 wt.%), the composites reached an effective microwave absorption bandwidth (RL <-10 dB) of 6.76 GHz, as well as a maximum RL of -54.4 dB at 12.76 GHz. This S-PPy/RGO aerogel is undoubtedly a good candidate as a lightweight and high-performance microwave absorbing material [110]. A broadband and tunable high-performance microwave absorber comprising an ultralight and highly compressible graphene foam (GF) was reported by Zhang *et al.* The GF showed substantially enhanced microwave absorbing properties with a qualified frequency bandwidth of 50.5 GHz, which was 80.9% of the overall bandwidth. Moreover, the microwave absorbing performance was tuned via physical compression. Compressive strain of 90% increased the qualified bandwidth to 60.5 GHz, which is approximately 70% wider than that for the best microwave absorbing material reported in the literature. An extraordinary specific microwave absorbing performance as high as 2.2×10^5 dB·cm^{-2}·g^{-1}, which is two orders of magnitude higher than those previously reported, was obtained owing to the ultralow mass density. The 3D conductive network of the GF offers tremendous opportunities for the application of graphene as an ultralight and tunable high-performance broadband microwave absorbing material [111]. Shen *et al.* prepared compressible graphene-coated polymer foams with ultralow density via a simple solution-based dip-coating technique for a tunable EMI shielding performance (Fig. 7). Commercial PU sponges with a highly porous network structure were used for absorbing GOs. The resultant PU/graphene (PUG) foams had a density as low as ~0.027-0.030 g/cm^3 and good absorption-dominant EMI SE, because of the good conduction dissipation and the microwave loss from the multiple reflections and scattering due to the inner 3D conductive graphene network. Moreover, the shielding performance of the PUG foams was simply tuned through mechanical compression, with the SE ranging from the average value of 40 dB to 24 dB when composites with 10 wt.% graphene loading were compressed by 75%, exhibiting promise for adjustable EMI shielding [104]. Shen *et al.* also described other types of GFs—including a microcellular GF [112] and multifunctional polyetherimide/graphene@Fe_3O_4 composite foams [113]—for electromagnetic-wave attenuation and obtained good electromagnetic-wave suppression. Zhang *et al.* studied the microwave absorbing performance of a series of GFs with different chemical compositions and physical structures by adjusting the GO concentration of the initial solution and the thermal reduction temperature. The results showed that the microwave absorbing properties of the GFs were strongly correlated with the C/O ratio, the conjugated carbon content, and the microstructure of the graphene skeleton. A minimum absorption value of −34.0 dB and a qualified bandwidth of 14.3 GHz (RL <−10 dB) were achieved for GFs with a density of only 1.6 mg/cm^3. The average absorption intensity and the specific microwave absorbing efficiency of the GFs were significantly higher than those of other foamy materials reported previously. The study indicated that GFs with the proper chemical composition and physical structure can achieve a good balance between impedance matching and electromagnetic loss, delivering excellent microwave absorbing properties [114]. Chen *et al.* described the preparation of a lightweight graphene/PDMS foamy composite with outstanding SE and mechanical flexibility. The foam composites were fabricated by using foam nickel as the sacrificed template. Here, graphene was first grown on the nickel surface via CVD, and then PDMS was cured on the surface of graphene. Finally, the graphene/PDMS foamy composite was obtained by etching the nickel frame with an HCl solution. The as-prepared composite had a density of 0.06 g/cm^3 and exhibited EMI SE as high as 30 dB in the frequency range of 30 MHz–1.5 GHz and 20 dB in the X-band. The specific EMI SE reached 500 dB·cm^3/g, far exceeding the performance of metals and carbon-based composites. Additionally, the composites showed excellent flexibility, and even under repeated mechanical deformation, the EMI shielding properties remained stable, indicating marvelous application potential in various fields [115]. Ling *et al.* demonstrated the facile preparation of lightweight microcellular polyetherimide/graphene composite foams via a phase-separation process and investigated their EMI shielding performance. The as-prepared porous composites had a low density of approximately 0.3 g/cm^3 and a percolation threshold of 0.18 vol.%. The specific EMI SE was significantly increased from 17 to 44 dB/(g/cm^3), which was attributed to the foaming process [116].

5 MXenes and MXenes-based composites for EMI shielding and microwave absorption

5.1 MXene and its polymer composites

Recently, with the rapid rise of 2D conductive materials besides graphene, e.g., MXenes, 2D materials are playing increasingly constructive roles in electromagnetic-wave attenuation. Compared with graphene, MXenes are composed of different kinds of elements and have thickness of several atom-layers; thus, they can exhibit dipolar and charge polarization in the through-thickness direction. Additionally, because of the substitution of hydroxyl groups and fluorine elements at A sites in the etching process, metal–oxygen or metal–halogen bonds are formed, and numerous defects are introduced, resulting in strong dipolar polarization and defect polarization. Moreover, along the in-plane direction, there exists large electron mobility, causing significant conduction loss under an alternating electromagnetic field. Thus, in contrast to the single-atom layer structure of graphene, MXenes have additional routes for dissipating electromagnetic energy. Furthermore, with the continuous expansion of the MXenes family, types of MXenes with magnetic and dielec-

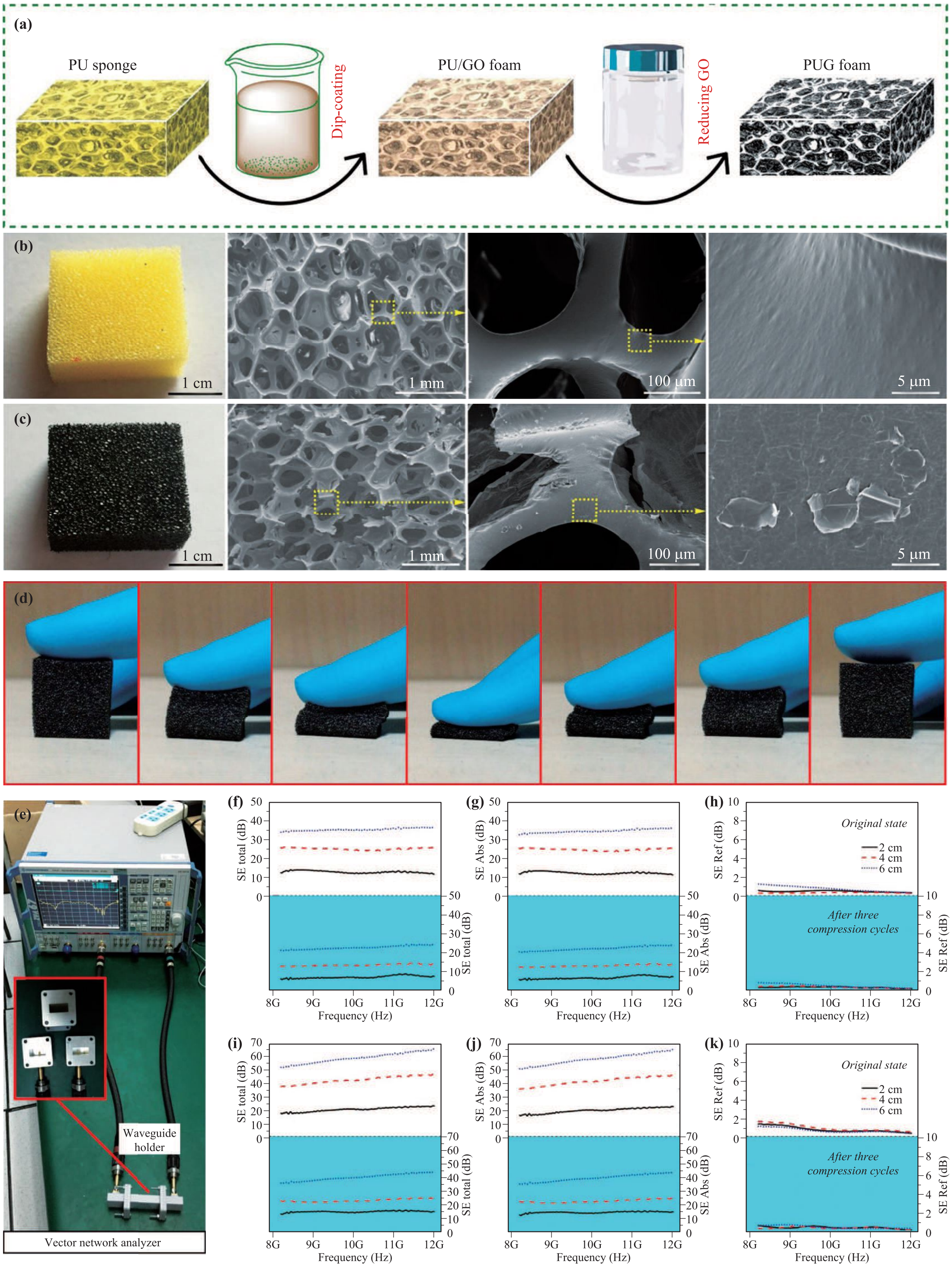

Fig. 7 **(a)** Overall fabrication process of the PUG foams, including dip-coating GO sheets onto the PU frameworks and then hydrothermally reducing by hydrazine vapor; **(b, c)** optical and SEM images of the original PU sponge and corresponding PUG-5 foam (containing 5 wt.% r-GO); **(d)** compressing and releasing process of the PUG-5 foam, showing excellent compressibility; **(e)** experiment setup for EMI shielding measurement: vector network analyzer with the waveguide. **(f–h)** SE total, SE absorption, and SE reflection of the PUG-5 foams with different thicknesses of ~ 2, ~ 4, and ~ 6 cm at the original state and after the first three compression cycles. **(i–k)** SE total, SE absorption, and SE reflection of the PUG-10 foams (containing 5 wt.% rGO) with different thicknesses of ~ 2, ~ 4, and ~ 6 cm at the original state and after the first three compression cycles [104]. Reproduced from Ref. [104]. Copyright © 2016, with permission from the American Chemical Society.

tric properties have been discovered [117], which will undoubtedly enrich the roles of MXenes in electromagnetic-wave attenuation and provide additional options for the manufacture of highly effective microwave absorbers.

In the past several years, the utilization of MXenes in EMI shielding and microwave absorption was extremely attractive owing to their ultrahigh microwave attenuation ability. Shahzad *et al.* reported a 45-μm-thick $Ti_3C_2T_x$ film that exhibited EMI SE of 92 dB (>50 dB for a 2.5-μm film) (Fig. 8). This was the highest SE value among synthetic materials with comparable thickness, by a large margin: significantly better than the metals silver and copper. In consideration of its lightweight and exfoliative features, this material has great promise for developing flexible, ultrathin, and ultralight microwave attenuating materials. The author ascribed the high EMI SE to the excellent electrical conductivity and multiple internal reflection [118]. Han *et al.* studied the EM absorption and shielding properties of MXenes-based wax composites in the X-Band. A localized sandwich structure with a layered morphology was established, and an exceptional EM absorbing capability in the X-band was observed. The results showed that a composite with 50 wt.% annealed MXenes had a minimum reflection coefficient of −48.4 dB at 11.6 GHz, which was attributed to the formation of TiO_2 nanocrystals and amorphous carbon. Moreover, superior SE with high absorption effectiveness was achieved. The total and absorbing SE of 1-mm-thick Ti_3C_2 MXenes/wax composites reached 76.1 and 67.3 dB, respectively, and the annealed Ti_3C_2 MXenes/wax composites had total and absorbing SE values of 32 and 24.2 dB, respectively, indi-

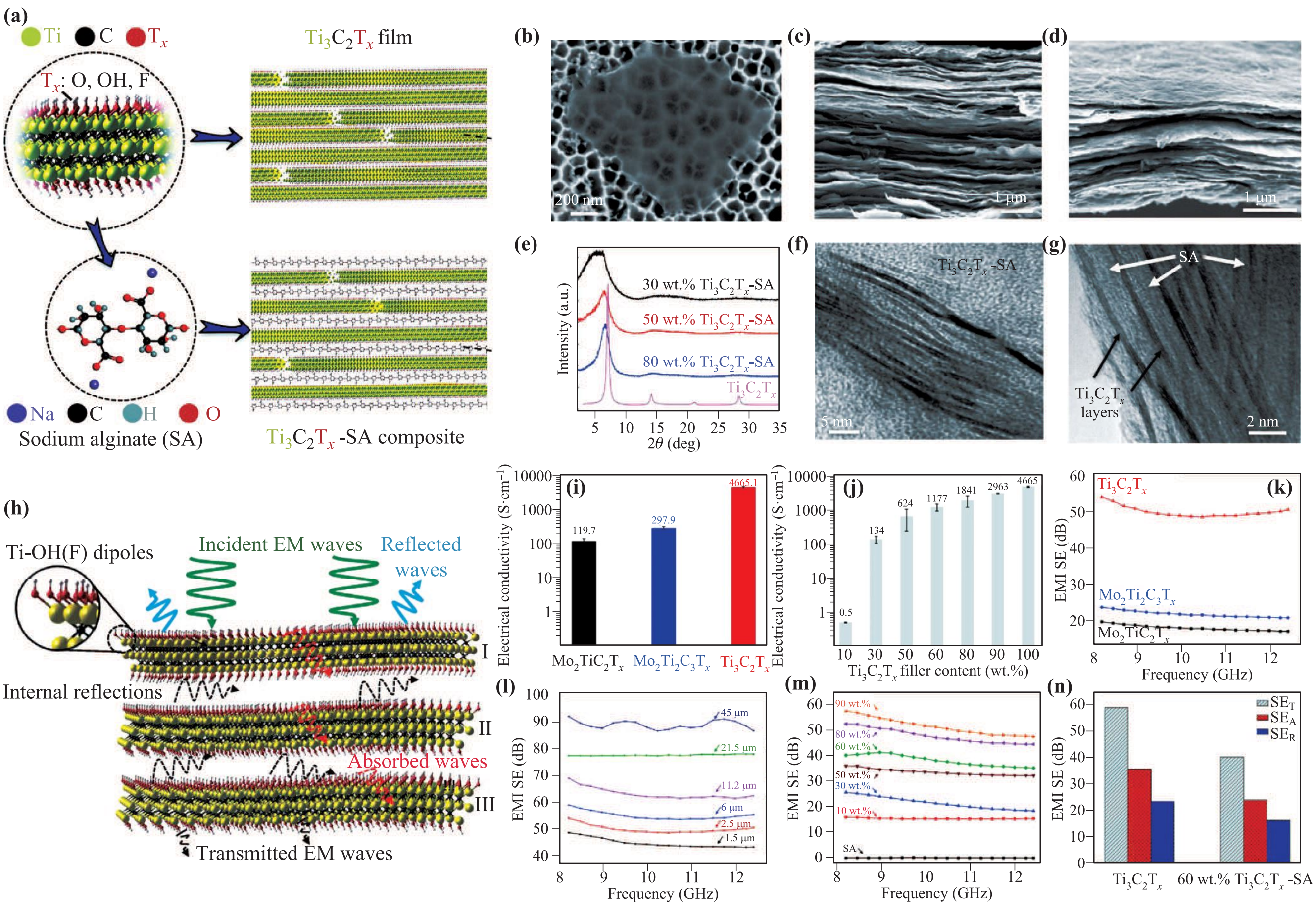

Fig. 8 **(a)** Schematic of $Ti_3C_2T_x$ and $Ti_3C_2T_x$-SA composite films; **(b)** SEM image of a $Ti_3C_2T_x$ flake on a filter. (c and d) SEM images of **(c)** 50 wt % $Ti_3C_2T_x$-SA composite and **(d)** pure $Ti_3C_2T_x$; **(e)** XRD patterns of pristine $Ti_3C_2T_x$ and its composite with SA at different loadings; (f and g) TEM images of 80 and 30 wt % $Ti_3C_2T_x$-SA composite films, respectively; **(h)** proposed EMI shielding mechanism; **(i)** electrical conductivity of $Mo_2TiC_2T_x$, $Mo_2Ti_2C_3T_x$, and $Ti_3C_2T_x$; **(j)** Electrical conductivity of $Ti_3C_2T_x$-SA composites with filler content varing from 10 to 90 wt % in SA matrix; **(k)** EMI SE of $Mo_2TiC_2T_x$, $Mo_2Ti_2C_3T_x$, $Ti_3C_2T_x$ at a thickness of ∼ 2.5 μm; **(l)** EMI SE of $Ti_3C_2T_x$ at different thicknesses; **(m)** EMI SE of $Ti_3C_2T_x$-SA composites at a thickness of 8 to 9 μm; (F) total EMI SE (EMI SET) and its absorption (SEA) and reflection (SER) mechanism in $Ti_3C_2T_x$ and 60 wt % $Ti_3C_2T_x$-SA samples at 8.2 GHz [108]. Reproduced from Ref. [108]. Copyright © 2016, with permission from Science mag (AAAS).

cating the strong microwave absorbing ability of MXenes [119]. Qing *et al.* exfoliated Ti_3AlC_2 powders in HF to prepare Ti_3C_2 nanosheets and investigated their electromagnetic properties in the frequency range of 12.4–18 GHz. The composites showed high relative complex permittivity and microwave absorption compared with those filled with the same content of Ti_3AlC_2 powder, and the RL of the composites filled with the Ti_3C_2 nanosheets exceeded −11 dB in the frequency range of 12.4–18 GHz at a thickness of 1.4 mm [120]. Feng *et al.* demonstrated the enhanced microwave attenuation capability of Ti_3C_2-based microwave absorbing materials in the frequency range of 2–18 GHz. Ti_3C_2 nanosheet/paraffin composites showed enhanced microwave absorbing performance with an effective absorbing bandwidth of 6.8 GHz (11.2–18 GHz) at 2 mm and an optimal RL of −40 dB at 7.8 GHz. The mechanisms of the dielectric responses of the Ti_3C_2 MXene nanosheets were discussed, and three typical electric polarizations of Ti_3C_2—interfacial electric polarization, electric polarization in the nanosheet plane direction, and electric polarization in the through-thickness direction—were illustrated by Cole–Cole diagrams. The enhanced microwave absorbing properties were attributed to the high dielectric loss, which was accompanied by the strong multiple reflections between MXene layers [121]. Liu *et al.* reported hydrophobic, flexible, and lightweight MXene foams for EMI shielding. Hydrophobic MXene foams were prepared by assembling MXene sheets into films through vacuum filtration, followed by a hydrazine-induced foaming process. Compared with the unfoamed film with SE of 53 dB, a greatly enhanced EMI SE of ∼70 dB was achieved in the MXene foam owing to the highly efficient microwave attenuation in the favorable porous structure [122]. Additionally, highly conductive transition-metal carbide/carbonitride(MXene)@PS composites were prepared via electrostatic assembly. Under electrostatic interaction, negative MXene nanosheets were attached onto the positive PS microspheres to form core/shell structures, which were subsequently compressed into bulk composites under a high pressure. The resultant nanocomposites exhibited a very low percolation threshold of 0.26 vol%, remarkable conductivity of 1081 $S\cdot m^{-1}$, and outstanding EMI shielding performance of >54 dB in the whole X-and with maximum SE of 62 dB at low MXene loading of 1.90 vol%. These are among the best performances for electrically conductive polymer nanocomposites [123].

5.2 MXenes-based multifunctional composites

Multifunctional MXenes-based composites have also been studied for the enhancement of the microwave attenuation performance. Li *et al.* reported *in situ*-grown CNT-modified Ti_3C_2 MXenes composites with improved electromagnetic wave absorption properties. One-dimensional (1D) CNTs were grown *in situ* on $Ti_3C_2T_x$ MXenes via a simple catalytic CVD process and were uniformly distributed in the interlayers of the 2D $Ti_3C_2T_x$ MXene flakes. Compared with the pristine $Ti_3C_2T_x$ MXenes, the hierarchical sandwich microstructure greatly improved the microwave absorption properties of the composites in the frequency range of 2–18 GHz. The minimum RL reached −52.9 dB, and the effective absorption bandwidth reached 4.46 GHz at a filler content of 35 wt.% and a thickness of 1.55 mm. The effective absorption bandwidth reached 14.54 GHz (3.46–18 GHz) with the adjustment of the film thickness from 1.55 to 5 mm. The microwave absorption was mainly derived from polarization loss and conduction loss [124]. Li *et al.* reported the facile preparation of $Ti_3C_2T_x$-coated $Ni_{0.5}Zn_{0.5}Fe_2O_4$ composites via a co-precipitation method. An as-synthesized $Ti_3C_2T_x$/ferrite composite with 5 wt.% $Ti_3C_2T_x$ MXenes loading exhibited a large RL (−42.5 dB) at 13.5 GHz, and the effective absorption bandwidth reached 3 GHz (12–15 GHz) in the K-band. The possible electromagnetic wave absorption mechanisms include magnetic loss, dielectric loss, conduction loss, multiple reflections, and scattering [125]. Qian *et al.* fabricated urchin-like ZnO-MXene nanocomposites via a facile coprecipitation process. The nanocomposites (mass ratio of ZnO-MXene to wax = 1:3) exhibited enhanced electromagnetic wave absorbing performance with an optimum RL of −26.30 dB, which is significantly better than that of pristine $Ti_3C_2T_x$ (−6.70 dB), owing to their unique semiconductive networks and larger interfacial area. The electromagnetic absorption performance was well controlled in the range of 14.0–18.0 GHz by adjusting the growth time of ZnO [126]. Qing *et al.* demonstrated epoxy composites synergistically reinforced with nitrogen-doped graphene and titanium carbide nanosheets as microwave absorbers. The electromagnetic properties of these hybrid absorbers were adjusted by controlling the microstructure and dielectric characteristics of the N-doped graphene and Ti_3C_2 nanosheets. The minimum RL reached −52 dB, and the effective bandwidth (RL < -10 dB) ranged from 10.9 to 18 GHz for a 1.4-mm-thick sample. These results suggest that the N-doped graphene and Ti_3C_2 nanosheets composites were highly promising lightweight, thin, broadband-absorption microwave absorbers [127]. The microwave absorption performance of layered PVB/$Ba_3Co_2Fe_{24}O_{41}$/Ti_3C_2 MXene composites was also studied. Polyvinyl butyral (PVB) was used as an isolated matrix for better impedance matching, and layered structures comprising different substances were employed for the attenuation of electromagnetic waves via different mechanisms. Experimental results showed that the as-synthesized PVB/Z-type $Ba_3Co_2Fe_{24}O_{41}/Ti_3C_2$ MXene composites had an optimal RL as small as −46.3 dB at 5.8 GHz at an absorber thickness of only 2.8 mm and an effective absorption bandwidth (RL <−10 dB) of 1.6 GHz [128].

5.3 Annealed MXenes for microwave attenuation

Owing to their special few-atom-thick 2D configuration and multi-element composition, single-layer or few-layer MXenes can generate layered multiphase composites *in situ* after oxidation. For example, $Ti_3C_2T_x$ MXene can be oxidized into 2D disordered carbon/TiO_2 nanoparticle composites with a laminated structure. The highly disordered thin carbon layers play an important role in electromagnetic wave absorption, and the *in situ*-generated TiO_2 nanoparticles on $Ti_3C_2T_x$ sheets can not only prevent carbon layers from restacking but also enhance the dielectric loss. Han *et al.* reported laminated carbon/TiO_2 hybrid microwave absorbers derived from $Ti_3C_2T_x$ MXenes and studied their electromagnetic absorbing capability. Disordered 2D carbon layers were obtained by annealing multilayer Ti_3C_2 MXene in a CO_2 atmosphere (Fig. 9). The minimum RL of laminated carbon/TiO_2 composites reached −36 dB, and the effective absorption bandwidth ranged from 3.6 to 18 GHz at a tunable thickness from 1.7 to 5 mm. When the thickness of the carbon/TiO_2/paraffin composite (45 wt.% C/TiO_2 hybrids loaded in a wax matrix) was 1.7 mm, the effective absorption bandwidth covered the whole Ku-band (12.4–18 GHz) [129]. Li *et al.* reported the fabrication of Ti_2CT_x MXenes and its derivatives with various heterogeneous structures via etching and a facile oxidation treatment. Ti_2CT_x/TiO_2, C/TiO_2, and TiO_2 composites were obtained from Ti_2CT_x MXenes at different oxidation temperatures. Compared with pristine Ti_2CT_x MXene, the enhanced electromagnetic wave absorption ability of the as-prepared Ti_2CT_x/TiO_2 and C/TiO_2 nanocomposites was attributed to their improved interfacial polarization loss caused by the generated heterogeneous interfaces and the strong conduction loss due to the completely exfoliated carbon layers. The C/TiO_2 nanocomposites showed a minimum reflection coefficient of −50.3 dB at 7.1 and 14.2 GHz and an ef-

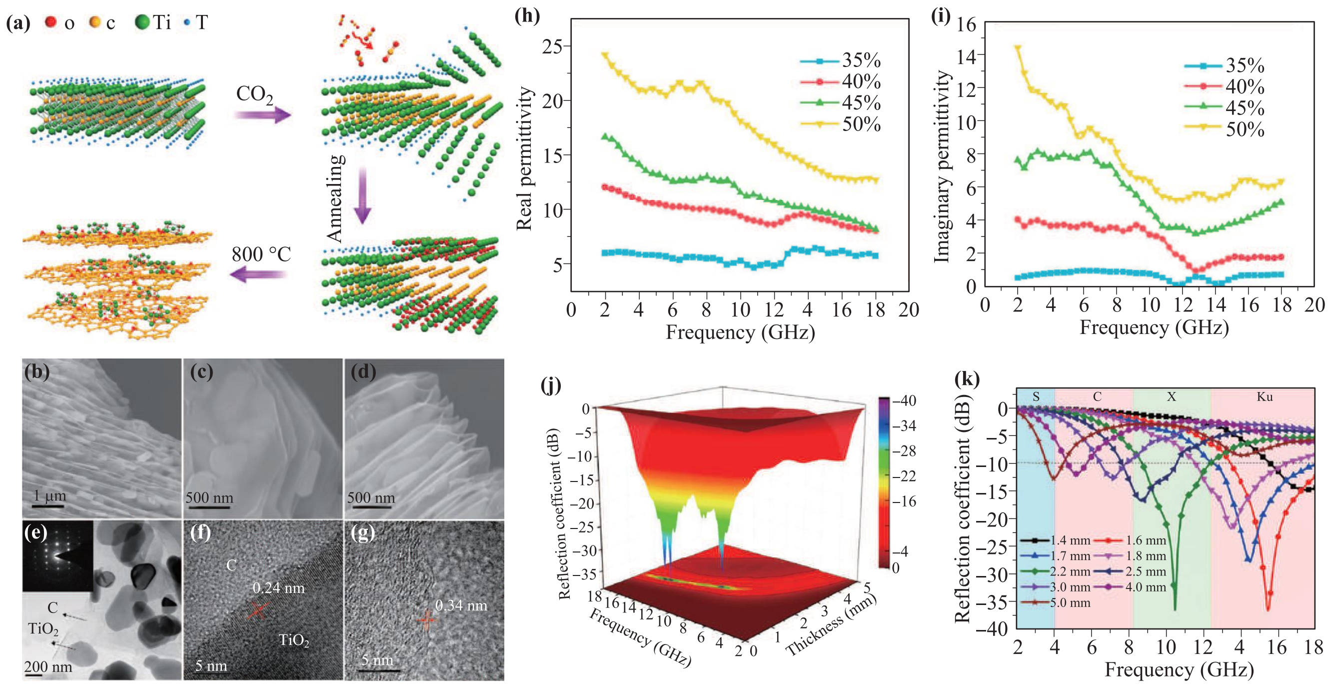

Fig. 9 **(a)** Schematic of the structural evolution from $Ti_3C_2T_x$ to C/TiO_2 hybrids by heat treatment at 800 °C in CO_2 atmosphere, where "T" represents the terminating groups consisting of O, OH, and F; (b, c, and d) SEM images of as-synthesized C/TiO_2 hybrids derived from multilayered $Ti_3C_2T_x$ showing TiO_2 particles sandwiched between electron-beam transparent carbon layers; **(e)** TEM image of a single C/TiO_2 hybrids, and the upper left inset is the corresponding SAED pattern; **(f)** HRTEM images of the interface between carbon layer and rutile TiO_2; **(g)** the edge showing a bilayer structure of as-exfoliated carbon layer; **(h, i)** real (ε') and **(b)** imaginary (ε'') permittivity versus frequency (2–18 GHz) for the composites with different loadings of C/TiO2 hybrids in the paraffin matrix; **(j, k)** 3D plot and reflection coefficient (RC) curves versus frequency (2–18 GHz) and thickness (0–5 mm) of the sample with 45 wt % C/TiO_2 hybrids (S-800, annealed at 800 °C) in the paraffin matrix [129]. Reproduced from Ref. [129]. Copyright © 2017, with permission from American Chemical Society.

fective absorption bandwidth of 4.7 GHz at a thickness of 2.1 mm, indicating their excellent electromagnetic wave absorption ability [130].

In general, MXenes and MXenes-based composites have shown enormous potential in EMI shielding and are undoubtedly among the most excellent candidates for microwave attenuation in the future. The mechanism for achieving extraordinary electromagnetic-wave SE and microwave absorption ability is worthy of in-depth research, and the electromagnetic properties of MXenes-based multinary composites should be further investigated for further enhancing their wave-absorbing performance and broadening the effective absorption bandwidth.

6 MoS_2 nanosheets for electromagnetic-wave attenuation

MoS_2 is the representative 2D material in transitional-metal chalcogenides and has exhibited great promise for applications in photoelectronics owing to its unique semiconductor properties. Owing to their good interfacial polarization and dielectric loss, exfoliated 2D MoS_2 nanosheets have a good attenuation ability for electromagnetic waves. Compared with graphene, transition-metal chalcogenides have lower conductivity and a smaller dielectric constant and thus provide better impedance matching with free space. In combination with other highly conductive 2D materials, such as graphene or MXenes, transitional-metal chalcogenide nanosheets can usually increase the impedance of graphene or MXene-based composites and thus reduce the surface reflection, improving the microwave absorbing performance.

Liang *et al.* investigated the application of 2D MoS_2 nanosheets for attenuating electromagnetic waves (Fig. 10), finding that the MoS_2 nanosheets were good electromagnetic-wave absorbers because of their large interfacial polarization and dielectric loss. The optimal microwave RL of the MoS_2 nanosheets reached −47.8 dB at 12.8 GHz, which was attributed to their good electrical conductivity and the polarization effect. Additionally, MoS_2 exhibited an effective electromagnetic wave absorption bandwidth of 5.2 GHz (RL <−10 dB) at thicknesses of 1.9 and 2.0 mm. All the results indi-

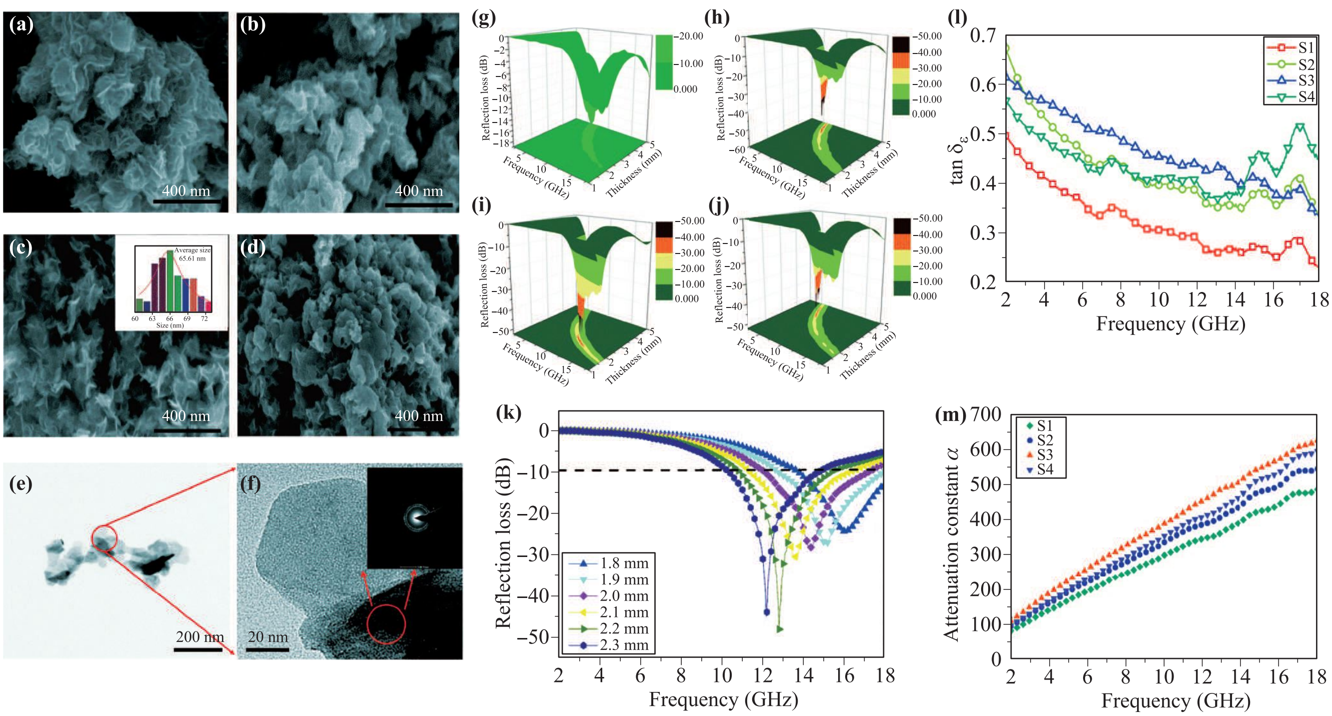

Fig. 10 **(a–d)** SEM images of the MoS_2 nanosheets prepared at different hydrothermal temperatures, **(a)** S1, 160 °C; **(b)** S2, 170 °C; **(c)** S3, 180 °C; **(d)** S4, 190 °C; **(e)** TEM image of S3; **(f)** HRTEM image of S3, in which, (f) is acquired from red areas of (e), and the inset in (c) is the size distribution of S3; **(g–j)** 3D plots of RL values for MoS_2 with different hydrothermal temperatures of S1 (g), S2 (h), S3 (i), and S4 (j) in the frequency range of 2–18 GHz; **(k)** RL curves of MoS2 with a hydrothermal temperature of 180 1C at thicknesses ranging from 1.8 to 2.3 mm in the frequency range of 2–18 GHz; **(l)** dielectric loss tangents of MoS_2 with different hydrothermal temperatures; **(m)** attenuation loss a of the MoS_2 samples [121]. Reproduced from Ref. [121]. Copyright © 2016, with permission from the Royal Society of Chemistry.

cated that the MoS_2 nanosheets are a good candidate for microwave absorbers, with a broad effective absorption bandwidth at a small thickness [131]. Zhang *et al.* reported the tunable high-performance microwave absorption performance of 3D MoS_2 hierarchical nanospheres in the broadband region. The 3D nanospheres were assembled spontaneously using 2D MoS_2 lamina on a large scale via a simple hydrothermal process. The electromagnetic wave absorption properties of hierarchical MoS_2 nanospheres/PVDF composites were investigated in the broad frequency range of 2–40 GHz. The results indicated that the peculiar hierarchical structure of MoS_2 was beneficial for microwave absorption, in contrast to bulk and microsize MoS_2, and the microwave absorption performance of the composites was effectively tuned by changing the absorber thickness and filler content. The minimum RL of MoS_2/PVDF composites with filler loading of 25 wt.% was −26.11 dB at 11.36 GHz at a thickness of 2.5 mm, and the frequency bandwidth (RL <−10 dB) ranged from 9.92 to 13.36 GHz. In the range of 18–40 GHz, the minimum RL was −27.47 dB at 18.47 GHz and −32.67 dB at 28.93 GHz for 30 wt.% and 20 wt.% MoS_2-loaded PVDF nanocomposites at thicknesses of 1.5 and 3.5 mm, respectively. The main microwave absorption mechanism involves various polarizations, destructive interference theory, and multiple reflections [132].

To further improve the electromagnetic performance, MoS_2-based multinary composites were studied. Quan *et al.* introduced graphene into MoS_2-based composites to adjust the dielectric properties for a better balance of impedance matching and energy conservation, because pure graphene or pure MoS_2 is insufficient for attenuating electromagnetic waves owing to either strong surface reflection or weak dissipation. They fabricated MoS_2/RGO composites via a facile hydrothermal approach. The dielectric constant of the composites was regulated by changing the mass ratio of the precursors, and an optimal balance between the impedance matching and energy conservation was obtained. The minimum RL was −67.1 dB at 14.8 GHz, and the effective electromagnetic wave absorption bandwidth (RL <−10 dB) was 5.92 GHz (12.08–18.00 GHz) at a small thickness of 1.95 mm. The study demonstrated that unilateral superior performance could not guarantee good microwave absorbing performance, and the effective combination of the impedance matching, attenuation ability, and absorber thickness was essential for improving the microwave absorbing properties [133]. Recently, MoS_2 and graphene/GO composites have been intensively studied for the enhancement of microwave absorption owing to their complementary electromagnetic properties [134–138]. In addition to the 2D–2D stacked structure, Sun *et al.* described other MoS_2-based mixed-dimensional van der Waals heterostructures for microwave absorption. They investigated the microwave absorbing performance of three types of stacked structures: the 2-0 type, comprising 2D MoS_2 and zero-dimensional (0D) nickel nanoparticles, exhibited a minimum RL of −19.7 dB and an effective absorption bandwidth of 2.92 GHz; the 2-1 type, comprising 2D MoS_2 and 1D CNTs, exhibited a minimum RL of −47.9 dB and an effective absorption bandwidth of 5.60 GHz; and the 2-3 type, comprising 2D MoS_2 and 3D carbon layers, exhibited a minimum RL of −69.2 dB and an effective absorption bandwidth of 4.88 GHz. The relaxation behavior originating from the interfacial polarization played an important role in attenuating electromagnetic waves, and the enhancement of the microwave absorbing performance in the order of 2-0 < 2-1 < 2-3 was attributed to the increasing conductivity and effective interfacial area of the composites [139]. Zhang *et al.* described the facile synthesis of NiS_2@MoS_2 core–shell nanospheres for the enhancement of the microwave absorption. Because of the characteristic impedance matching, synergistic effects, dipole and interface polarization, multiple reflections, and quarter-wavelength matching, nanocomposites with a filler content of 20 wt.% exhibited enhanced microwave absorption properties. The minimum RL reached −41.05 dB at 12.08 GHz, and the absorption bandwidth (RL <−10 dB) reached 4.4 GHz at a thickness of 2.2 mm [140]. Additionally, a conductive polymer was also introduced into the MoS_2 composite system for improving the microwave absorbing performance. Zhang *et al.* reported the growth of PANI nanoneedles on MoS_2 nanosheets. The length–diameter ratio of the PANI nanoneedles on the MoS_2 nanosheets was readily tuned by controlling the polymerization time, resulting in the tunable electrical conductivity and dielectric properties of the MoS_2/PANI composites. The minimum RL values of the MoS_2 nanosheets reached −44.4 dB at 11.48 GHz and a thickness of 3.0 mm, and the RL of the MoS_2/PANI nanoneedle composites reached −44.8 dB at 14.5 GHz for a film thickness of only 1.6 mm. The effective electromagnetic wave absorption bandwidth (RL <−10 dB) for the MoS_2/PANI nanoneedles composites was 2.82 GHz owing to the synergistic effect of the PANI nanoneedles and MoS_2 nanosheets [141].

Ternary or multicomponent MoS_2-based composites were also studied. Ding *et al.* demonstrated the decoration of an $FeNi_3$ nanoalloy on 3D composites composed of RGOs and molybdenum disulfide and found that the ternary composites exhibited excellent electromagnetic wave absorption properties. The composites were synthesized via a two-step hydrothermal reaction. RGO/MoS_2 composites were first synthesized in a hydrothermal process, and then the RGO/MoS_2 nanosheets were decorated with $FeNi_3$ nanoalloys via a second hydrothermal process. The electromagnetic wave absorption performance of $FeNi_3$@RGO/MoS_2 composites with different filler contents in a paraffin matrix were investigated, and with the increase of the filler content, the electromagnetic absorbing performance improved significantly. The maximum absorption bandwidth was 4.72 GHz at a film thickness of 2.0 mm, and the corresponding minimum RL value was −30.39 dB at 14.72 GHz when the filler loading amount was 40%. The strong microwave absorption property was ascribed to both the dielectric loss and magnetic loss, and in the low-frequency region, the magnetic loss played an important role, and the dielectric loss occupied the main part of microwave absorption in the high-frequency area [142]. Guo *et al.* described the microwave absorption and EMI shielding performance of RGO@MoS_2/PVDF composites. When the filling ratio was 5.0 wt.%, the minimum RL of the RGO@MoS_2/PVDF composites reached −43.1 dB at 14.48 GHz, and the effective frequency bandwidth (RL <-10 dB) ranged from 3.6 to 17.8 GHz at a film thickness of 1–5 mm, indicating that the composites possessed a broadband microwave absorption ability. RGO@MoS_2/PVDF composites with a filling ratio of 25 wt.% exhibited EMI SE up to 27.9 dB, where the absorption was dominant [143]. Li *et al.* reported the synthesis and microwave absorption performance of RGO/MoS_2@Fe_3O_4 ternary composites. In a two-step hydrothermal process, Fe_3O_4 nanoparticles were successfully distributed on the surface of RGO/MoS_2 nanosheets. The saturation magnetization of the RGO/MoS_2@Fe_3O_4 composite was 15.64 emu/g. The minimum RL value was −49.43 dB at 8.95 GHz when the content of RGO/MoS_2@Fe_3O_4 in the paraffin matrix was 16.7 wt.%, and the corresponding maximum absorption bandwidth was 4.33 GHz at a film thickness of 3.0 mm [144].

According to the aforementioned results, 2D MoS_2 nanosheets are excellent microwave absorbers because of not only their peculiar 2D structure but also their appropriate electromagnetic parameters, giving rise to large interfacial polarization losses and a multimode attenuation mechanism. In combination with other types of absorbers, MoS_2 nanosheets can play multifarious roles, as impedance modulators, microwave attenuators, or structural support.

7 Other 2D materials for electromagnetic-wave attenuation

Compared with transitional-metal chalcogenides, oxides and hydroxides have a lower conductivity, and when mixed with highly conductive graphene or MXenes, they can adjust the conductivity of composites more effectively for better impedance matching. Additionally, oxides and hydroxides are generally good dielectric materials, and some of them have a large dielectric constant and can thus be used to dissipate electromagnetic waves via dielectric loss. Numerous 2D oxides and hydroxides with excellent dielectric properties have been discovered and have played important roles in electrical and electronic applications, such as dielectric substrates, dielectric layers of capacitors, and gate dielectrics. The typical dielectric oxide nanosheets include titania-based nanosheets, such as $Ti_{0.87}O_2$, and perovskite oxide nanosheets, such as $Bi_4Ti_3O_{12}$, $LaNb_2O_7$, $(Ca,Sr)_2Nb_3O_{10}$, and $CaLaNb_2TiO_{10}$. These oxides exhibit a large dielectric constant—generally >100 [145] —which is favorable for microwave attenuation. The widely used hydroxide nanosheets are clays, principally comprising layered double hydroxides (LDHs), such as hydrotalcite and montmorillonite (MMT). They can be exfoliated into a well-defined 2D structure via osmotic swelling [146]. LDHs and MMT are good isolators and can behave as a good complement to 2D conductors and semiconductors in the electrical and electronic fields for the modulation of electromagnetic parameters.

Applications of 2D oxides and hydroxides for microwave absorption have been reported. Gashti *et al.* investigated the electromagnetic properties of aluminum–clay nanocomposites and found that the composites had good electromagnetic-wave shielding performance owing to the dipole polarization and multiple reflections [147]. Salih *et al.* reported that the addition of Zn/Al-NO_3 LDH to polyvinyl chloride (PVC) improved the dielectric properties of the PVC. An increase of the LDH concentration in the PVC matrix led to an increase of the dielectric constant and the dielectric loss factor. The results suggest that these composites can be used as microwave absorbers at low microwave frequencies [148]. Lv *et al.* reported magnetic organic modified zinc–aluminum LDH/polyimide (PI) composites for electromagnetic shielding applications. During imidization, organic modified zinc–aluminum LDHs lose their hydroxyl group, and the partial decomposition of a sodium dodecyl sulfate modifier resulted in loose contact between the PI and the zinc–aluminum LDHs. The saturated magnetization of heated organic modified zinc–aluminum LDHs was enhanced slightly owing to the structural improvement in the Fe_3O_4 crystalline domain. The good soft magnetic and dielectric properties endowed the composites with good potential for electromagnetic shielding [149]. Parvinzadeh *et al.* demonstrated the synthesis of an iron-pillared bentonite clay-based nanoadsorbent via the thermal aging technique. X-ray diffraction and Fourier transform infrared spectroscopy indicated the intercalation of polyoxocation oligomers of iron between clay layers, and thermogravimetric analysis indicated that the iron particles generated on the clay surface significantly improved the thermal stability of the clay particles. The electromagnetic properties of the clay particles were investigated, revealing that the electromagnetic transmission of the clay could be tailored by the intercalation of iron polyoxocation oligomers, and strong microwave attenuation was achieved. The results suggest that iron-pillared clay particles can be used in various polymer nanocomposites for enhancing the absorption of electromagnetic waves [150]. Quan *et al.* reported the microwave absorption performance of CoFeAl-LDH/GO hybrids. The hybrids were prepared via metal-ion absorption and subsequent *in situ* growth of LDH on a GO surface. Because of the extra dipolar polarization induced by the donated electron from GO and the interfacial polarization due to the Maxell–Wagner–Sillars effect, the absorption properties of the LDH/GO hybrids were greatly improved, and the minimum RL and the qualified bandwidth reached −23.8267 dB and 7.36 GHz, respectively, at a thickness of 2.5 mm, indicating that the structural design played an important role in the microwave attenuation [151].

Thus far, the application of ultrathin 2D oxide nanosheets for the attenuation of electromagnetic waves has not been reported, possibly owing to the immature manufacture technology for realizing the large-scale low-cost production of 2D oxide nanosheets. However, considering their large dielectric constant and tremendous specific surface area, in combination with other microwave absorbing materials, 2D oxide nanosheets will undoubtedly play a positive role in microwave attenuation.

In addition to oxides, 2D nitrides were studied for electromagnetic applications. The intensively studied 2D nitrides mainly include C_3N_4 nanosheets and hexagonal boron nitride (BN) nanosheets. In the literature, nitrides are not used alone for microwave attenuation. They are commonly employed as an additive for the preparation of multifunctional microwave absorbers, for the enhancement of either the thermal conductivity or the impedance matching. C_3N_4 is a lightweight semiconductor having a moderate resistivity for the conduction loss of electromagnetic waves, and BN is an isolator having good thermal conductivity, which can enhance the thermal conduction ability of the composites and decrease the surface reflection of electromagnetic waves by improving the impedance matching.

Lv *et al.* prepared graphene/g-C_3N_4 composites for microwave absorption by loading g-C_3N_4 nanosheets on graphene through a simple liquid-phase approach. Because of the appropriate resistance, g-C_3N_4 on graphene acted as a resistor and yielded large current attenuation under an electromagnetic field, converting electromagnetic energy into heat energy via the Joule effect. The optimal RL was −29.6 dB at 14.5 GHz for a thin coating layer of 1.5 mm. The corresponding effective absorption bandwidth reached 5.2 GHz (12.8–18 GHz) at a filling ratio of only 10 wt.% [152]. Zivkovic *et al.* studied the microwave absorption and thermal conductivity performance of BN powder-filled epoxy composites. The addition of BN did not significantly affect the dielectric constant or microwave absorbing properties of the composites but improved the thermal conductivity of the composites remarkably [153]. Kang *et al.* prepared sandwich-like hybrids of RGO and hexagonal BN (h-BN) via heat treatment of a self-assembled structure of GO and ammonia borane (AB). The ideal emperature for transforming the hybrids into inorganic sandwiches was 900 °C. Additionally, h-BN was generated *in situ* under heat treatment and embedded into the RGO frameworks. The h-BN content was tuned by controlling the mass ratio of AB to GO and the heat-treatment temperature. The complex permittivity and the microwave absorption were tuned by changing the h-BN content. When the mass ratio of GO/AB was 1:1, the composites showed a good microwave absorption capability in the range of 6–18 GHz. A minimum RL of −40.5 dB was obtained at 15.3 GHz for the wax composite filled with 25 wt.% GO/AB hybrids at a film thickness of 1.6 mm. The qualified frequency bandwidth reached 5 GHz. The layer-by-layer structure of the hybrids could give rise to theincreasing approaches and probability of electron migrating and hopping, yielding a strong dielectric loss and good impedance matching for microwave consumption [154]. Zhang *et al.* fabricated an ordered multilayer film composed of a GO/polymer and a BN/polymer through a layer-by-layer casting method. The special layer-by-layer architecture of the film not only led to the superior electrical and thermal conductive performance in the in-plane direction but also effectively blocked the electrical conductive path in the through-plane direction owing to the introduction of the isolated BN layer. Moreover, the ordered multilayer film exhibited good EMI SE (37.92 dB), excellent electrical insulation with breakdown strength of 1.52 MV/m, and high thermal conductivity (12.62 W/mK) in the in-plane direction, indicating the potential of the ordered multilayer film as an ideal EMI shielding material with excellent electrical insulation and high thermal conductivity for application in electronic devices [155].

Recently, with the family of 2D materials expanding continuously, novel 2D materials have increasingly been explored, and the electromagnetic properties of some of these have been investigated. For example, Wu *et al.* studied the electromagnetic absorption performance of few-layer BP (FL-BP). The FL-BP was prepared via the liquid-phase exfoliation method and exhibited high electromagnetic absorbing performance in multi-frequency bands. A composite filled with 30 wt.% of FL-BP with a thickness of 2.5 mm showed an effective absorption bandwidth of 6.20 GHz. The minimum RL in the Ku-band and X-band reached −46.5 and −41.6 dB, respectively, when the thickness of the composite films was tuned. The microwave absorbing bandwidth of the FL-BP was broader than those of many other 2D material-based absorbers. Furthermore, when the loading ratio was increased to 50 wt.%, the FL-BP-based absorber exhibited a broad effective absorption bandwidth in the S-band [156]. In addition to black phosphorene, other 2D materials—such as silicene, stanene, and 2D oxyhalides—might also present good or unique electromagnetic performance owing to their unusual conductive and dielectric properties, and their applications for microwave attenuation are expected to be further developed.

8 Conclusion and outlook

This review provides a relatively comprehensive introduction of the application of 2D materials for the attenuation of electromagnetic waves. Graphene and GOs are currently the most widely studied and used 2D materials for microwave attenuation, because of their multiple attenuation mechanisms. As a microwave shield or an absorber, graphene has several obvious advantages. First, it has an ultrathin thickness and ultralow mass density, which are very beneficial for the preparation of ultrathin and lightweight microwave absorbers. Second, it has an extremely large specific surface area, which can significantly increase the interfacial reflection and interface polarization for the attenuation of electromagnetic waves. Third, graphene has high conductivity and a large dielectric constant, which can result in a large dielectric loss of electromagnetic energy. Fourth, GOs contain a large amount of functional groups and defects, giving rise to dipole polarization loss and defect polarization loss of electromagnetic waves. Fifth, graphene is highly processable, making it compatible with various matrices, and can behave as a universal additive in a variety of matrices. Sixth, graphene has good mechanical strength and can form a robust freestanding film alone or by compounding with other materials for the modulation of mechanical and electrical properties over a wide range to satisfy different requirements in electromagnetic applications. However, graphene alone cannot generate ideal microwave absorption properties, owing to its severe impedance mismatch with free space; thus, it is necessary to introduce other functional components to the graphene-based system for not only better impedance matching but also multimode attenuation, to decrease the RL and broaden the absorption bandwidth. Generally, conductive polymers, metals, semiconductive inorganic or organic matter, dielectric polymers and ceramics, magnetic metals and ferrites, etc., can be added to graphene for the enhancement of the dielectric and magnetic loss. In addition to the multicomponent system, structural design is an effective approach for improving the microwave absorption ability. The most widely used structures for the enhancement of microwave absorption include multilayer structures, core–shell structures, hierarchical structures, porous foam structures, and combinations of these. Such structures always have two basic purposes: improving the impedance matching and increasing the dissipation ability. They either facilitate the entrance of electromagnetic waves into the absorber by decreasing the surface reflection, increase the interfacial area of composites for stronger interfacial polarization and multiple reflections, or form numerous small heterogeneous cavities for the enhanced dissipation of electromagnetic waves.

MXene is another high-efficiency 2D microwave shield and absorber. Similar to graphene, it has good conductivity and a large specific surface area. MXene has exhibited the highest EMI SE among synthetic materials—even higher than the metals copper and silver. More importantly, the absorption loss is dominant in the attenuation of electromagnetic waves. Several factors lead to the high EMI SE and microwave absorbing ability of MXenes. MXene has high electrical conductivity and a large dielectric constant and can yield large surface reflection and conduction loss. MXene is ultrathin, with a thickness far smaller than the skin depth; thus, electromagnetic waves can penetrate into the interior of MXene-based composites to generate multiple reflections and transmission for sufficient dissipation. The surface of MXene contains numerous functional groups, such as –OH, –O–, and –F, as well as defect sites, resulting in strong dipole polarization and defect polarization, which further enhances the consumption of electromagnetic energy.

Graphene and MXene are both highly conductive. Although a high conductivity is conducive to enhancing conduction loss, a mismatched impedance results in large surface reflection, which is unfavorable for high-performance microwave absorption. Therefore, improving the impedance matching while enhancing the microwave attenuation is a critical issue worthy of study. The introduction of nonconductive 2D materials into highly conductive 2D materials is an effective method for the impedance adjustment of composites. For instance, 2D MoS_2 nanosheets are semiconductive, and when they are introduced into graphene-based or MXenes-based composites, the conductivity and dielectric constant of the composites decrease, and $\sqrt{\frac{\mu_r}{\varepsilon_r}}$ increases, approaching the impedance of free space. According to the transmission-line theory, better impedance matching results in smaller interfacial reflection. In addition, electromagnetic waves can better penetrate into the interior of the absorber and are more fully dissipated. The addition of MoS_2 to graphene or MXene can significantly decrease the RL and boost the absorption bandwidth of the composite system. Other 2D materials, such as oxides, hydroxides, nitrides, and BP, can also act as impedance modulators and dielectric media for the improvement of the impedance matching and the enhancement of the interfacial polarization and multiple reflections. Thus, the incorporation of multinary 2D materials is a versatile method for the composition regulation and structural design of complex absorbers and is an effective approach for optimizing the performance of microwave absorbers.

In addition to 2D materials, other materials can be added to 2D material-based systems. These materials typically include conductive polymers, metals, carbon, dielectric ceramics, and magnetic metals and ferrites. The introduction of such materials can greatly increase the microwave absorption ability of the composite system and broaden the absorption bandwidth, which is attributed to the multimode reflection and absorption mechanisms.

Although remarkable success has been achieved in 2D material-based absorbers, the exploitation of lightweight, ultrathin, strong, and flexible microwave absorbers faces numerous challenges. These challenges generally arise from the nature of microwaves or materials and are thus are very difficult to overcome. First, the wavelength of microwaves is long—generally on the order of millimeters or larger—much bigger than the thickness of ultrathin film, and thus makes dimensional interference effects, such as 1/4-wavelength equation, disabled in such films. Second, the skin depth of nonmetallic materials is large at microwave frequencies. For example, the skin depth of graphite is close to 16 μm at 10 GHz, which means that microwaves can directly penetrate the ultrathin film without obvious loss, making it difficult to achieve high-efficiency loss in ultrathin films. Third, regarding the materials used, many performance parameters are not frequency-dependent; thus, broadband absorption is difficult to achieve in single- and few-material systems. Fourth, high absorption is always accompanied with large reflection, and it is difficult to enhance the absorption while keeping the reflection unchanged or reducing it in ultrathin films. However, the development of ultrathin microwave absorbers is not hopeless. As described previously, MXene-based materials have shown superior EMI SE exceeding that of silver and copper—although with significantly lower bulk conductivity than silver and copper—which provides considerable inspiration and motivation for developing ultrathin absorbers. It appears that the ordered-assembly structure of nanoscale materials is the most straightforward way to achieve ultrathin high-efficiency absorbers. In the known cases, the effects of 2D materials for microwave attenuation are generally better than those of 1D and 0D materials and multicomponent composites, such as composites comprising diverse nanoferrites with different magnetocrystalline anisotropy fields H_a, are more beneficial for broadband microwave absorption. Therefore, to develop well-designed multicomponent 2D material-based composites or 3D nanoporous materials such as MOFs and nanoporous foams, are the most promising approaches to achieve an ultrathin high-efficiency microwave shield and absorber.

In summary, owing to their low cost, good processability, peculiar morphology, and large specific surface area, 2D materials can act as the skeleton, filler, or coating in composites, for optimizing the composition and structure. We believe that, depending on the reasonable structure and composition design, the potential of 2D materials in microwave attenuation can be exploited and that 2D materials will play increasingly important roles in shielding and absorbing electromagnetic waves and probably bring a revolutionary change towards the elimination of electromagnetic pollution in the future. This will allow the large-scale production and application of ultrathin, ultralight, high-strength, and high-efficiency microwave shields and absorbers.

Acknowledgements This work was supported by the National Key R&D Program of China (Grant No. 2016YFE0204200), and the National Natural Science Foundation of China (NSFC, Grant Nos. 51702009 and 21771017).

References

1. M. Ezawa, A topological insulator and helical zero mode in silicene under an inhomogeneous electric field, *New J. Phys.* 14(3), 033003 (2012)
2. Q. Liu, X. Zhang, L. B. Abdalla, A. Fazzio, and A. Zunger, Switching a normal insulator into a topological insulator via electric field with application to phosphorene, *Nano Lett.* 15(2), 1222 (2015)
3. F. F. Zhu, W. J. Chen, Y. Xu, C. L. Gao, D. D. Guan, C. H. Liu, D. Qian, S. C. Zhang, and J. F. Jia, Epitaxial growth of two-dimensional stanene, *Nat. Mater.* 14(10), 1020 (2015)
4. C. Xu, L. Wang, Z. Liu, L. Chen, J. Guo, N. Kang, X. L. Ma, H. M. Cheng, and W. Ren, Large-area high-quality 2D ultrathin Mo_2C superconducting crystals, *Nat. Mater.* 14(11), 1135 (2015)
5. C. Gong, L. Li, Z. Li, H. Ji, A. Stern, Y. Xia, T. Cao, W. Bao, C. Wang, Y. Wang, Z. Q. Qiu, R. J. Cava, S. G. Louie, J. Xia, and X. Zhang, Discovery of intrinsic ferromagnetism in two-dimensional van der Waals crystals, *Nature* 546(7657), 265 (2017)
6. B. Huang, G. Clark, E. Navarro-Moratalla, D. R. Klein, R. Cheng, K. L. Seyler, D. Zhong, E. Schmidgall, M. A.

McGuire, D. H. Cobden, W. Yao, D. Xiao, P. Jarillo-Herrero, and X. Xu, Layer-dependent ferromagnetism in a van der Waals crystal down to the monolayer limit, *Nature* 546(7657), 270 (2017)

7. N. Miao, B. Xu, N. C. Bristowe, J. Zhou, and Z. Sun, Tunable magnetism and extraordinary sunlight absorbance in indium triphosphide monolayer, *J. Am. Chem. Soc.* 139(32), 11125 (2017)
8. N. Miao, B. Xu, L. Zhu, J. Zhou, and Z. Sun, Z. Sun, 2d intrinsic ferromagnets from van der Waals antiferromagnets, *J. Am. Chem. Soc.* 140(7), 2417 (2018)
9. G. R. Bhimanapati, Z. Lin, V. Meunier, Y. Jung, J. Cha, S. Das, D. Xiao, Y. Son, M. S. Strano, V. R. Cooper, L. B. Liang, S. G. Louie, E. Ringe, W. Zhou, S. S. Kim, R. R. Naik, B. G. Sumpter, H. Terrones, F. N. Xia, Y. L. Wang, J. Zhu, D. Akinwande, N. Alem, J. A. Schuller, R. E. Schaak, M. Terrones, and J. A. Robinson, Recent advances in two-dimensional materials beyond graphene, *ACS Nano* 9(12), 11509 (2015)
10. D. H. Deng, K. S. Novoselov, Q. Fu, N. F. Zheng, Z. Q. Tian, and X. H. Bao, Catalysis with two-dimensional materials and their heterostructures, *Nat. Nanotechnol.* 11(3), 218 (2016)
11. C. L. Tan, X. H. Cao, X. J. Wu, Q. Y. He, J. Yang, X. Zhang, J. Z. Chen, W. Zhao, S. K. Han, G. H. Nam, M. Sindoro, and H. Zhang, Recent advances in ultrathin two-dimensional nanomaterials, *Chem. Rev.* 117(9), 6225 (2017)
12. H. J. Yin and Z. Y. Tang, Ultrathin two-dimensional layered metal hydroxides: An emerging platform for advanced catalysis, energy conversion and storage, *Chem. Soc. Rev.* 45(18), 4873 (2016)
13. J. S. Li, H. Huang, Y. J. Zhou, C. Y. Zhang, and Z. T. Li, Research progress of graphene-based microwave absorbing materials in the last decade, *J. Mater. Res.* 32(07), 1213 (2017)
14. H. Lv, Y. Guo, Z. Yang, Y. Cheng, L. P. Wang, B. Zhang, Y. Zhao, Z. J. Xu, and G. Ji, A brief introduction to the fabrication and synthesis of graphene based composites for the realization of electromagnetic absorbing materials, *J. Mater. Chem. C* 5(3), 491 (2017)
15. S. A. Schelkunoff, Electromagnetic Waves, New York: Van Nostrand, 1943
16. F. Qin and C. Brosseau, A review and analysis of microwave absorption in polymer composites filled with carbonaceous particles, *J. Appl. Phys.* 111(6), 061301 (2012)
17. Y. Naito and K. Suetake, Application of ferrite to electromagnetic wave absorber and its characteristics, *IEEE T. Microw. Theory* 19(1), 65 (1971)
18. M. Wu, Y. D. Zhang, S. Hui, T. D. Xiao, S. Ge, W. A. Hines, J. I. Budnick, and G. W. Taylor, Microwave magnetic properties of $Co_{50}/(SiO_2)_{50}$ nanoparticles, *Appl. Phys. Lett.* 80(23), 4404 (2002)
19. O. Acher and S. Dubourg, Generalization of Snoek's law to ferromagnetic films and composites, *Phys. Rev. B* 77(10), 104440 (2008)
20. J. M. Thomassin, C. Jerome, T. Pardoen, C. Bailly, I. Huynen, and C. Detrembleur, Polymer/carbon based composites as electromagnetic interference (EMI) shielding materials, *Mater. Sci. Eng. Rep.* 74(7), 211 (2013)
21. Y. I. Bhattacharjee, I. Arief, and S. Bose, Recent trends in multi-layered architectures towards screening electromagnetic radiation: challenges and perspectives, *J. Mater. Chem. C* 5(30), 7390 (2017)
22. S. Geetha, K. K. Satheesh Kumar, C. R. K. Rao, M. Vijayan, and D. C. Trivedi, EMI shielding: Methods and materials-a review, *J. Appl. Polym. Sci.* 112(4), 2073 (2009)
23. D. Micheli, R. Pastore, C. Apollo, P. B. Morles, M. Marchetti, and G. Gradoni, in: Electromagnetic Characterization of Composite Materials and Microwave Absorbing Modeling, edited by B. Reddy, India: InTech, 2011, p. 359
24. K. S. Novoselov, A. K. Geim, S. V. Morozov, D. Jiang, Y. Zhang, S. V. Dubonos, I. V. Grigorieva, and A. A. Firsov, Electric field effect in atomically thin carbon films, *Science* 306(5696), 666 (2004)
25. S. Stankovich, D. A. Dikin, G. H. B. Dommett, K. M. Kohlhaas, E. J. Zimney, E. A. Stach, R. D. Piner, S. T. Nguyen, and R. S. Ruoff, Graphene-based composite materials, *Nature* 442(7100), 282 (2006)
26. S. K. Hong, K. Y. Kim, T. Y. Kim, J. H. Kim, S. W. Park, J. H. Kim, and B. J. Cho, Electromagnetic interference shielding effectiveness of monolayer graphene, *Nanotechnology* 23(45), 455704 (2012)
27. B. Shen, W. Zhai, and W. Zheng, Ultrathin flexible graphene film: An excellent thermal conducting material with efficient EMI shielding, *Adv. Funct. Mater.* 24(28), 4542 (2014)
28. C. Wang, X. J. Han, P. Xu, X. L. Zhang, Y. C. Du, S. R. Hu, J. Y. Wang, and X. H. Wang, The electromagnetic property of chemically reduced graphene oxide and its application as microwave absorbing material, *Appl. Phys. Lett.* 98(7), 072906 (2011)
29. P. Kumar, F. Shahzad, S. Yu, S. M. Hong, Y. H. Kim, and C. M. Koo, Large-area reduced graphene oxide thin film with excellent thermal conductivity and electromagnetic interference shielding effectiveness, *Carbon* 94, 494 (2015)
30. Z. Lu, L. Ma, J. Tan, H. Wang, and X. Ding, Transparent multi-layer graphene/polyethylene terephthalate structures with excellent microwave absorption and electromagnetic interference shielding performance, *Nanoscale* 8(37), 16684 (2016)
31. X. Bai, Y. H. Zhai, and Y. Zhang, Green approach to prepare graphene-based composites with high microwave absorption capacity, *J. Phys. Chem. C* 115(23), 11673 (2011)

32. Y. J. Chen, G. Xiao, T. S. Wang, Q. Y. Ouyang, L. H. Qi, Y. Ma, P. Gao, C. L. Zhu, M. S. Cao, and H. B. Jin, Porous Fe_3O_4/carbon core/shell nanorods: Synthesis and electromagnetic properties, *J. Phys. Chem. C* 115(28), 13603 (2011)

33. K. Batrakov, P. Kuzhir, S. Maksimenko, A. Paddubskaya, S. Voronovich, P. Lambin, T. Kaplas, and Y. Svirko, Flexible transparent graphene/polymer multilayers for efficient electromagnetic field absorption, *Sci. Rep.* 4(1), 7191 (2015)

34. V. K. Singh, A. Shukla, M. K. Patra, L. Saini, R. K. Jani, S. R. Vadera, and N. Kumar, Microwave absorbing properties of a thermally reduced graphene oxide/nitrile butadiene rubber composite, *Carbon* 50(6), 2202 (2012)

35. S. T. Hsiao, C. C. M. Ma, H. W. Tien, W. H. Liao, Y. S. Wang, S. M. Li, C. Y. Yang, S. C. Lin, and R. B. Yang, Effect of covalent modification of graphene nanosheets on the electrical property and electromagnetic interference shielding performance of a waterborne polyurethane composite, *ACS Appl. Mater. Interfaces* 7(4), 2817 (2015)

36. B. Quan, X. Liang, G. Ji, Y. Cheng, W. Liu, J. Ma, Y. Zhang, D. Li, and G. Xu, Dielectric polarization in electromagnetic wave absorption: Review and perspective, *J. Alloys Compd.* 728, 1065 (2017)

37. X. J. Zhao, W. P. Liu, X. B. Jiang, K. Liu, G. R. Peng, and Z. J. Zhan, Exploring the relationship of dielectric relaxation behavior and discharge efficiency of P(VDF-HFP)/PMMA blends by dielectric spectroscopy, *Mater. Res. Express* 3(7), 075304 (2016)

38. F. Wu, Y. L. Xia, Y. Wang, and M. Y. Wang, Two-step reduction of self-assembled three-dimensional (3D) reduced graphene oxide (RGO)/zinc oxide (ZnO) nanocomposites for electromagnetic absorption, *J. Mater. Chem. A* 2(47), 20307 (2014)

39. P. B. Liu and Y. Huang, Synthesis of reduced graphene oxide-conducting polymers-Co_3O_4 composites and their excellent microwave absorption properties, *RSC Advances* 3(41), 19033 (2013)

40. J. N. Ma, W. Liu, B. Quan, X. H. Liang, and G. B. Ji, Incorporation of the polarization point on the graphene aerogel to achieve strong dielectric loss behavior, *J. Colloid Interface Sci.* 504, 479 (2017)

41. X. H. Liang, B. Quan, G. B. Ji, W. Liu, H. Q. Zhao, S. S. Dai, J. Lv, and Y. W. Du, Tunable dielectric performance derived from the metal–organic framework/reduced graphene oxide hybrid with broadband absorption, *ACS Sustain. Chem. & Eng.* 5(11), 10570 (2017)

42. X. N. Chen, F. C. Meng, Z. W. Zhou, X. Tian, L. M. Shan, S. B. Zhu, X. L. Xu, M. Jiang, L. Wang, D. Hui, Y. Wang, J. Lu, and J. H. Gou, One-step synthesis of graphene/polyaniline hybrids by in situ intercalation polymerization and their electromagnetic properties, *Nanoscale* 6(14), 8140 (2014)

43. W. L. Song, J. Wang, L. Z. Fan, Y. Li, C. Y. Wang, and M. S. Cao, Interfacial engineering of carbon nanofiber-graphene-carbon nanofiber heterojunctions in flexible lightweight electromagnetic shielding networks, *ACS Appl. Mater. Interfaces* 6(13), 10516 (2014)

44. T. K. Gupta, B. P. Singh, R. B. Mathur, and S. R. Dhakate, Multi-walled carbon nanotube-graphene-polyaniline multiphase nanocomposite with superior electromagnetic shielding effectiveness, *Nanoscale* 6(2), 842 (2014)

45. T. K. Gupta, B. P. Singh, V. N. Singh, S. Teotia, A. P. Singh, I. Elizabeth, S. R. Dhakate, S. K. Dhawan, and R. B. Mathur, MnO_2 decorated graphene nanoribbons with superior permittivity and excellent microwave shielding properties, *J. Mater. Chem. A* 2(12), 4256 (2014)

46. X. J. Zhang, G. S. Wang, Y. Z. Wei, L. Guo, and M. S. Cao, Polymer-composite with high dielectric constant and enhanced absorption properties based on graphene-CuS nanocomposites and polyvinylidene fluoride, *J. Mater. Chem. A* 1(39), 12115 (2013)

47. X. J. Zhang, G. S. Wang, W. Q. Cao, Y. Z. Wei, M. S. Cao, and L. Guo, Fabrication of multi-functional PVDF/RGO composites via a simple thermal reduction process and their enhanced electromagnetic wave absorption and dielectric properties, *RSC Advances* 4(38), 19594 (2014)

48. M. K. Han, X. W. Yin, L. Kong, M. Li, W. Y. Duan, L. T. Zhang, and L. F. Cheng, Graphene-wrapped ZnO hollow spheres with enhanced electromagnetic wave absorption properties, *J. Mater. Chem. A* 2(39), 16403 (2014)

49. Y. L. Ren, H. Y. Wu, M. M. Lu, Y. J. Chen, C. L. Zhu, P. Gao, M. S. Cao, C. Y. Li, and Q. Y. Ouyang, Quaternary nanocomposites consisting of graphene, Fe_3O_4@Fe core@shell, and ZnO nanoparticles: Synthesis and excellent electromagnetic absorption properties, *ACS Appl. Mater. Interfaces* 4(12), 6436 (2012)

50. Y. Li and G. Li, Physics of Ferrites, Beijing: Science Press, 1978, p. 335

51. S. T. Zhang and W. Li, Condensed State Magnetic Physics, Beijing: Science Press, 2003, p. 393

52. X. J. Zhang, G. S. Wang, W. Q. Cao, Y. Z. Wei, J. F. Liang, L. Guo, and M. S. Cao, Enhanced microwave absorption property of reduced graphene oxide (RGO)-$MnFe_2O_4$ nanocomposites and polyvinylidene fluoride, *ACS Appl. Mater. Interfaces* 6(10), 7471 (2014)

53. Z. T. Zhu, X. Sun, H. R. Xue, H. Guo, X. L. Fan, X. C. Pan, and J. P. He, Graphene-carbonyl iron cross-linked composites with excellent electromagnetic wave absorption properties, *J. Mater. Chem. C* 2(32), 6582 (2014)

54. Y. Qing, D. Min, Y. Zhou, F. Luo, and W. Zhou, Graphene nanosheet- and flake carbonyl iron particle-filled epoxy-silicone composites as thin-thickness and wide-bandwidth microwave absorber, *Carbon* 86, 98 (2015)

55. T. T. Chen, F. Deng, J. Zhu, C. F. Chen, G. B. Sun, S. L. Ma, and X. J. Yang, Hexagonal and cubic Ni nanocrystals grown on graphene: Phase-controlled synthesis, characterization and their enhanced microwave absorption properties, *J. Mater. Chem.* 22(30), 15190 (2012)

56. X. H. Li, J. Feng, Y. P. Du, J. T. Bai, H. M. Fan, H. L. Zhang, Y. Peng, and F. S. Li, One-pot synthesis of $CoFe_2O_4$/graphene oxide hybrids and their conversion into FeCo/graphene hybrids for lightweight and highly efficient microwave absorber, *J. Mater. Chem. A Mater. Energy Sustain.* 3(10), 5535 (2015)

57. L. N. Wang, X. L. Jia, Y. F. Li, F. Yang, L. Q. Zhang, L. P. Liu, X. Ren, and H. T. Yang, Synthesis and microwave absorption property of flexible magnetic film based on graphene oxide/carbon nanotubes and Fe_3O_4 nanoparticles, *J. Mater. Chem. A* 2(36), 14940 (2014)

58. D. P. Sun, Q. Zou, Y. P. Wang, Y. J. Wang, W. Jiang, and F. S. Li, Controllable synthesis of porous Fe_3O_4@Zno sphere decorated graphene for extraordinary electromagnetic wave absorption, *Nanoscale* 6(12), 6557 (2014)

59. H. Lv, G. Ji, X. Liang, H. Zhang, and Y. Du, A novel rod-like MnO_2@Fe loading on graphene giving excellent electromagnetic absorption properties, *J. Mater. Chem. C* 3(19), 5056 (2015)

60. L. Wang, Y. Huang, X. Sun, H. J. Huang, P. B. Liu, M. Zong, and Y. Wang, Synthesis and microwave absorption enhancement of graphene@Fe_3O_4@SiO_2@NiO nanosheet hierarchical structures, *Nanoscale* 6(6), 3157 (2014)

61. A. P. Singh, P. Garg, F. Alam, K. Singh, R. B. Mathur, R. P. Tandon, A. Chandra, and S. K. Dhawan, Phenolic resin-based composite sheets filled with mixtures of reduced graphene oxide, gamma-Fe_2O_3 and carbon fibers for excellent electromagnetic interference shielding in the X-band, *Carbon* 50(10), 3868 (2012)

62. H. L. Xu, H. Bi, and R. B. Yang, Enhanced microwave absorption property of bowl-like Fe_3O_4 hollow spheres/reduced graphene oxide composites, *J. Appl. Phys.* 111, 07A522 (2012)

63. K. Singh, A. Ohlan, V. H. Pham, B. R, S. Varshney, J. Jang, S. H. Hur, W. M. Choi, M. Kumar, S. K. Dhawan, B.S. Kong, and J. S. Chung, Nanostructured graphene/Fe_3O_4 incorporated polyaniline as a high performance shield against electromagnetic pollution, *Nanoscale* 5(6), 2411 (2013)

64. Y. Chen, Y. Li, M. Yip, and N. Tai, Electromagnetic interference shielding efficiency of polyaniline composites filled with graphene decorated with metallic nanoparticles, *Compos. Sci. Technol.* 80, 80 (2013)

65. Y. J. Chen, Z. Y. Lei, H. Y. Wu, C. L. Zhu, P. Gao, Q. Y. Ouyang, L. H. Qi, and W. Qin, Electromagnetic absorption properties of graphene/Fe nanocomposites, *Mater. Res. Bull.* 48(9), 3362 (2013)

66. X. C. Zhao, Z. M. Zhang, L. Y. Wang, K. Xi, Q. Q. Cao, D. H. Wang, Y. Yang, and Y. W. Du, Excellent microwave absorption property of graphene-coated Fe nanocomposites, *Sci. Rep.* 3(1), 3421 (2013)

67. G. Z. Wang, Z. Gao, G. P. Wan, S. W. Lin, P. Yang, and Y. Qin, High densities of magnetic nanoparticles supported on graphene fabricated by atomic layer deposition and their use as efficient synergistic microwave absorbers, *Nano Res.* 7(5), 704 (2014)

68. J. Feng, F. Z. Pu, Z. X. Li, X. H. Li, X. Y. Hu, and J. T. Bai, Interfacial interactions and synergistic effect of CoNi nanocrystals and nitrogen-doped graphene in a composite microwave absorber, *Carbon* 104, 214 (2016)

69. C. G. Hu, Z. Y. Mou, G. W. Lu, N. Chen, Z. L. Dong, M. J. Hu, and Qu, graphene-Fe_3O_4 nanocomposites with high-performance microwave absorption, *Phys. Chem. Chem. Phys.* 15(31), 13038 (2013)

70. X. H. Li, H. B. Yi, J. W. Zhang, J. Feng, F. S. Li, D. S. Xue, H. L. Zhang, Y. Peng, and N. J. Mellors, Fe_3O_4-graphene hybrids: Nanoscale characterization and their enhanced electromagnetic wave absorption in gigahertz range, *J. Nanopart. Res.* 15(3), 1472 (2013)

71. X. L. Zheng, J. Feng, Y. Zong, H. Miao, X. Y. Hu, J. T. Bai, and X. H. Li, Hydrophobic graphene nanosheets decorated by monodispersed superparamagnetic Fe_3O_4 nanocrystals as synergistic electromagnetic wave absorbers, *J. Mater. Chem. C* 3(17), 4452 (2015)

72. T. S. Wang, Z. H. Liu, M. M. Lu, B. Wen, Q. Y. Ouyang, Y. J. Chen, C. L. Zhu, P. Gao, C. Y. Li, M. S. Cao, and L. H. Qi, Graphene-Fe_3O_4 nanohybrids: Synthesis and excellent electromagnetic absorption properties, *J. Appl. Phys.* 113(2), 024314 (2013)

73. D. Z. Chen, G. S. Wang, S. He, J. Liu, L. Guo, and M. S. Cao, Controllable fabrication of mono-dispersed RGO-hematite nanocomposites and their enhanced wave absorption properties, *J. Mater. Chem. A* 1(19), 5996 (2013)

74. L. Kong, X. W. Yin, Y. J. Zhang, X. Y. Yuan, Q. Li, F. Ye, L. F. Cheng, and L. T. Zhang, Electromagnetic wave absorption properties of reduced graphene oxide modified by maghemite colloidal nanoparticle clusters, *J. Phys. Chem. C* 117(38), 19701 (2013)

75. M. Fu, Q. Z. Jiao, Y. Zhao, and H. S. Li, Vapor diffusion synthesis of $CoFe_2O_4$ hollow sphere/graphene composites as absorbing materials, *J. Mater. Chem. A* 2(3), 735 (2014)

76. M. Zong, Y. Huang, H. W. Wu, Y. Zhao, Q. F. Wang, and X. Sun, One-pot hydrothermal synthesis of rGO/$CoFe_2O_4$ composite and its excellent microwave absorption properties, *Mater. Lett.* 114, 52 (2014)

77. X. H. Li, J. Feng, H. Zhu, C. H. Qu, J. T. Bai, and X. L. Zheng, Sandwich-like graphene nanosheets decorated with superparamagnetic $CoFe_2O_4$ nanocrystals and their application as an enhanced electromagnetic wave absorber, *RSC Advances* 4(63), 33619 (2014)

78. M. Fu, Q. Z. Jiao, and Y. Zhao, Preparation of $NiFe_2O_4$ nanorod-graphene composites via an ionic liquid assisted one-step hydrothermal approach and their microwave absorbing properties, *J. Mater. Chem. A* 1(18), 5577 (2013)

79. J. Z. He, X. X. Wang, Y. L. Zhang, and M. S. Cao, Small magnetic nanoparticles decorating reduced graphene oxides to tune the electromagnetic attenuation capacity, *J. Mater. Chem. C* 4(29), 7130 (2016)

80. H. L. Lv, Y. H. Guo, G. L. Wu, G. B. Ji, Y. Zhao, and Z. C. J. Xu, Interface polarization strategy to solve electromagnetic wave interference issue, *ACS Appl. Mater. Interfaces* 9(6), 5660 (2017)

81. X. B. Li, S. W. Yang, J. Sun, P. He, X. P. Pu, and G. Q. Ding, Enhanced electromagnetic wave absorption performances of Co_3O_4 nanocube/reduced graphene oxide composite, *Synth. Met.* 194, 52 (2014)

82. M. Verma, A. P. Singh, P. Sambyal, B. P. Singh, S. K. Dhawan, and V. Choudhary, Barium ferrite decorated reduced graphene oxide nanocomposite for effective electromagnetic interference shielding, *Phys. Chem. Chem. Phys.* 17(3), 1610 (2015)

83. B. Qu, C. L. Zhu, C. Y. Li, X. T. Zhang, and Y. J. Chen, Coupling hollow Fe_3O_4-Fe nanoparticles with graphene sheets for high-performance electromagnetic wave absorbing material, *ACS Appl. Mater. Interfaces* 8(6), 3730 (2016)

84. A. P. Singh, M. Mishra, A. Chandra, and S. K. Dhawan, Graphene oxide/ferrofluid/cement composites for electromagnetic interference shielding application, *Nanotechnology* 22(46), 465701 (2011)

85. W. L. Song, L. Z. Fan, M. S. Cao, M. M. Lu, C. Y. Wang, J. Wang, T. T. Chen, Y. Li, Z. L. Hou, J. Liu, and Y. P. Sun, Facile fabrication of ultrathin graphene papers for effective electromagnetic shielding, *J. Mater. Chem. C* 2(25), 5057 (2014)

86. W. L. Song, M. S. Cao, M. M. Lu, J. Yang, H. F. Ju, Z. L. Hou, J. Liu, J. Yuan, and L. Z. Fan, Alignment of graphene sheets in wax composites for electromagnetic interference shielding improvement, *Nanotechnology* 24(11), 115708 (2013)

87. W. L. Song, M. S. Cao, M. M. Lu, S. Bi, C. Y. Wang, J. Liu, J. Yuan, and L. Z. Fan, Flexible graphene/polymer composite films in sandwich structures for effective electromagnetic interference shielding, *Carbon* 66, 67 (2014)

88. N. Yousefi, X. Sun, X. Lin, X. Shen, J. Jia, B. Zhang, B. Tang, M. Chan, and J. K. Kim, Highly aligned graphene/polymer nanocomposites with excellent dielectric properties for high-performance electromagnetic interference shielding, *Adv. Mater.* 26(31), 5480 (2014)

89. A. P. Singh, M. Mishra, D. P. Hashim, T. N. Narayanan, M. G. Hahm, P. Kumar, J. Dwivedi, G. Kedawat, A. Gupta, B. P. Singh, A. Chandra, R. Vajtai, S. K. Dhawan, P. M. Ajayan, and B. K. Gupta, Probing the engineered sandwich network of vertically aligned carbon nanotube-reduced graphene oxide composites for high performance electromagnetic interference shielding applications, *Carbon* 85, 79 (2015)

90. H. L. Lv, Z. H. Yang, P. L. Wang, G. B. Ji, J. Z. Song, L. R. Zheng, H. B. Zeng, and Z. C. J. Xu, A voltage-boosting strategy enabling a low-frequency, flexible electromagnetic wave absorption device, *Adv. Mater.* 30(15), 1706343 (2018)

91. J. Feng, Y. Hou, Y. Wang, and L. Li, Synthesis of hierarchical $ZnFe_2O_4$@SiO_2@rGO core-shell microspheres for enhanced electromagnetic wave absorption, *ACS Appl. Mater. Interfaces* 9(16), 14103 (2017)

92. Y. F. Pan, G. S. Wang, and Y. H. Yue, Fabrication of Fe_3O_4@SiO_2@rGO nanocomposites and their excellent absorption properties with low filler content, *RSC Advances* 5(88), 71718 (2015)

93. S. Li, Y. Huang, X. Ding, N. Zhang, M. Zong, M. Wang, and J. Liu, Synthesis of core-shell FeCo@SiO_2 particles coated with the reduced graphene oxide as an efficient broadband electromagnetic wave absorber, *J. Mater. Sci.: Mater. Electron.* 28(21), 15782 (2017)

94. X. Liu, L. S. Wang, Y. Ma, Y. Qiu, Q. Xie, Y. Chen, and D. L. Peng, Facile synthesis and microwave absorption properties of yolk-shell ZnO-Ni-C/RGO composite materials, *Chem. Eng. J.* 333, 92 (2018)

95. D. X. Yan, H. Pang, B. Li, R. Vajtai, L. Xu, P. G. Ren, J. H. Wang, and Z. M. Li, Structured reduced graphene oxide/polymer composites for ultra-efficient electromagnetic interference shielding, *Adv. Funct. Mater.* 25(4), 559 (2015)

96. X. Jian, B. Wu, Y. Wei, S. X. Dou, X. Wang, W. He, and N. Mahmood, Facile synthesis of Fe_3O_4/GCS composites and their enhanced microwave absorption properties, *ACS Appl. Mater. Interfaces* 8(9), 6101 (2016)

97. Q. Song, F. Ye, X. Yin, W. Li, H. Li, Y. Liu, K. Li, K. Xie, X. Li, Q. Fu, L. Cheng, L. Zhang, and B. Wei, Carbon nanotube-multilayered graphene edge plane core-shell hybrid foams for ultrahigh-performance electromagnetic-interference shielding, *Adv. Mater.* 29(31), 1701583 (2017)

98. L. Wang, Y. Huang, C. Li, J. J. Chen, and X. Sun, Hierarchical graphene@Fe_3O_4 nanocluster@carbon@MnO_2 nanosheet array composites: Synthesis and microwave absorption performance, *Phys. Chem. Chem. Phys.* 17(8), 5878 (2015)

99. X. M. Bian, L. Liu, H. B. Li, C. Y. Wang, Q. Xie, Q. L. Zhao, S. Bi, and Z. L. Hou, Construction of three-dimensional graphene interfaces into carbon fiber textiles for increasing deposition of nickel nanoparticles: Flexible hierarchical magnetic textile composites for strong electromagnetic shielding, *Nanotechnology* 28(4), 045710 (2017)

100. Y. Wang, Y. Fu, X. Wu, W. Zhang, Q. Wang, and J. Li, Synthesis of hierarchical core-shell $NiFe_2O_4$@MnO_2 composite microspheres decorated graphene nanosheet for enhanced microwave absorption performance, *Ceram. Int.* 43(14), 11367 (2017)

101. X. Zhang, Y. Huang, X. Chen, C. Li, and J. Chen, Hierarchical structures of graphene@$CoFe_2O_4$@SiO_2@TiO_2 nanosheets: Synthesis and excellent microwave absorption properties, *Mater. Lett.* 158, 380 (2015)

102. H. L. Yu, T. S. Wang, B. Wen, M. M. Lu, Z. Xu, C. L. Zhu, Y. J. Chen, X. Y. Xue, C. W. Sun, and M. S. Cao, Graphene/polyaniline nanorod arrays: Synthesis and excellent electromagnetic absorption properties, *J. Mater. Chem.* 22(40), 21679 (2012)

103. Y. L. Ren, C. L. Zhu, S. Zhang, C. Y. Li, Y. J. Chen, P. Gao, P. P. Yang, and Q. Y. Ouyang, Three-dimensional SiO_2@Fe_3O_4 core/shell nanorod array/graphene architecture: Synthesis and electromagnetic absorption properties, *Nanoscale* 5(24), 12296 (2013)

104. B. Shen, Y. Li, W. Zhai, and W. Zheng, Compressible graphene-coated polymer foams with ultralow density for adjustable electromagnetic interference (EMI) shielding, *ACS Appl. Mater. Interfaces* 8(12), 8050 (2016)

105. V. Eswaraiah, V. Sankaranarayanan, and S. Ramaprabhu, Functionalized graphene-PVDF foam composites for EMI shielding, *Macromol. Mater. Eng.* 296(10), 894 (2011)

106. H. B. Zhang, Q. Yan, W. G. Zheng, Z. He, and Z. Z. Yu, Tough graphene-polymer microcellular foams for electromagnetic interference shielding, *ACS Appl. Mater. Interfaces* 3(3), 918 (2011)

107. D. X. Yan, P. G. Ren, H. Pang, Q. Fu, M. B. Yang, and Z. M. Li, Efficient electromagnetic interference shielding of lightweight graphene/polystyrene composite, *J. Mater. Chem.* 22(36), 18772 (2012)

108. H. Zhang, A. J. Xie, C. P. Wang, H. S. Wang, Y. H. Shen, and X. Y. Tian, Novel RGO/alpha-Fe_2O_3 composite hydrogel: Synthesis, characterization and high performance of electromagnetic wave absorption, *J. Mater. Chem. A* 1(30), 8547 (2013)

109. W. L. Song, X. T. Guan, L. Z. Fan, W. Q. Cao, C. Y. Wang, and M. S. Cao, Tuning three-dimensional textures with graphene aerogels for ultra-light flexible graphene/texture composites of effective electromagnetic shielding, *Carbon* 93, 151 (2015)

110. F. Wu, A. M. Xie, M. X. Sun, Y. Wang, and M. Y. Wang, Reduced graphene oxide (rGO) modified spongelike polypyrrole (PPy) aerogel for excellent electromagnetic absorption, *J. Mater. Chem. A* 3(27), 14358 (2015)

111. Y. Zhang, Y. Huang, T. F. Zhang, H. C. Chang, P. S. Xiao, H. H. Chen, Z. Y. Huang, and Y. S. Chen, Broadband and tunable high-performance microwave absorption of an ultralight and highly compressible graphene foam, *Adv. Mater.* 27(12), 2049 (2015)

112. B. Shen, Y. Li, D. Yi, W. Zhai, X. Wei, and W. Zheng, Microcellular graphene foam for improved broadband electromagnetic interference shielding, *Carbon* 102, 154 (2016)

113. B. Shen, W. Zhai, M. Tao, J. Ling, and W. Zheng, Lightweight, multifunctional polyetherimide/graphene@Fe_3O_4 composite foams for shielding of electromagnetic pollution, *ACS Appl. Mater. Interfaces* 5(21), 11383 (2013)

114. Y. Zhang, Y. Huang, H. H. Chen, Z. Y. Huang, Y. Yang, P. S. Xiao, Y. Zhou, and Y. S. Chen, Composition and structure control of ultralight graphene foam for high-performance microwave absorption, *Carbon* 105, 438 (2016)

115. Z. Chen, C. Xu, C. Ma, W. Ren, and H. M. Cheng, Lightweight and flexible graphene foam composites for high-performance electromagnetic interference shielding, *Adv. Mater.* 25(9), 1296 (2013)

116. J. Ling, W. Zhai, W. Feng, B. Shen, J. Zhang, and W. G. Zheng, Facile preparation of lightweight microcellular polyetherimide/graphene composite foams for electromagnetic interference shielding, *ACS Appl. Mater. Interfaces* 5(7), 2677 (2013)

117. J. He, P. Lyu, and P. Nachtigall, New two-dimensional Mn-based MXenes with room temperature ferromagnetism and half-metallicity, *J. Mater. Chem. C* 4(47), 11143 (2016)

118. F. Shahzad, M. Alhabeb, C. B. Hatter, B. Anasori, S. Man Hong, C. M. Koo, and Y. Gogotsi, Electromagnetic interference shielding with 2D transition metal carbides (MXenes), *Science* 353(6304), 1137 (2016)

119. M. Han, X. Yin, H. Wu, Z. Hou, C. Song, X. Li, L. Zhang, and L. Cheng, Ti_3C_2 mxenes with modified surface for high-performance electromagnetic absorption and shielding in the X-band, *ACS Appl. Mater. Interfaces* 8(32), 21011 (2016)

120. Y. Qing, W. Zhou, F. Luo, and D. Zhu, Titanium carbide (mxene) nanosheets as promising microwave absorbers, *Ceram. Int.* 42(14), 16412 (2016)

121. W. L. Feng, H. Luo, Y. Wang, S. F. Zeng, L. W. Deng, X. S. Zhou, H. B. Zhang, and S. M. Peng, Ti_3C_2 mxene: A promising microwave absorbing material, *RSC Advances* 8(5), 2398 (2018)

122. J. Liu, H. B. Zhang, R. Sun, Y. Liu, Z. Liu, A. Zhou, and Z. Z. Yu, Hydrophobic, flexible, and lightweight MXene foams for high-performance electromagnetic-interference shielding, *Adv. Mater.* 29(38), 1702367 (2017)

123. R. H. Sun, H. B. Zhang, J. Liu, X. Xie, R. Yang, Y. Li, S. Hong, and Z. Z. Yu, Highly conductive transition metal carbide/carbonitride(MXene)@polystyrene nanocomposites fabricated by electrostatic assembly for highly efficient electromagnetic interference shielding, *Adv. Funct. Mater.* 27(45), 1702807 (2017)

124. X. L. Li, X. W. Yin, M. K. Han, C. Q. Song, H. L. Xu, Z. X. Hou, L. T. Zhang, and L. F. Cheng, Ti_3C_2 mxenes modified with in situ grown carbon nanotubes for enhanced electromagnetic wave absorption properties, *J. Mater. Chem. C* 5(16), 4068 (2017)

125. Y. B. Li, X. Zhou, J. Wang, Q. H. Deng, M. A. Li, S. Y. Du, Y. H. Han, J. Lee, and Q. Huang, Facile preparation of in situ coated $Ti_3C_2T_x/Ni_{0.5}Zn_{0.5}Fe_2O_4$ composites and their electromagnetic performance, *RSC Advances* 7(40), 24698 (2017)
126. Y. Qian, H. W. Wei, J. D. Dong, Y. Z. Du, X. J. Fang, W. H. Zheng, Y. T. Sun, and Z. X. Jiang, Fabrication of urchin-like ZnO-MXene nanocomposites for high-performance electromagnetic absorption, *Ceram. Int.* 43(14), 10757 (2017)
127. Y. Qing, H. Nan, F. Luo, and W. Zhou, Nitrogen-doped graphene and titanium carbide nanosheet synergistically reinforced epoxy composites as high-performance microwave absorbers, *RSC Advances* 7(44), 27755 (2017)
128. H. B. Yang, J. J. Dai, X. Liu, Y. Lin, J. J. Wang, L. Wang, and F. Wang, Layered $PVB/Ba_3Co_2Fe_{24}O_{41}/Ti_3C_2$ mxene composite: Enhanced electromagnetic wave absorption properties with high impedance match in a wide frequency range, *Mater. Chem. Phys.* 200, 179 (2017)
129. M. K. Han, X. W. Yin, X. L. Li, B. Anasori, L. T. Zhang, L. F. Cheng, and Y. Gogotsi, Laminated and two-dimensional carbon-supported microwave absorbers derived from mxenes, *ACS Appl. Mater. Interfaces* 9(23), 20038 (2017)
130. X. Li, X. Yin, M. Han, C. Song, X. Sun, H. Xu, L. Cheng, and L. Zhang, A controllable heterogeneous structure and electromagnetic wave absorption properties of Ti_2CT_x mxene, *J. Mater. Chem. C* 5(30), 7621 (2017)
131. X. Liang, X. Zhang, W. Liu, D. Tang, B. Zhang, and G. Ji, A simple hydrothermal process to grow MoS_2 nanosheets with excellent dielectric loss and microwave absorption performance, *J. Mater. Chem. C* 4(28), 6816 (2016)
132. X. J. Zhang, S. Li, S. W. Wang, Z. J. Yin, J. Q. Zhu, A. P. Guo, G. S. Wang, P. G. Yin, and L. Guo, Self-supported construction of three-dimensional MoS_2 hierarchical nanospheres with tunable high-performance microwave absorption in broadband, *J. Phys. Chem. C* 120(38), 22019 (2016)
133. B. Quan, X. Liang, G. Xu, Y. Cheng, Y. Zhang, W. Liu, G. Ji, and Y. Du, A permittivity regulating strategy to achieve high-performance electromagnetic wave absorbers with compatibility of impedance matching and energy conservation, *New J. Chem.* 41(3), 1259 (2017)
134. L. Bai, Y. Wang, F. Li, D. An, Z. Zhang, and Y. Liu, Enhanced electromagnetic wave absorption properties of MoS_2-graphene hybrid nanosheets prepared by a hydrothermal method, *J. Sol-Gel Sci. Technol.* 84(1), 104 (2017)
135. A. Xie, M. Sun, K. Zhang, W. Jiang, F. Wu, and M. He, In situ growth of MoS_2 nanosheets on reduced graphene oxide (rGO) surfaces: Interfacial enhancement of absorbing performance against electromagnetic pollution, *Phys. Chem. Chem. Phys.* 18(36), 24931 (2016)
136. Y. Wang, D. Chen, X. Yin, P. Xu, F. Wu, and M. He, Hybrid of MoS_2 and reduced graphene oxide: A lightweight and broadband electromagnetic wave absorber, *ACS Appl. Mater. Interfaces* 7(47), 26226 (2015)
137. X. Wang, W. Zhang, X. Ji, B. Zhang, M. Yu, W. Zhang, and J. Liu, 2D MoS_2/graphene composites with excellent full Ku band microwave absorption, *RSC Advances* 6(108), 106187 (2016)
138. X. Ding, Y. Huang, S. Li, N. Zhang, and J. Wang, 3D architecture reduced graphene oxide-MoS_2 composite: Preparation and excellent electromagnetic wave absorption performance, *Compos. Part A: Appl. Sci. Manuf.* 90, 424 (2016)
139. Y. Sun, W. Zhong, Y. Wang, X. Xu, T. Wang, L. Wu, and Y. Du, MoS_2-based mixed-dimensional van der waals heterostructures: A new platform for excellent and controllable microwave-absorption performance, *ACS Appl. Mater. Interfaces* 9(39), 34243 (2017)
140. X. J. Zhang, S. W. Wang, G. S. Wang, Z. Li, A. P. Guo, J. Q. Zhu, D. P. Liu, and P. G. Yin, Facile synthesis of NiS_2@MoS_2 core-shell nanospheres for effective enhancement in microwave absorption, *RSC Advances* 7(36), 22454 (2017)
141. W. L. Zhang, D. Jiang, X. Wang, B. N. Hao, Y. D. Liu, and J. Liu, Growth of polyaniline nanoneedles on MoS_2 nanosheets, tunable electroresponse, and electromagnetic wave attenuation analysis, *J. Phys. Chem. C* 121(9), 4989 (2017)
142. X. Ding, Y. Huang, S. Li, N. Zhang, and J. Wang, $FeNi_3$ nanoalloy decorated on 3d architecture composite of reduced graphene oxide/molybdenum disulfide giving excellent electromagnetic wave absorption properties, *J. Alloys Compd.* 689, 208 (2016)
143. A. P. Guo, X. J. Zhang, S. W. Wang, J. Q. Zhu, L. Yang, and G. S. Wang, Excellent microwave absorption and electromagnetic interference shielding based on reduced graphene oxide@MoS_2/poly(vinylidene fluoride) composites, *ChemPlusChem* 81(12), 1305 (2016)
144. M. Li, X. Cao, S. Zheng, and S. Qi, Ternary composites $RGO/MoS_2@Fe_3O_4$: Synthesis and enhanced electromagnetic wave absorbing performance, *J. Mater. Sci.: Mater. Electron.* 28(22), 16802 (2017)
145. M. Osada and T. Sasaki, Two-dimensional dielectric nanosheets: Novel nanoelectronics from nanocrystal building blocks, *Adv. Mater.* 24(2), 210 (2012)
146. R. Z. Ma and T. Sasaki, Two-dimensional oxide and hydroxide nanosheets: Controllable high-quality exfoliation, molecular assembly, and exploration of functionality, *Acc. Chem. Res.* 48(1), 136 (2015)
147. M. P. Gashti and S. Eslami, Structural, optical and electromagnetic properties of aluminum-clay nanocomposites, *Superlattices Microstruct.* 51(1), 135 (2012)
148. E. Y. Salih, Z. Abbas, S. H. H. Al Ali, and M. Z. Hussein, Dielectric behaviour of $Zn/Al-NO_3$ LDHs filled with polyvinyl chloride composite at low microwave frequencies, *Adv. Mater. Sci. Eng.* 2014, 1 (2014)

149. F. Z. Lv, Y. Y. Wu, Y. H. Zhang, J. W. Shang, and P. K. Chu, Structure and magnetic properties of soft organic ZnAl-LDH/polyimide electromagnetic shielding composites, *J. Mater. Sci.* 47(4), 2033 (2012)

150. M. Parvinzadeh, and S. Eslami, Optical and electromagnetic characteristics of clay-iron oxide nanocomposites, *Res. Chem. Intermed.* 37(7), 771 (2011)

151. B. Quan, X. H. Liang, G. B. Ji, J. Lv, S. S. Dai, G. Y. Xu, and Y. W. Du, Laminated graphene oxide-supported high-efficiency microwave absorber fabricated by an in-situ growth approach, *Carbon* 129, 310 (2018)

152. H. Lv, H. Zhang, and G. Ji, Development of novel graphene/g-C_3N_4 composite with broad-frequency and light-weight features, *Part. Part. Syst. Charact.* 33(9), 656 (2016)

153. A. Murk and I. Zivkovic, Boron nitride loading for thermal conductivity improvement of composite microwave absorbers, *Electron. Lett.* 48(18), 1130 (2012)

154. Y. Kang, Z. Jiang, T. Ma, Z. Chu, and G. Li, Hybrids of reduced graphene oxide and hexagonal boron nitride: Lightweight absorbers with tunable and highly efficient microwave attenuation properties, *ACS Appl. Mater. Interfaces* 8(47), 32468 (2016)

155. X. Zhang, X. Zhang, M. Yang, S. Yang, H. Wu, S. Guo, and Y. Wang, Ordered multilayer film of (graphene oxide/polymer and boron nitride/polymer) nanocomposites: An ideal EMI shielding material with excellent electrical insulation and high thermal conductivity, *Compos. Sci. Technol.* 136, 104 (2016)

156. F. Wu, A. Xie, M. X. Sun, W. C. Jiang, and K. Zhang, Few-layer black phosphorus: A bright future in electromagnetic absorption, *Mater. Lett.* 193, 30 (2017)